Characterisation and functional analysis of receptor-like cytoplasmic kinase MARIS and protein phosphatases ATUNIS1 and ATUNIS2 in tip-growing plant cells

Inaugural-Dissertation

zur

Erlangung des Doktorgrades

der Mathematisch-Naturwissenschaftlichen Fakultät

der Universität zu Köln

vorgelegt von

Christina Maria Franck

aus Moosburg a.d. Isar, Deutschland

Köln, 2018

Berichterstatter: Dr. Aurélien Boisson-Dernier
                    Prof. Dr. Martin Hülskamp

Prüfungsvorsitzender: Prof. Dr. Siegfried Roth

Tag der mündlichen Prüfung: 15. Januar 2018

ZUSAMMENFASSUNG

Pflanzenzellen sind von einer Zellwand umgeben, einer stabilen aber dynamischen extrazellulären Matrix, die viele verschiedene Funktionen für die Pflanze übernimmt. Da sie den ersten Kontaktpunkt zwischen Pflanze und Umwelt darstellt, manifestieren sich viele Umweltveränderungen und Standortherausforderungen in Form von Zellwandmodifikationen. Diese werden von Sensoren in der Zellwand erkannt, die eine Signalkaskade aktivieren, die zu transkriptionellen und translationellen Veränderungen in der Pflanzenzelle führt. Diese Sensorproteine werden Rezeptorartige Kinasen (RLKs) genannt. Die *Catharantus roseus* RLK1-artige Unterfamilie von Rezeptorartigen Kinasen hat über die vergangenen 10 Jahre zunehmend Aufmerksamkeit erregt. Ihre Mitglieder sind in unterschiedlichsten Funktionsbereichen in der Pflanze involviert, von abiotischem Stress-Management über Befruchtung, Immunabwehr und Hormon-Signalwegen, bis hin zu Morphogenese und Pflanzenwachstum (Franck et al., eingereicht). Zellwachstum ist ein sehr komplexer Prozess, der strikte Koordinierung der Zellwandintegrität (CWI) mit der zellinternen Wachstumsmaschinerie erfordert. Wenn die Zellwand zu weich ist, kann dies zum Platzen der Pflanzenzelle führen, wenn sie zu steif ist, könnte dies einen Wachstumsstopp zur Folge haben. Um diesen Wachstumsregulationsmechanismus zu untersuchen, sind Zellen, die Spitzenwachstum betreiben wie Pollenschläuche und Wurzelhaare, optimal geeignet, da es sich hierbei um "einzellige" Systeme handelt, die unidirektional wachsen.

Der CWI-Signalweg in Pollenschläuchen (PTs) wird von zwei redundanten, Spitzen-lokalisierten *Cr*RLK1Ls mit den Namen ANXUR1/2 (ANX1/2) gesteuert. *anx1 anx2* Doppel-Nullmutanten Pflanzen sind männlich steril. *In vitro* sind *anx1 anx2* Pollenkörner nicht in der Lage, PTs zu auszubilden und platzen nachdem sie nur kleine Wölbungen gebildet haben (Boisson-Dernier et al., 2009; Miyazaki et al., 2009). Im Gegensatz dazu bilden *ANX1/2*-Überexpressionslinien kurze PTs mit breiten Spitzen aus, die letztendlich aufgrund von übermäßigen Zellwandmaterialablagerungen aufhören, zu wachsen (Boisson-Dernier et al., 2013). Die zwei partiell redundanten NADPH Oxidasen RbohH und RbohJ, die der Sauerstoffradikale bildenden Oxidasen (Rboh) Familie angehören, agieren unterhalb von ANX1/2. *rbohH rbohJ* Doppelmutantenpollen zeigen ein vergleichbares Erscheinungsbild bezüglich vorzeitigem Platzen wie *anx1 anx2* Pollen (Boisson-Dernier et al., 2013).

Der Wurzelhaar (RH) CWI-Signalweg wird vom *Cr*RLK1L-Mitglied FERONIA (FER) gesteuert, der nächsten Verwandten von ANX1/2. *fer* Mutanten weisen platzende RHs auf (Duan et al., 2010). Interessanterweise wurde vorgeschlagen, dass NADPH Oxidase RbohC (RHD2) - ein Homolog zu RbohH/J - unterhalb von FER agiert (Foreman et al., 2003). *rhd2* Mutanten weisen auch platzende RHs auf.

In dieser Dissertation zeige ich die Entdeckung dreier neuer Signalwegkomponenten auf, die unterhalb von ANX1/2 im CWI-Signalweg fungieren. In einer EMS-induzierten *anx1 anx2* Sterilitäts-Suppressorselektion haben wir 32 Suppressormutanten identifiziert, die sogenannten *Impotenz Rettungsmutanten (ipr*s). Zwei dieser, *ipr19* und *ipr7*, wurden zur genaueren Untersuchung ausgewählt. Die *ipr19* Mutation bewirkt einen R240C Aminosäureaustausch in der bis *dato* uncharakterisierten Rezeptorartigen Cytoplasmatischen Kinase (RLCK) MARIS (MRI). Die *ipr7* Mutation führt zu einem D94N Austausch im konservierten Kernstück der katalytischen Domäne einer Proteinphosphatase namens ATUNIS1 (AUN1). *AUN1* hat ein sehr nah verwandtes Homolog, *AUN2 (TOPP8)*, das 89.8% Sequenzidentität mit *AUN1* teilt. Wir zeigen, dass alle drei Gene im ANX1/2-abhängigen CWI-Signalweg in Pollen agieren und dass *MRI* zudem im FER-abhängigen

CWI-Signalweg in RHs fungiert. Bei MRI handelt es sich um einen positiven Regulator beider Signalwege, wohingegen AUN1/2 negative Regulatoren des Spitzenwachstums sind. Außerdem zeigen wir, dass es sich bei $MRI^{[R240C]}$ um eine dominant hypermorphe und bei $AUN1^{[D94N]}$ um eine dominant amorphe Mutation handelt.

ABSTRACT

Plant cells are surrounded by a cell wall, a rigid yet dynamic extracellular-matrix that fulfills many different functions for the plant. As first contact point between a plant and its environment, many environmental changes and challenges manifest in modifications of the cell wall. These changes are recognized by sensors within the cell wall that recognize a specific modification and trigger a signal cascade in response, in order to induce transcriptional or translational changes within the plant cell. These sensor proteins are called receptor-like kinases (RLKs). The *Catharantus roseus* RLK1-like (*Cr*RLK1L) subfamily of RLKs has gained increasing attention over the past decade. Family members are involved in diverse functions ranging from abiotic stress responses, fertilization, immunity and hormone signaling to plant morphogenesis and plant growth (Franck et al., submitted). Cell growth is a very complex process, as it requires tight coordination between the cell wall integrity (CWI) and the internal growth machineries. If the cell wall is too soft, the plant cell might burst, if it is too rigid, the cell might cease growth. To study this growth-regulatory mechanism, tip-growing cells such as pollen tubes and root hairs are apt models as they are "unicellular" systems that elongate unidirectionally.

In pollen tubes (PTs), the CWI pathway is governed by two redundant, tip-localized *Cr*RLK1Ls named ANXUR1/2 (ANX1/2). *anx1 anx2* double knock-out plants are male sterile. *In vitro, anx1 anx2* pollen grains are unable to form PTs and burst after forming little bulges (Boisson-Dernier et al., 2009; Miyazaki et al., 2009). In contrast, *ANX1/2* over-expressor lines form short PTs with wide tips that eventually stop growing due to cell wall material over-accumulations at the PT tip (Boisson-Dernier et al., 2013). Two partially redundant NADPH oxidases of the Respiratory burst oxidase homologue (Rboh) family, RbohH and RbohJ, act downstream of ANX1/2. *rbohH rbohJ* double mutant pollen shows a similar precocious bursting phenotype as *anx1 anx2* pollen (Boisson-Dernier et al., 2013).

The root hair (RH) CWI pathway is governed by the *Cr*RLK1L member FERONIA (FER), the closest homologue of ANX1/2. *fer* mutants exhibit bursting RHs (Duan et al., 2010). Interestingly, NADPH oxidase RBOHC (RHD2) - a homologue of RbohH/J - was proposed to act downstream of FER (Foreman et al., 2003). *rhd2* mutants exhibit bursting RHs as well.

In this PhD thesis, I report the finding of three novel downstream components of the ANX1/2-dependent CWI pathway. In an EMS-mediated *anx1 anx2* sterility suppressor screen, we identified 32 suppressor mutants, the *impotence rescue mutants (ipr*s). Two of these, *ipr19* and *ipr7*, were selected for closer examination. The *ipr19* mutation triggers a R240C amino acid substitution in the yet uncharacterized receptor-like cytoplasmic kinase (RLCK) MARIS (MRI). The *ipr7* mutation causes a D94N substitution in the core catalytic domain of protein phosphatase TOPP9 that we termed ATUNIS1 (AUN1). *AUN1* has a very close homologue, *AUN2 (TOPP8)* that shares 89.8% sequence identity with *AUN1*. We show that all three genes act in the ANX1/2-dependent CWI pathway in pollen and that MRI acts in the FER-dependent CWI pathway in RHs. While MRI is a positive regulator in both pathways, AUN1/2 are negative regulators of tip-growth. Also, we demonstrate that $MRI^{[R240C]}$ is a dominant hypermorphic mutation, while $AUN1^{[D94N]}$ is a dominant amorphic mutation.

ACKNOWLEDGEMENTS

First, I'd like to thank my supervisor and first referee ***Aurélien Boisson-Dernier*** for giving me the chance to help building up the AG Boisson as his very first PhD student. Thank you for three years that were never boring, for constantly challenging me to do even better and most importantly, for always lending an open ear to any concerns, thoughts or crazy ideas. I want to thank ***Martin Hülskamp*** for having me in the lab and accepting to be the second referee in my thesis committee. Thank you for taking time to listen to any concerns and providing support when needed. Furthermore, I would like to thank ***Siegfried Roth*** for being willing to chair the PhD defense. I also want to thank ***Swen Schellmann*** for being part of the defense committee and the small occasional pranks. Additionally, I'd like to thank ***Thomas Dresselhaus*** for giving helpful feedback on my project results in an informal PhD advisory meeting.

I want to thank ***Gabriele Thorn*** for all the support and help during the past three years. Thanks for "adopting me" in the secretary's office for the first three months of my PhD and always being there if I needed any advice or just wanted to chat.

Also, a big thanks goes to our lab technician ***Roswitha Lentz*** for being awesome, always having an open ear to problems and being the perfect counter to any stress that could possibly arise during everyday life at the lab. I also want to thank lab officer ***Birgit Kernebeck*** for putting up with our artsy collection of empty PET bottles in the office, for always having a piece of advice if needed and for the fun conversations. Next, I want to thank my fellow/former office mates ***Jens Westermann, Mona Mapar, Irene Klinkhammer, Alex Schurz*** and ***Sabine Lohmer*** for the relaxed and joyful atmosphere, the many discussions we had about basically everything work and non-work related and all the snacks that I got from everyone during my time here. Thanks for always having an open ear to any problem.

I also want to thank ***Uschi Claßen*** for her friendly, welcoming attitude and for always being concerned about the wellbeing of fellow lab members.

I'd like to thank former lab members ***Hemal Bhasin*** and ***Arpa Sutipatanasomboon*** for our fun times inside and outside of the lab, the many discussions and their helpful advice with the protein work. Also, a big thanks goes to ***Lisa Stephan*** for making the freezing days in the cold room considerably less dull and for the unexpected cold room freeletics sessions. Also, thanks a lot for all your advice and help with the protein work as well as the opportunity to chat about literally everything. I want to thank my "twin sister" ***Jessi Pietsch, Eva Koebke, Heike Wolff*** and ***Marc Jacoby*** for spontaneous good times at the kitchen and for always welcoming me in their office. I also want to thank my former office members ***Andrea Schrader*** and ***Bipei Zhang*** for enriching discussions and good times I spent there.

Also, I want to thank our students ***Sebastian*** and ***Simon*** for their contributions to our small workgroup and for our enjoyable lunchtime discussions at the Mensa.

I want to thank ***my family*** for always being there, if needed and supporting me through any tough decision and stressful time. Thanks for being the reliable anchor that I can always come back to.

Lastly, I want to thank **_Jens_** for our awesome collaboration in and outside of the lab. Without you, life would be a lot less fun. Thanks for always being there for me.

TABLE OF CONTENTS

LIST OF ABBREVIATIONS

ACA9	*Autoinhibited Ca^{2+} ATPase 9*
amiRNA ralfl4/19	*artificial microRNA Rapid Alkalinization Factor-like 4/19*
ANX1/2	ANXUR1/2
arl1/2	*anxur rescue line 1/2*
AUN1/2	ATUNIS1/2
BF	Bursting Fraction
Ca^{2+}	Calcium
CFP	Cyan Fluorescent Protein
Col-0	Columbia-0
*Cr*RLK1L	*Catharantus roseus* Receptor-Like Kinase 1 Like
CW	Cell Wall
CWI	Cell Wall Integrity
dCAPS	Derived Cleaved Amplified Polymorphic Sequence
ECD	Extracellular Domain
EMS	Ethyl Methyl Sulfonate
FER	FERONIA
ipr	*impotence rescue mutant*
L*er*	Landsberg *erecta*
LAT52	*Anther-specific Gene LAT52*
MRI	MARIS
NADPH	Nicotinamide Adenine Dinucleotide Phosphate
ox	over-expressor
PCR	Polymerase Chain Reaction
PMEs	Pectin Methyl Esterases
prc1-1	*procruste1-1*
PT	Pollen Tube
qrt	*quartet*
RALF	Rapid Alkalinization Factor
RbohH/J	Respiratory burst oxidase homologue H/J
RH	Root Hair
RHD2 (RbohC)	Root Hair Defective 2
RLCK	Receptor-like Cytoplasmic Kinase
RLK	Receptor-like Kinase
ROS	Reactive Oxygen Species
SNP	Single Nucleotide Polymorphism
SUP	Suppressor
THE1	THESEUS1
TMD	Transmembrane Domain
TOPP	Type One Protein Phosphatase
WT	Wild Type
YFP	Yellow Fluorescent Protein

LIST OF FIGURES

LIST OF TABLES

1. INTRODUCTION

1.1 The cell wall is a plant adaption to its environment

Plants are sessile organisms, unlike humans they are unable to move or change location if the surrounding environmental conditions are not fulfilling their requirements. Instead, they have to adapt to their surroundings in the most efficient way. They show spectacular adaptive traits to protect themselves from environmental challenges. Some plants develop thorns, spines or prickles which are modified shoots, leaves or epidermis tissue, respectively, in order to fight off herbivore attacks (Simpson, 2010). Others exhibit glandular trichomes producing essential oils with fungicidal activity (Mashigo et al., 2015) or etherical oil to ward off insects like aphids (Wagner et al., 1991). Other plants use glands to excrete superfluous salt (Yuan et al., 2016). Additionally, all plant cells are surrounded by an extracellular matrix called the cell wall (CW) that contains mainly cellulose, hemicellulose and pectin (Cosgrove et al., 2005) (Fig. 1). Cellulose primarily is an unbranched (1,4) - linked β-D-glucan. It is synthesized at the plasma membrane. Many cellulose molecules arrange in a parallel manner to form crystalline cellulose microfibrils of 3-5 nm width. Mechanically, these are very strong and extremely resistant to enzymatic attack. Their ribbon-like structure makes them the optimal scaffold material giving stability to the CW. The cellulose fibers are crosslinked by hemicelluloses. The latter are structurally similar to cellulose but unable to form microfibrils by themselves due to branches and other modifications. Just like pectins, hemicelluloses are synthesized in the golgi apparatus and transported to the CW surface by vesicles. Two of the most abundant hemicelluloses are xyloglucan and arabinoxylan. Their structure varies slightly in different plant species. Pectins function as "glue" that holds the CW together. They are a heterogeneous group of polysaccharides with distinctive domains thought to be covalently linked with each other (Ridley et al., 2001; Willats et al., 2001; Vincken et al., 2003). Rhamnogalacturan I, homogalacturonan and xylogalacturonan are the most prominent pectins. The latter two exhibit carboxyl groups that are often found methyl-esterified, which is a structural modification that blocks these pectins from linking with each other and thus from forming gels (Cosgrove et al., 2005). Arabinans and arabinogalactans are neutral pectins that have been proposed to promote CW flexibility (Jones et al., 2003) and have been demonstrated to bind to cellulose (Lin et al., 2015). The pectin composition is also responsible for the rigidity or softness of the CW. At first glance, the CW might look less spectacular than other adaptations but in fact it executes multiple very different functions important for plant life.

1.2 The cell wall fulfills versatile tasks

Firstly, the cellulose in the CW is not easily digestible for herbivores and thus is a measure to impair herbivore feeding. Furthermore, as first barrier between the plant cell and its environment, the CW acts as scout for the cell. Cellular interactions, like cell-cell communication during pathogen attacks, fertilization or abiotic stress responses cause modifications of the CW. By using CW sensors, the plant cell closely monitors the status of the latter and any modification is reported via signal-transduction mechanisms to the inside of the cell. These induce transcriptional or translational changes, which allow the plant cell to appropriately react to any situation. Furthermore, the CW is the skeleton of the plant.
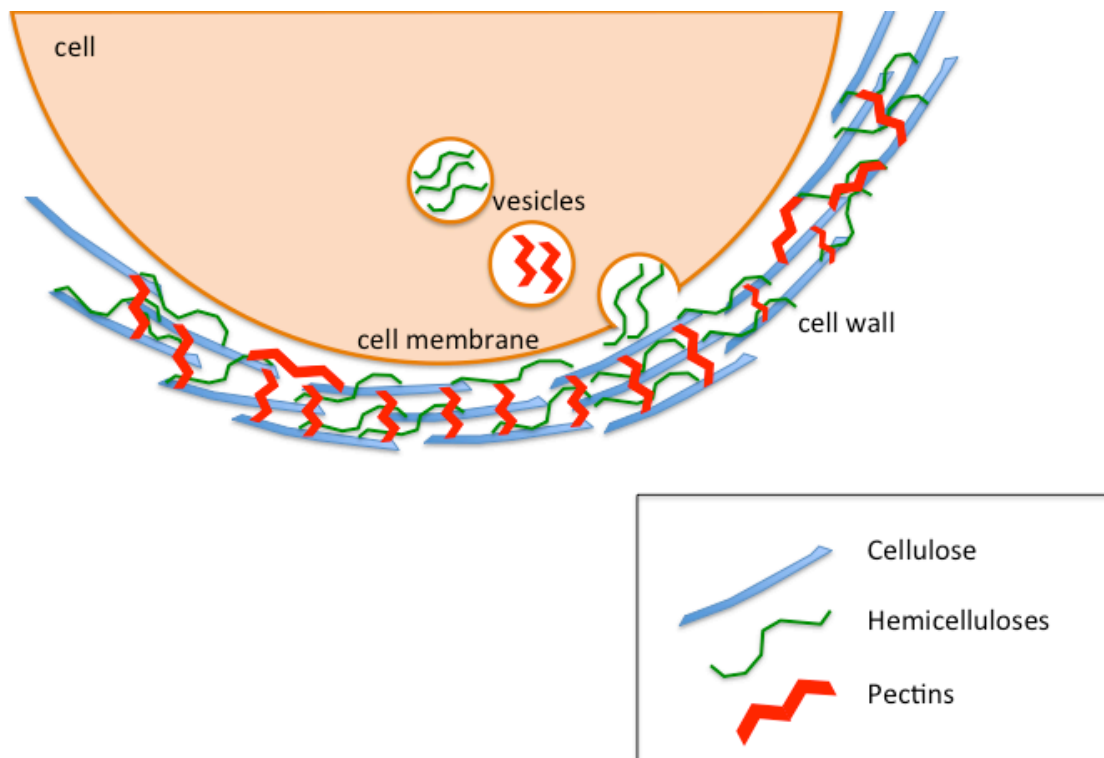
Fig. 1 Schematic representation of the cell wall with cellulose, hemicelluloses and pectins.

It withstands the positive turgor pressure within the plant cells and thus grants a growing plant stability. Also, it is capable of withstanding negative pressure found for example in conductive vessels. Additionally, the CW is important for cellular shape and growth. By being able to modulate CW rigidity, the plant cell can control the growth speed. If the CW is too rigid, plant cell growth might be stalled, if it is too soft, the plant cell might lose its integrity and burst. To prevent any of these events, the cell has to closely monitor its CW integrity (CWI) and relay this information to the internal growth machinery.

This process is not limited to plants, in fact, there are multiple CWI pathways in various organisms. In the budding yeast *Saccharomyces cerevisiae*, for example, the CWI pathway is well characterized (Levin, 2005). This is especially interesting as the challenges and functional requirements encountered by plant and yeast cells are quite similar (Levin, 2011; Free, 2013; Hamann, 2014). In yeast, the CWI maintenance mechanism is activated by CW damaging agents, osmotic shock, biotic and abiotic stresses, as well as cytoskeleton reorganization (Levin, 2011; Hamann, 2014). Signals are initiated via receptors at the plasma membrane and are relayed to transcription factors within the nucleus via a complex signaling cascade involving Rho1, Guanine exchange factors (GEFS), GTPase activating proteins (GAPs) and mitogen-activated protein (MAP) kinases amongst other members. Thus, the question arises how plants mediate CWI maintenance.

1.3 Pollen tubes as model systems for investigating cell growth

In order to properly investigate the very complex process of cell growth, a good model system needs to be chosen. We conducted our experiment in *Arabidopsis thaliana,* more specifically on pollen tubes (PTs), as they hold many advantages. PTs are very apt models to study growth processes as they are "unicellular" systems that elongate in one direction only, which is at the tip. They are amenable to genetics and to "omics" technology and they react to pharmacological treatments. Furthermore, they can be easily cultivated *in vitro*, they maintain their polarity and they are suitable for live imaging. Also, PTs are among the fastest growing cells with average growth rates between 3-6 µm/min in *Arabidopsis* (Lassig et al., 2014; Franck et al., 2017) and growth rates up to 240 µm/min for fast-growing species such as *Tradescantia* or *Hemerocallis* (Michard et al., 2009), indicating that their CWI maintenance system has to be robust.

In plant reproduction, PTs are responsible for delivering the sperm cells to the receptive ovules (Cheung et al., 1996; Johnson and Preuss, 2012). This mission is a fierce competition as the number of ovules is limited per pistil and so is the possibility to contribute to the next generation.

1.4 The pollen tube is important for plant reproduction

Fertilization generally describes the fusion of two haploid gametes to give rise to a diploid organism. In order to reach the female reproductive cells, sperm cells in angiosperms have to travel up to several millimeters in *Arabidopsis* and up to 30 cm in maize (Dresselhaus et al., 2016). The PT is commonly used as a vehicle to transport the sperm cells.

During plant reproduction, a pollen grain lands on the receptive stigma, where it undergoes adhesion and re-hydration before it germinates (Johnson and Lord, 2006; Dresselhaus and Franklin-Tong, 2013) (Fig. 2). The vegetative cell within the pollen starts elongating and exits the pollen grain through one of the three colpi, designated apertures where no sporopollenin is deposited. Thus, the PT emerges. It elongates by tip-growth and is set to deliver the male germ unit, consisting of two sperm cells and the vegetative nucleus that are connected with each other. The PT penetrates the pistil tissue and grows through the nutrient-rich transmitting tract until it is attracted by a receptive ovule and grows towards it. During this journey towards the ovule, extensive signaling between the PT and the maternal tissues of the stigma, style, transmitting tract and ovule takes place to ensure optimal guidance, e.g. via chemotactic cues (Márton et al., 2004; Okuda et al., 2009; Takeuchi et al., 2012; Márton et al., 2012). The PT penetrates the micropyle, an opening in the integuments surrounding the female gametophyte, and is received by the filiform apparatus, a callose-rich complex of CW invaginations of the synergid cells. The PT enters one of the latter, while the other one degrades. This is thought to be a first barrier to avoid polyspermy. Recently however, it has been proposed that the PT might be entering the synergids at a site more distinct from the filiform apparatus (Leshem et al., 2013). The PT eventually ruptures within the receptive synergid and releases the two sperm cells (Kessler and Grossniklaus, 2011). One of the latter fertilizes the egg cell while the other one fertilizes the central cell, giving rise to the diploid embryo and the triploid endosperm nurturing the embryo, respectively (Baroux et al., 2002; Bleckmann et al., 2014). This process is called double fertilization.
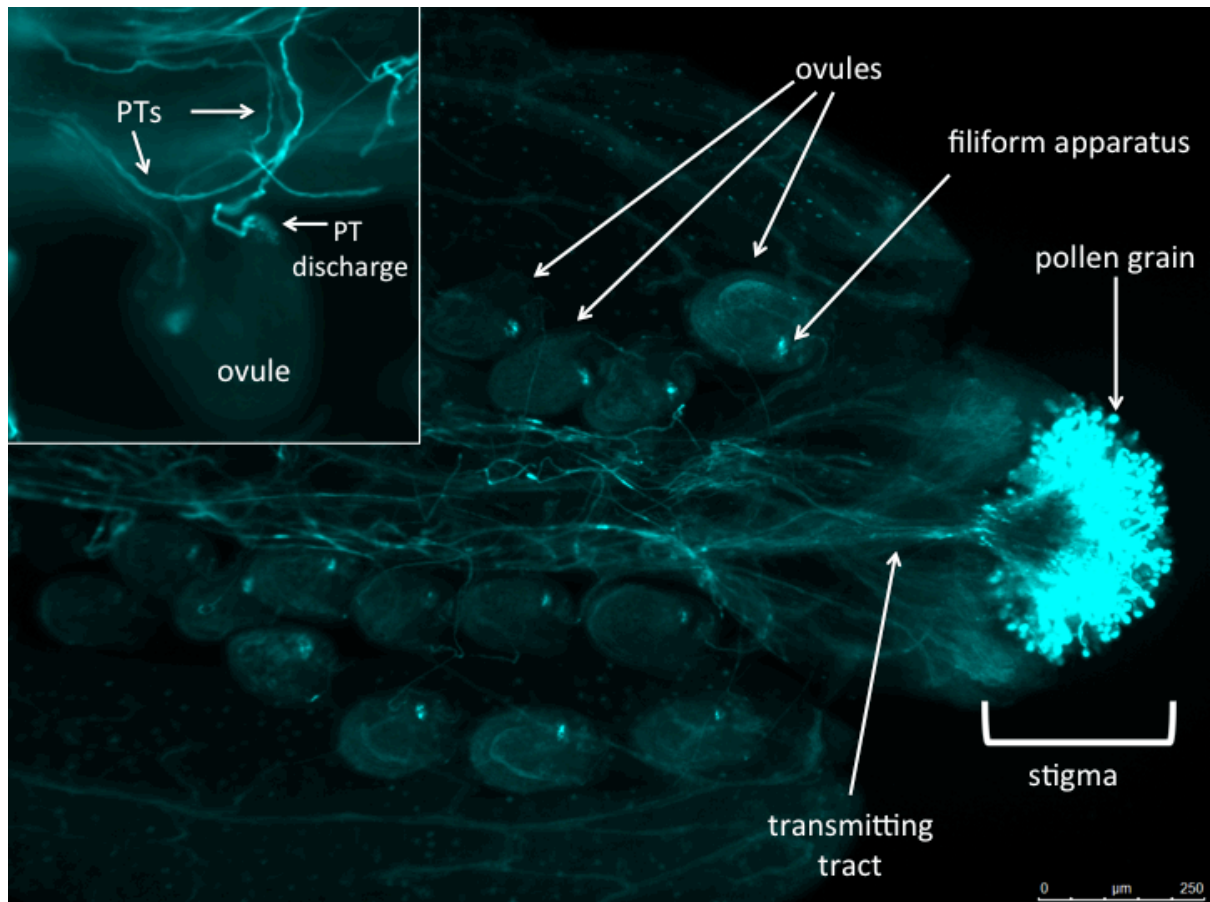
Fig. 2 Plant reproduction visualized by Aniline blue staining of a pollinated WT pistil. Pollen grains land on the stigma where they hydrate and germinate. They form PTs that penetrate the female tissues and grow towards the ovules through the transmitting tract. At the ovule, a PT arrives at the filiform apparatus, a callose-rich region formed by the synergid cells. The PT enters one of the synergids and eventually bursts to deliver the sperm cells.

1.5 Pollen tube growth control

1.5.1 Cell wall integrity

To successfully contribute to the next generation, a PT has to grow as fast as possible. Thus, it has to optimally control the properties of its CW. A CW too rigid will stall its growth while a CW too soft bears the danger of precocious loss of integrity.

The PT CW consists of low levels of cellulose and higher levels of pectins and callose (Mollet et al., 2013). The callose is only found in the distal part of the PT. Also, most pectins in the distal region are de-methylesterified and can crosslink with each other via Ca^{2+} ions (Bosch and Hepler, 2005). Overall, this renders the PT CW distal from the PT tip less soft than proximal to the tip, allowing for tip-growth. Meanwhile, newly synthesized methylesterified pectins are secreted at the PT tip (Chebli et al., 2012). They are soft and elastic and cannot crosslink with each other unless de-methylesterified by Pectin Methyl Esterases (PMEs). As novel pectins are secreted, the de-methylesterified pectins are slowly moved to the periphery (Guan et al., 2013). If the CW material supply is too slow, the PT CW at the tip might become too rigid, resulting in precocious bursting of the PT. If the supply is too fast, the tip might become too soft, and the PT might cease growing. Thus, the delivery of novel CW material needs to be strictly coordinated with the internal growth machinery.

1.5.2 Internal growth machinery

New CW material is transported via vesicle trafficking in the PT. Vesicle streaming takes place in a reverse fountain-like pattern with mostly endocytotic vesicles in the distal region and endo- and exocytotic vesicles in the tip region (Chebli et al., 2013) (Fig. 3). It is dependent on a functional actin cytoskeleton. The PT has to keep a balance between endocytosis and exocytosis of vesicles. If this balance is disrupted, lack of CW material at the tip can result in bursting of the PT. The other scenario is that CW material over-accumulation can result in stall of growth.

To guarantee efficient transport of vesicles, the PT is in need of an intact and dynamic cytoskeleton. The cytoskeleton is mainly composed of two elements, microtubules (MTs) and actin microfilaments (F-actin) (reviewed in Qin and Yang, 2011). MTs are important for organelle movement and tip-growth efficiency as well as organizing the exocytosis organization center (Raudaskoski et al., 1994; Fuchs et al., 2005; Mourino-Perez et al., 2006). However, they are not essential for tip-growth in contrast to F-actin. Axially aligned, long F-actin cables are responsible for the movement of organelles and vesicles as well as the regulation of cytoplasmic streaming (Staiger et al., 1994; Cai and Cresti, 2009). Actin nucleation factor Formin 3 (AFH3) is responsible for the formation of actin cables in the shank part of the PT (Ye et al., 2009). Downregulation of *AFH3* by RNAi abolishes the actin cables and alters the cytoplasmic streaming pattern. As a result, PTs are short and wide. In the subapical zone of the PT, actin cables are shorter and thinner and form a ring-like F-actin structure. They are assembled by Formin 5 (FH5) localized at the plasma membrane (Cheung et al., 2010). *FH5RNAi* PTs exhibit diminished subapical F-actin and show abnormal twists and turns, indicating that the F-actin in the subapical zone is important for polar growth maintenance (Fu et al. 2001; Cheung et al., 2010).

Furthermore, the dynamics of these short, thin actin cables in the subapical zone is regulated by ROP1, a ROP-GTPase belonging to the Rho family (Fu et al., 2001). Over-expression of ROP1 leads to depolarized PT growth due to transformation of the small actin cables into a network of fine filaments and introduction of a transverse actin band behind the tip. RAC/ROPs are major molecular switches in plants, which shuttle between an active, GTP-bound state and an inactive, GDP-bound state (Nibau et al., 2006; Nibau and Cheung, 2011; Franck et al., submitted). This requires GAPs and GEFs just as in the CWI pathway in *Saccharomyces cerevisiae* that was previously mentioned (Berken et al., 2005; Levin, 2005). If ROPGAP1 was over-expressed in ROP1 over-expressing PTs or the latter were treated with Latrunculin B, normal actin polymerization and tip-growth could be restored (Fu et al., 2001). Also, ROP-interactive CRIB motif–containing (RIC) proteins are important for polarized PT growth (Wu et al., 2001). Over-expression of RIC3 and RIC4 was shown to cause depolarized PT growth similar to ROP1 over-expression. RIC10 is important for promoting PT elongation but is not involved in the maintenance of polarized cell growth. The remaining 8 RIC proteins have PT growth inhibitory effects. Furthermore, ROP1 has been shown to control PT growth by activating RIC4, which mediates F-actin assembly, and RIC3, which mediates the formation of another important element of the internal growth machinery, the tip-localized calcium (Ca^{2+}) gradient (Gu et al., 2005). Ca^{2+} regulates the F-actin dynamics at the PT tip by promoting F-actin depolymerization.

A stable Ca^{2+}- gradient at the tip with regular cytosolic Ca^{2+}- oscillations is key for steady PT growth (Cárdenas et al., 2008; Michard et al., 2008; Iwano et al., 2009; Steinhorst et al., 2013) (Fig. 3). If this gradient is unstable, PT growth irregularities like growth oscillations might occur (Boisson-Dernier et al., 2013; Lassig et al., 2014). These bear the same risks as

uncoupling endo- and exocytosis, as rapid growth requires a lot of CW material.

Furthermore, a stable tip-focused gradient of reactive oxygen species (ROS) must be maintained in the PT (Potocky et al., 2007) (Fig. 3). ROS are known to loosen the CW (Fry, 1998; Liszkay et al., 2004; Müller et al., 2009), allowing for tip-growth.

Lastly, a tip-focused pH gradient maintenance is also thought to play a role in PT growth control, although to date there has not been a successful dynamic measurement of PT pH. The PT tip has been reported to be more acidic than the distal region (Cardénas et al., 2008) with a constitutive alkaline band at the base of the so-called clear zone behind the tip (Feijó et al., 1999) (Fig. 3). This suits the observation that a lower pH in the CW is also correlated with higher extensibility (Rayle et al., 1970).

A growing PT has to coordinate these aspects of the internal growth machinery with the CWI. This means that the plant requires a sensor within the CW that detects changes and relays the information to the inside of the cell to initiate appropriate reactions. In plant cells, this task is executed by a family of proteins termed receptor-like kinases (RLKs).
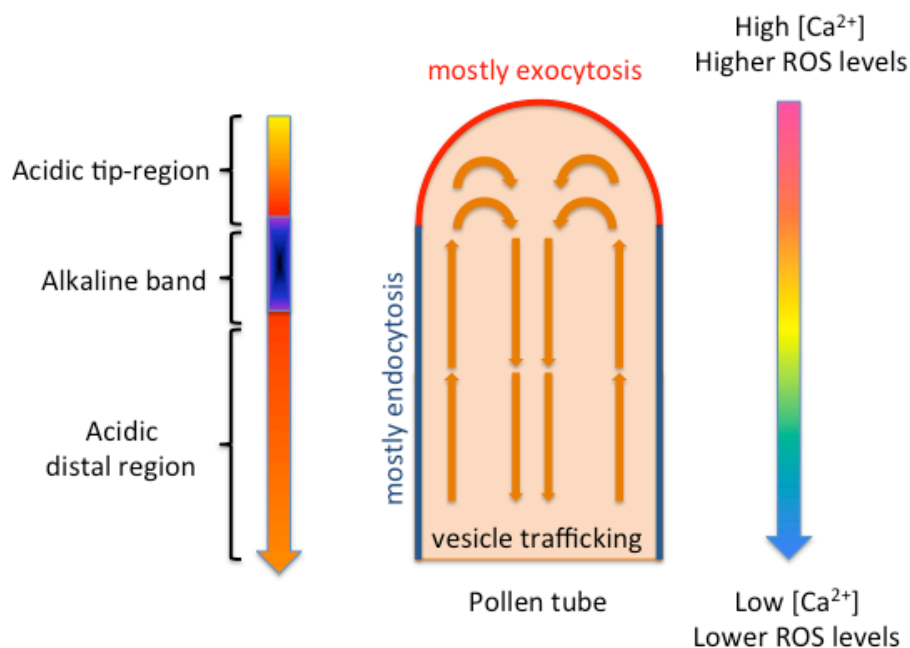
Fig. 3 Schematic representation of the internal growth machineries in a growing PT(center). The tip-region of the PT, where mostly exocytosis takes place, is marked in red, the distal region, where mostly endocytosis takes place, is marked in blue. Within the PT, vesicle streaming occurs in a reverse-fountain like pattern. A growing PT requires high $[Ca^{2+}]$-levels at the tip as well as higher ROS levels compared to the distal region. The pH of both tip-region and distal region is acidic, interrupted by an alkaline band at the transition zone between them.

1.6 RLKs are sensors within the cell wall

RLKs are generally composed of an extracellular domain (ECD) in the CW that binds ligands, a trans-membrane domain and an intracellular kinase domain triggering signal cascades in response to stimulation of the ECD (van der Geer et al., 1994) (Fig. 4). RLKs are a wide-ranged family. In the model plant *Arabidopsis thaliana*, there are more than 600 RLKs identified to date (Lehti-Shiu et al., 2009). For the CW, different types of RLKs are

important. CW-associated kinases (WAKs) were shown to be receptors for various pectins and are important for both pathogen response and cell expansion during plant development (Kohorn et al., 2012). Lectin receptor-kinases (LecRKs) bind to carbohydrates and might be important for cell-wall structure/plasma-membrane CW connection as well as plant innate immunity (Ringli et al., 2010; Singh et al., 2013). Proline-rich extensin receptor-kinases (PERKs) are involved in CW signaling and are involved during cell growth and putatively during stress tolerance (Kishor et al., 2015). Leucine-rich repeat-containing receptor kinases (LRRs) might interact with polysaccharide components of the CW and have functions during cellulose biosynthesis and putatively during stress responses (Ringli et al., 2010). Finally, malectin-like receptor kinases, also known as the *Catharanthus roseus* RLK1-like (*Cr*RLK1L) subfamily of RLKs, are named after the first isolated member *CrRLK1* from Madagascar periwinkle (Schulze-Muth et al., 1996). They are composed of one or two non-interchangeable, apoplastic malectin-like domains that putatively bind carbohydrates, a trans-membrane domain (TMD) and a conserved interchangeable kinase domain at the inside of the cell (Schallus et al., 2008; Lindner et al., 2012; Kessler et al., 2014; Franck et al., submitted). In *Arabidopsis,* 8 out of 17 *CrRLK1L* members have been characterized till date and they have versatile functions during plant morphogenesis, cell growth, reproduction, immunity, hormone signaling, and abiotic stress responses (Franck et al., submitted).

1.6.1 The *CrRLK1L* family members THESEUS1 and FERONIA

To give an example for the complexity of *Cr*RLK1L functions within the plant, the receptor-like kinases THESEUS1 and FERONIA will be described in this part.
The founding member of the *Cr*RLK1L subfamily of receptor-like kinases is THESEUS1 (THE1). It appeared in a suppressor screen for the short hypocotyl phenotype of the mutant *procruste1-1* (*prc1-1*) that is deficient in *CELLULOSE SYNTHETASE 6 (CESA6)* (Hématy et al., 2007). Mutations in *THE1* only affect *prc1-1* but not wild type plants. In a *prc1-1* background, *the1-1, the1-2, the1-3* and *the1-6* mutant plants have longer hypocotyls compared to *prc1-1* and they are resistant to treatment with the herbicide isoxaben that triggers ectopic lignification (Merz et al., 2017). Also, THE1 over-expression in *prc1-1* background leads to shorter hypocotyls and more ectopic lignification in seedlings than in untransformed *prc1-1* (Hématy et al., 2007). Thus, in context of a damaged CW, THE1 is activated to negatively regulate cell growth. Also, THE1 appears to be able to monitor the CW status.
The best-characterized member of the *Cr*RLK1L family is FERONIA (FER), named after an Etruscan deity of fertility. It is ubiquitously expressed in the plant and has a plethora of different functions. *fer* mutants are dwarfish, suggesting a role of FER in plant morphogenesis (Guo et al., 2009; Kessler et al., 2010). FER further has a function during root growth. It is bound by the peptide Rapid Alkalinization Factor 1 (RALF1) inhibiting root growth by triggering alkalinization of the extracellular matrix (Haruta et al., 2014). Moreover, *fer* mutants show defects in tip-growth: They exhibit distorted trichomes and bursting root hairs (Duan et al., 2010), indicating that FER acts in CWI maintenance. Interestingly, the *ralf1* mutant exhibits short root hairs as well, possibly due to precocious root hair bursting (Du et al., 2016). Additionally, during plant reproduction, PTs targeting *fer* ovules fail to rupture and release the sperm cells (Huck et al., 2003; Rotman et al., 2003; Escobar-Restrepo et al., 2007). Instead, they continue to grow, leaving the ovules unfertilized, which

indicates that FER is important for plant fertilization. Lastly, *FER* also plays a role in plant immunity. *fer* mutants appear to be less susceptible to *Golovinomyces orontii* (Kessler et al., 2010) and *Fusarium oxysporum* (Masachis et al., 2016) infections, pointing towards a negative role of FER during plant immunity, which is supported by several other studies (Deslauriers and Larsen, 2010; Keinath et al., 2010). However, Stegmann et al. (2017) recently demonstrated that FER positively influences PAMP-triggered immunity by acting as a scaffold for *flg22*-induced FLS2/BAK1 and *elf18*-induced EFR/BAK1 complex formation. This points towards a patho-system specific role of FERONIA in immunity.

Two other *Cr*RLK1Ls, named ANXUR1/2 (ANX1/2) after the husband of Feronia in Etruscan mythology, are predominantly expressed in pollen and localized at the plasma membrane at the PT tip (Boisson-Dernier et al., 2009). In the following, their functions during PT growth will be discussed in more detail.

1.6.2 The role of ANX1/2 during pollen tube growth

ANX1/2 show very strong expression in pollen, yet, T-DNA insertion single mutants of the genes do not have a phenotype. However, the *anx1 anx2* double knock-out mutant is male sterile. In the originally described double mutant, Boisson-Dernier et al. (2009) retrieved only 11 seeds in 277 siliques. When conducting an *in vitro* pollen germination assay, they discovered that 100% of *anx1 anx2* pollen were precociously bursting (Fig. 4). The pollen grains only manage to form little bulges but not to maintain PT growth (Boisson-Dernier et al., 2009; Miyazaki et al., 2009). Interestingly, when either ANX1-YFP or ANX2-YFP is expressed in a WT background, the pollen grains germinate less well (Boisson-Dernier et al., 2013). Also, the PTs remain shorter with wider tips, clearly being inhibited in growth. Ruthenium red staining for pectins revealed that the PTs over-accumulate pectinuous CW material at the PT tip. FRAP (Fluorescence Recovery after Photobleaching) experiments showed that this was due to a tilt of the balance between endo- and exocytosis towards exocytosis. Furthermore, with FM4-64 dye staining the plasma membrane, Boisson-Dernier et al. (2013) demonstrated that over-accumulation of CW material often is coupled with plasma-membrane invagination (Fig. 4). This indicates that the plasma membrane continues growing, but due to the thickness of the CW at the tip, the PT can no longer elongate. Thus, the receptor-like kinases ANX1/2 are positive regulators of PT growth by maintaining CWI.

1.7 Characterization of RbohH and RbohJ

ANX1/2 are thought to act upstream of the partially redundant ROS producing NADPH oxidases Respiratory Burst Oxidase Homologues H/J (RbohH/J) (Boisson-Dernier et al., 2013). They are localized to the plasma membrane of growing PTs with RbohH preferentially at the PT tip region and RbohJ more at the periphery (Lassig et al., 2014). Rbohs show homology to a catalytic subunit of the mammalian phagocyte oxidase (gp91^{phox}) (Torres et al., 1998). They are plasma membrane localized and have a C-terminal FAD/NADPH-binding site, six TMDs, and a putative EF-hand Ca^{2+}-binding motif in the extended N-terminal region (Ogasawara et al., 2008). The FAD-/NADPH-binding domain is responsible for ROS production and secretion to the apoplast. In the apoplast, the ROS O_2^- (superoxide) can be converted into H_2O_2, which is a very small molecule and can freely diffuse back into the cell.
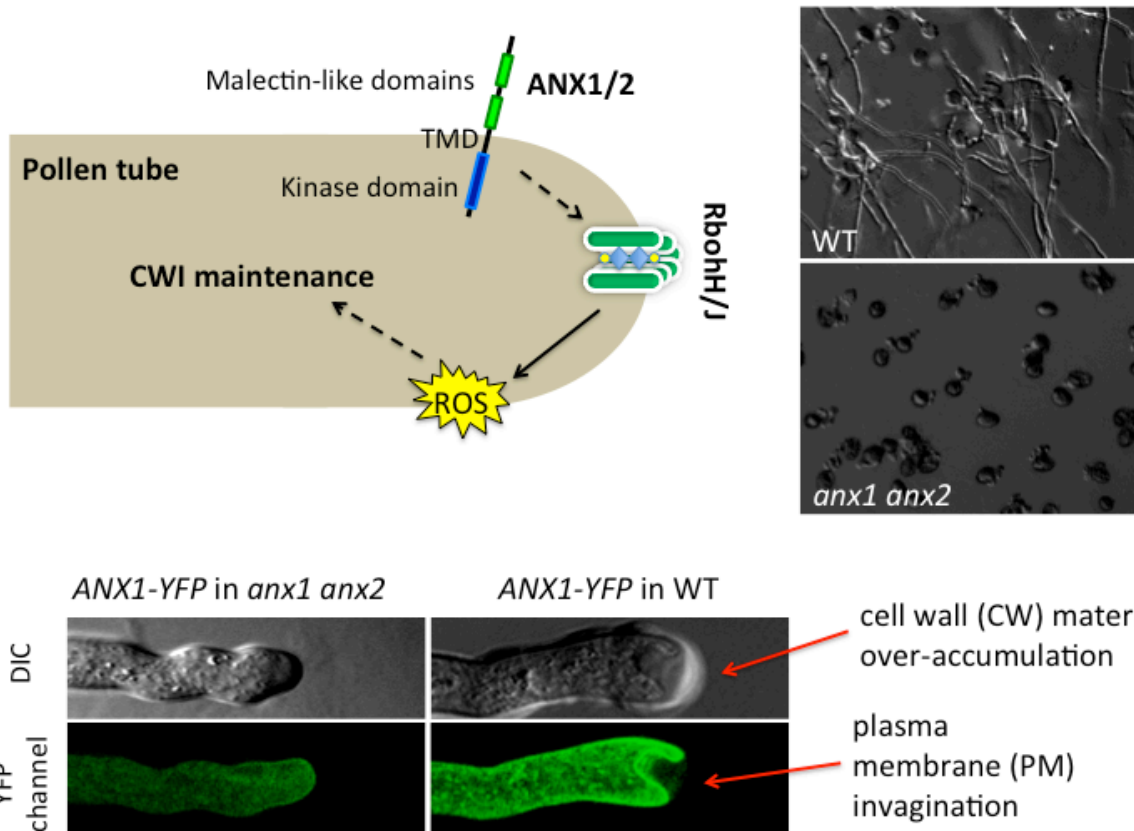
Fig. 4 The roles of ANX1/2 during PT growth. **Top left:** The CWI-pathway in PTs, governed by redundant *Cr*RLK1Ls ANX1/2 exhibiting two Malectin-like domains, a trans-membrane domain and a kinase domain. ANX1/2 trigger activation of ROS-producing NADPH-oxidases RbohH/J that mediate CWI maintenance. **Top right:** Upper panel shows WT pollen forming PTs in an *in vitro* pollen germination assay. Lower panel depicts pollen of *anx1 anx2* double knock-out mutants that are unable to form pollen grains and burst at 100% instead. **Bottom:** Comparison of *anx1 anx2* PTs complemented by ANX1-YFP and WT PTs over-expressing *ANX1-YFP*. While the *ANX1-YFP* complemented PT exhibits normal growth, the *ANX1-YFP* over-expressing PT has a wide tip from CW-material over-accumulations. Furthermore, it has an invaginated plasma-membrane. Modified from Boisson-Dernier et al. (2013).

The T-DNA insertion double knock-out mutant *rbohH rbohJ* plants are male sterile as well (Boisson-Dernier et al., 2013). *In vitro*, up to 80% of pollen grains burst precociously, reminding of *anx1 anx2* pollen grains. The remaining 20% are able to form short PTs that eventually burst as well. Interestingly, functional RbohH/J are required for observing *ANX1/2*- overexpression phenotypes, which indicates that RbohH/J act downstream of the two *Cr*RLK1Ls. Making use of the HyPer sensor for H_2O_2 detection, Boisson-Dernier et al. conducted live imaging on WT and *rbohH rbohJ* double mutant PTs. In WT PTs, irregular H_2O_2-oscillations originating from the periphery could be detected, that were absent in *rbohH rbohJ* PTs. This indicates that most of the H_2O_2 detected by the HyPer sensor is produced by RbohH/J. Interestingly, by using YellowCameleon3.6, a sensor for Ca^{2+} in combination with ratiometric imaging (Krebs et al., 2012; Franck et al., 2017), Boisson-Dernier et al. (2013) could detect lower overall Ca^{2+} levels in *rbohH rbohJ* PTs as well as an instability in the vital tip-focussed Ca^{2+} gradient. Overall, *rbohH rbohJ* PTs display an oscillatory growth behavior (Boisson-Dernier et al., 2013; Lassig et al., 2014) with phases of fast growth followed by

phases of growth arrest. Lassig et al. showed that phases of growth arrest correlate with phases of CW material accumulation at the PT tip. Apparently, the accumulated CW material is subsequently used up during phases of fast growth. Immediately before growth arrest, a peak of high Ca^{2+} concentration can be observed at the PT tip (Lassig et al., 2014; Franck et al., 2017). This suggested that Ca^{2+} signaling and ROS production are linked with each other with Ca^{2+} probably initiating a negative feedback loop to slow down the PT growth rate. In addition, it shows that RbohH/J are positive regulators of PT growth downstream of ANX1/2.

These two major findings lay the foundation for the PhD project described in this thesis. The hypothesis was that these genes might be acting in a still largely uncharacterized pathway, the cell wall integrity (CWI) pathway in PTs, governed by *ANX1/2*. The aim of this thesis was to characterize and identify potential novel key players of the pathway and to position them in the pathway relatively to the preexisting ones.

1.8 The suppressor screen

For this purpose, Boisson-Dernier et al. (2015) initiated a forward genetic screen to identify suppressor mutations of the *anx1 anx2* PT bursting phenotype. *In vivo,* the suppressor mutants would be easily detectable due to elongated siliques, as a reduction of PT bursting would result in more fertilized ovules and thus a higher amount of seeds per silique. Approximately, 7'000 ethyl methyl sulfonate (EMS) treated *anx1-2 anx2-2* M1 seeds were grown and screened for silique length (Boisson-Dernier et al., 2015). Ultimately, 32 true suppressor mutants were identified. Aniline blue staining for callose was executed to demonstrate whether the PT targeting of ovules was normal and whether the PT bursting was rescued *in vivo*. Also, the identified M1 mutants were used as pollen donors for *anx1-2 anx2-2* stigmas, where they led to an elongation of the silique, as expected. Consequently, this class of mutants was called *impotence rescue mutants (ipr*s*),* as previously described (Boisson-Dernier et al., 2015). Naturally, the different *ipr* mutants depict seed set rescue to various extents. Thus, two suppressor mutants, one with a strong rescue effect (*ipr19)* and one with a weak rescue effect (*ipr7)* were selected for detailed examination.

1.8.1 Discovery of MARIS and ATUNIS

As EMS mutagenesis usually causes multiple single-nucleotide polymorphisms (SNPs), a modified SNP-ratio mapping approach was applied (Lindner et al., 2012; Boisson-Dernier et al., 2015). At the time I took on the project, the causative SNPs in the respective genes had already been discovered. In the case of *ipr19*, a gene (*AT2G41970)* encoding a yet uncharacterized receptor-like cytoplasmic kinase (RLCK) of the RLCK-VIII family was concerned. The causative SNP (C718T) led to an arginine to cystein conversion at the 240th residue (R240C) in the conserved kinase domain of the protein (Fig. 8). The gene was named *MARIS (MRI)* after an Etruscan deity of fertility, as *MRI* is vital for PT growth (Boisson-Dernier et al., 2015). Regarding *ipr7,* the causative SNP (G280A) mapped to the gene *AT3G05580*, also known as *Type One Protein Phosphatase 9* (*TOPP9*). TOPP9 is a Serine/Threonine (Ser/Thr) -phosphatase. The SNP results in an Aspartate to Asparagine conversion at the 94th residue (D94N) in the conserved catalytic subunit. We named the gene *ATUNIS1 (AUN1)*, after an etruscan deity of death and rebirth, as the *AUN1[D94N]*

mutation causes the otherwise bursting *anx1 anx2* pollen grains to survive and form some PTs. Both *MRI* and *AUN1* will be described in detail in the following pages.

With the genes of interest identified, it is crucial to understand which types of mutations generally can arise in the *anx1-2 anx2-2* suppressor screen.

Gain-of-function mutation of a positive regulator
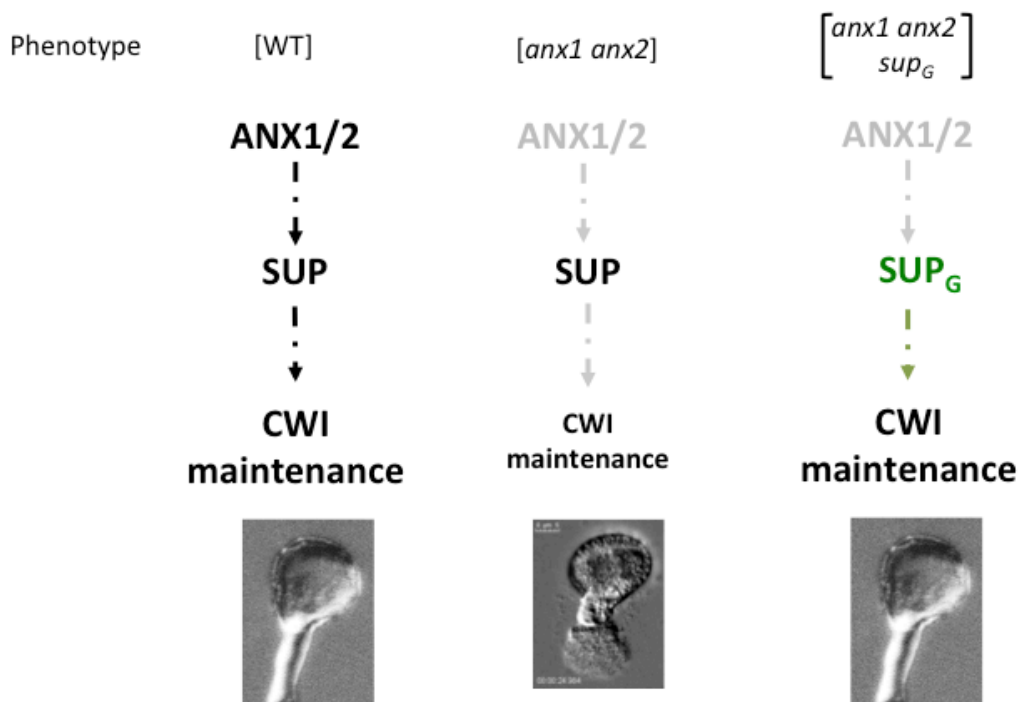
Fig. 5 Schematic representation of a gain-of-function mutation in a positive regulator.

1.8.2 Possible types of suppressor mutations

There are two different scenarios of mutations that could be discovered in such a suppressor screen. The first scenario is a gain-of-function mutation in a positive regulator (Fig. 5). This would render the regulator, referred to as SUP for suppressor in the following, constitutively active without prior need for activation. In this case, ANX1/2 would directly or indirectly activate SUP, which in turn would initiate the maintenance of CWI. Thus, the PT is able to grow normally. If ANX1/2 are not present, SUP is not activated and thus cannot prompt CWI maintenance. In consequence, the PT bursts. However, if a gain-of-function mutation in SUP (SUP$_G$) renders it constitutively active, SUP$_G$ no longer requires activation by ANX1/2 and in their absence, it can trigger the maintenance of CWI. Thus, PT bursting would be rescued.

The other possible scenario would be a loss-of-function mutation in a negative regulator, making SUP constitutively inactive without requiring prior inhibition (Fig. 6). Here, ANX1/2 would negatively regulate SUP that in turn prevents CWI maintenance. This enables normal PT growth. However, in absence of ANX1/2, SUP would not be inhibited and thus would shut down the maintenance of CWI. As a result, PT bursting is observed. If however SUP is

rendered constitutively inactive by a loss-of-function mutation (SUP$_L$), SUP$_L$ no longer requires prior inhibition by ANX1/2 and does not prevent CWI maintenance in their absence. Thus, PT bursting is averted.

Loss-of-function mutation of a negative regulator
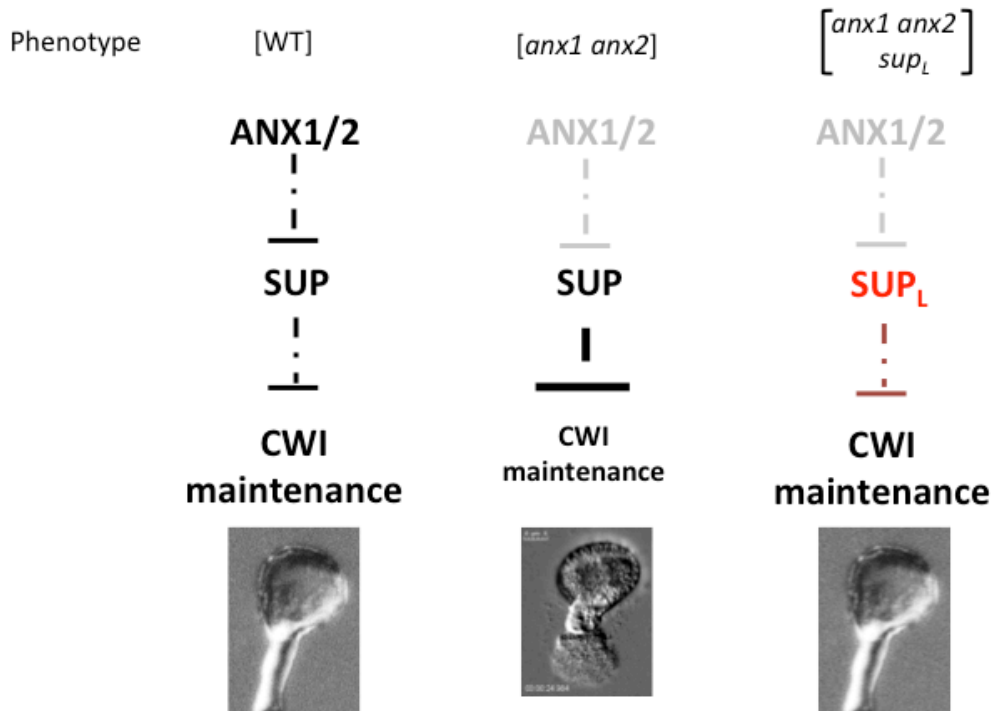
Fig. 6 Schematic representation of a loss-of-function mutation of a negative regulator.

The next chapters will focus on revealing whether MRI or AUN1 are part of the ANX1/2-dependent CWI pathway in PTs and if so, whether they have a positive or a negative regulatory function.

2. MATERIALS AND METHODS

2.1 Molecular cloning

In order to clone MRI, RNA was isolated from WT flowers and subsequently, a cDNA synthesis was conducted with Thermo Scientific RevertAid H Minus First Strand cDNA Synthesis Kit. The primer pairs ABD687 (introducing the *Sal*I site) and ABD688 (introducing the *Spe*I site and removing the stop codon) (Tab. 3) were used with the Phusion DNA polymerase (Finnzymes) as previously described in Boisson-Dernier et al. (2015). The fragment with 1.1kb length was ligated into pJet1.2 (Thermo Scientific) (Tab. 4), where it was sequenced and cloned into the *Sal*I/*Spe*I sites of pABD4 (*p*ACA9:TAP2(YFP)) (Tab. 5) to create pABD19 (*p*ACA9:MRI-TAP2(YFP)) (Tab. 6).

To generate pABD47 (*p*LAT52:MRI-CFP) and pABD49 (*p*LAT52:MRI[R240C]-CFP), *MRI* without stop-codon was amplified from cDNA of *ipr19/MRI* flowers with the Gateway-system (Katzen et al., 2007) compatible primer pair ABD737/ABD738. The resulting 1.1kb fragment amplified by Phusion was cloned into pDONR207 and transformed into *E. coli* heat-shock competent *DH5α* cells. 16 clones were sequenced, of which 6 were wild-type *MRI* and 10 were *MRI[R240C]*. Both *MRI* and *MRI[R240C]* were then cloned into pABD34 and pABD35. With ABD762/ABD763, the 1.1kb long *MRI* promoter was amplified and subsequently cloned into pJet1.2. After sequencing, the *Sac*I/*Spe*I sites were used to replace the *LAT52* promoter in pABD34 with *p*MRI, creating pABD83. Then, *MRI[R240C]* was cloned into pABD83, generating pABD85 (*p*MRI:*MRI[R240C]*-YFP).

In order to obtain AUN1 as well as AUN1[D94N], RNA was isolated from *ipr7/AUN1* flowers. cDNA synthesis was performed using the Thermo Scientific RevertAid H Minus First Strand cDNA Synthesis Kit with Gateway-compatible primer pairs ABD776/ABD777 and ABD776/ABD778 to amplify AUN1 without and with stop codon, respectively. The 950bp long fragments without stop-codons were cloned into pDONR207 and transformed into heat-shock sensitive *E. coli DH5α* cells. Restriction digestion with BsrG1 was performed on the resulting colonies and subsequently, minipreps were made to isolate the plasmid from the bacteria with the Thermo Scientific GeneJET Plasmid Miniprep Kit. After sequencing, *AUN1* and *AUN1[D94N]* were cloned into pABD34, yielding pCMF3 and pCMF5, respectively. To obtain *AUN1[H127A]*, primer pair ABD810/ABD811 was used on the *AUN1* CDS without stop codon in pDONR207 as a template for site-directed mutagenesis. The vector was then transformed in *E. coli* and sequenced. Afterwards, *AUN1[H127A]* was cloned into pABD34 as well (pCMF10).

2.2 DNA extraction

A small leaf disc was harvested from each respective seedling and mixed with 3 glass beads in 300μl Magic Buffer (50mM Tris/HCl pH7.2 (v/v), 300mM NaCl (v/v) and 10% Sucrose (w/v), all dissolved in ddH$_2$O) in a 2ml Eppendorf tube. The tissue was then ground in a QIAGEN Tissue Lyser at 30Hz for 1.5 min (this step was repeated, if required). 1μl of this extracted DNA was then used for PCR.

2.3 RNA extraction

Flowers were pooled and frozen in liquid nitrogen before being ground with a mortar. The RNeasy™ Plant Mini kit (QIAGEN) was used for RNA extraction.

2.4 PCR reactions

In order to determine the genotype of an individual plant with PCR, a 24µl PCR reaction was performed using 12.5µl DreamTaq™ Green PCR master mix (Thermo Scientific), 1µl DNA extract, 0.3µl forward and reverse primers (10µM) and 10.9µl ddH$_2$O. The PCR conditions were set as follows: 2 min of denaturation at 94°C, 35 cycles of denaturation at 94°C for 15 sec, followed by 15 sec of annealing at 58°C-60°C and 1 min of extension at 72°C. The final extension was set to 72°C for 2 min.

To confirm the causative SNP (G280A in *AT3G05580*), a derived cleaved amplified polymorpic sequence (dCAPS) marker assay was conducted on *ipr7/AUN1* and *ipr7/ipr7* plants. Therefore, a 20µl PCR reaction was used, composed of 2µl DNA extract, 0.1µl DreamTaq™ and 2µl of 10x DreamTaq™ Buffer (both Thermo Scientific), 0.8µl of 10mM dNTPs, 0.4µl of forward and reverse primers (10µM) and 14.3µl of ddH$_2$O. PCR conditions were set as described previously. After PCR, 0.4µl of *Taq*I and 2.27µl of 10xUnique *Taq*I buffer (Thermo Scientific) were mixed and added per sample. The PCR products were then digested at 65°C overnight and subsequently separated in a 3% agarose gel by gel electrophoresis. While WT plants produce a 170bp long fragment, *ipr7/ipr7* plants give rise to a 202bp long fragment. *ipr7/AUN1* plants exhibit both fragments, respectively.

To confirm the causative SNP (C718T) in *ipr19/MRI*, the dCAPS primer pair ABD724/ABD725 was used. After PCR amplification, the samples were digested with *Xho*I at 37°C over night and subsequently separated in a 3% agarose gel by gel electrophoresis. *ipr19/ipr19* plants exhibit a 200bp long fragment, while WT plants give rise to a 172bp long fragment. *ipr19/MRI* plants produce both fragments, respectively.

For the Phusion PCR, a total of 48µl of PCR reaction was used, composed of 0.5µl Phusion High-Fidelity DNA polymerase and 10µl 5x Phusion HF buffer (both Thermo Scientific), 2.5µl of forward and reverse primer (10µM), 1µl of DMSO, 2µl of 10mM dNTPs and 29.9µl ddH$_2$O. The PCR conditions were set as follows: 2min initial denaturation at 98°C, followed by 35 cycles of denaturation for 20 sec at 98°C, annealing at 62°C for 30 sec and extension for 1 min at 72°C. Final extension was set to 72°C for 5 min.

2.5 Heat-shock transformation of *E. coli* cells

Desired constructs were transformed into *E. coli DH5α* or *DB3.1* cells. Cells were thawed on ice and 5µl of the ligation or 10ng of the respective plasmid was added. Subsequently, the cells were incubated for another 15 min on ice for the DNA to adsorb to the cell surfaces. Next, cells were heat-shocked for 45 sec at 42°C and placed on ice for 2 min. 900µl for pre-warmed LB was added and the cells were incubated at 37°C for 1 hour with agitation. Thereafter, the cells were harvested and centrifuged at 3'000 rpm for 4 min and the LB was decanted but for approximately 100µl. The bacterial cells were resuspended and spread on an LB plate with appropriate antibiotics. The plates were incubated at 37°C overnight and colonies were picked the next day.

2.6 *Agrobacterium tumefaciens* electroporation

All of the abovementioned expression clones were transformed into electro-competent *Agrobacterium tumefaciens (GV3101)* strains. For this purpose, electroporation cuvettes were placed on ice and the competent cells were thawed on ice for 5 min. 50ng of the respective plasmid DNA was added and mixed with the cells. A BioRad electroporator was used (1.25kV, 200 ohms, 25µF). The cell-DNA-mixture was transferred to an ice-cooled cuvette and the cells were electro-shocked. Next, the mix was recovered in 900µl of warm LB medium and incubated for 1 hour at 28°C with agitation. Cells were harvested by centrifugation at 3'000 rpm for 4 min and the pellet was resuspended in 40µl LB medium. Then, the cells were plated on Rifampicin plates with the appropriate plasmid selection antibiotic and incubated for 2 days at 28°C.

2.7 Floral dipping

Floral dipping was conducted as previously described (Clough and Bent, 1998). 25ml liquid LB medium with appropriate antibiotics were inoculated with a fresh *Agrobacterium* colony at 28°C with agitation for 20 hours in a sterile flask. 0.5µl of the 25ml pre-culture were subsequently inoculated overnight in a sterile flask containing 250 ml of fresh LB with agitation at 28°C. On the next day, the cloudy *Agrobacteria* culture was harvested at 5'000 rpm for 20 min. The resulting pellet was resuspended in 200ml 5% Sucrose solution (w/v) for 20-40 min. The optical density (OD) at 600nm was measured and adjusted to 0.8. Sylwet L-77 (150µl/L) was added to the solution right before the onset of floral dipping.
The height of the plant material was 7-15cm with many immature florets. Plants were dipped into the *Agrobacteria* solution with agitation for 1 - 1.5 min. Subsequently, the pots were placed horizontally in a closed environment on top of watered tissues for one day before eventually being transferred to the greenhouse.

2.8 Seed sterilization, plant material and growth conditions

Seeds were subjected to 70% EtOH with 0.05% SDS for 10 minutes under constant shaking. Subsequently, the 70% EtOH was replaced by 96% EtOH and the seeds were agitated for another 10 minutes. Under the sterile hood, they were transferred to sterile filters and subsequently sown on half-strength Murashige and Skoog basal (MS) (Duchefa Biochemie bv) and Sucrose medium plates with appropriate antibiotics - if required - and vertically placed in a fridge at 4°C for two days. Subsequently, they were transferred to a growth chamber under long day conditions (16 hours light, 8 hours dark) at 22°C, approximate relative humidity of 60% and 150-300nmol light intensity. After 7 days, the seedlings were transferred to soil in a greenhouse under long day conditions.
The mutants used in this study can be found in Tab. 1 with information on when they were published or how they were obtained. The transgenic lines used are listed in Tab. 2.

Mutant name	Locus	Ecotype	Molecular markers
amiRNA ralfl 4/19 (obtained from Nadine Duss and Ueli Grossniklaus (UZH), unpublished)	At1g28270 At2g33775	Col-0	
anx1-2 anx2-2 (Boisson-Dernier et al., 2015)	AT3G04690 AT5G28680	Col-0	
anx1-1/anx1-1 anx2-1/ANX2-1 (Boisson-Dernier et al., 2013)	AT3G04690 AT5G28680	Col-0	PCR: ABD603/ABD604 PCR: ABD603/600
rbohH-3 rbohJ-3 (Boisson-Dernier et al., 2013)	AT5G60010 AT3G45810	Col-0	
fer-4 (GABI_106A06)	AT3G51550	Col-0	
fer-1 (Escobar-Restrepo et al., 2007)	AT3G51550	L*er*	
mri-1/MRI (CSHL_GT21229)	AT2G41970	L*er*	PCR: ABD681/ABD682 PCR: ABD682/ABD747
mri-2 (GABI_820D05)	AT2G41970	Col-0	PCR: ABD735/ABD736 PCR: ABD735/ABD614
mri-2/MRI (from reciprocal crosses of *mri-2* x Col-0)	AT2G41970	Col-0	PCR: ABD735/ABD736 PCR: ABD735/ABD614
ipr19/MRI (Boisson-Dernier et al., 2015)	AT2G41970	Col-0	dCAPS: ABD724/ABD725
aun1-1 (SALK_045433C)	AT3G05580	Col-0	PCR: ABD728/ABD729 PCR: ABD728/ABD600
aun2-1 (SALK_137888)	AT5G27840	Col-0	PCR: ABD779/ABD731 PCR: ABD779/ABD600
aun1-1/AUN1 aun2-1/AUN2-1 (from reciprocal crosses of *aun1-1/AUN1 aun2-1/aun2-1* x Col-0)	AT3G05580	Col-0	PCR: ABD728/ABD729 PCR: ABD728/ABD600
aun1-1/AUN1 aun2-1/aun2-1 (from crosses of *aun1-1/AUN1 aun2-1/aun2-1* x Col-0)	AT3G05580	Col-0	PCR: ABD728/ABD729 PCR: ABD728/ABD600
aun1-1 aun2-1 (from crosses of *aun1-1* x *aun2-1*)	AT3G05580 AT5G27840	Col-0	PCR: ABD728/ABD729 PCR: ABD728/ABD600 PCR: ABD779/ABD731 PCR: ABD779/ABD600
aun1-2 (GABI_600E08)	AT3G05580	Col-0	PCR: ABD728/ABD731 PCR: ABD731/ABD600
aun2-2 (SALK_125184)	AT5G27840	Col-0	PCR: ABD779/ABD731 PCR: ABD779/ABD600

aun1-2 aun2-2 (from crosses of *aun1-2* x *aun2-2*)	AT3G05580 AT5G27840	Col-0	PCR: ABD728/ABD731 PCR: ABD731/ABD600 PCR: ABD779/ABD731 PCR: ABD779/ABD600
ipr7/AUN1 (original suppressor mutant from *anx1-2 anx2-2* suppressor screen)	AT3G05580	Col-0	dCAPS: ABD726/ABD727

Tab. 1 List of mutants used in this study with locus, ecotype background and molecular markers.

Transgenic line	Genotype	AGI code	Vector Resistance
anx1-1 anx2-1 with MRI-CFP	Col-0 *anx1-1 anx2-1*	AT2G41970	pLAT52:MRI-CFP BASTA
anx1-1 anx2-1 with MRI[R240C]-CFP	Col-0 *anx1-1 anx2-1*	AT2G41970	pLAT52:MRI[R240C]-CFP BASTA
rbohH-3 rbohJ-3 with MRI-CFP	Col-0 *rbohH-3 rbohJ-3*	AT2G41970	pLAT52:MRI-CFP BASTA
rbohH-3 rbohJ-3 with MRI[R240C]-CFP	Col-0 *rbohH-3 rbohJ-3*	AT2G41970	pLAT52:MRI[R240C]-CFP BASTA
WT with MRI-CFP	Col-0	AT2G41970	pLAT52:MRI-CFP BASTA
WT with MRI[R240C]-CFP	Col-0	AT2G41970	pLAT52:MRI[R240C]-CFP BASTA
mri-1/MRI with MRI-YFP	Col-0 *mri-1/MRI*	AT2G41970	pACA9:MRI-YFP Hygromycin
mri-1/mri-1 with MRI-YFP	Col-0 *mri-1/mri-1*	AT2G41970	pACA9:MRI-YFP Hygromycin
fer-4 with MRI[R240C]-YFP	Col-0 *fer-4*	AT2G41970	pMRI:MRI[R240C]-YFP BASTA
amiRNA ralfl4/19 with AUN1-YFP	Col-0 *amiRNA ralfl4/19*	AT3G05580	pLAT52:AUN1-YFP BASTA
amiRNA ralfl4/19 with AUN1[D94N]-YFP	Col-0 *amiRNA ralfl4/19*	AT3G05580	pLAT52:AUN1[D94N]-YFP BASTA
anx1-1 anx2-1 with AUN1-YFP	Col-0 *anx1-1 anx2-1*	AT3G05580	pLAT52:AUN1-YFP BASTA
anx1-1 anx2-1 with AUN1[D94N]-YFP	Col-0 *anx1-1 anx2-1*	AT3G05580	pLAT52:AUN1[D94N]-YFP BASTA
rbohH-3 rbohJ-3 with AUN1-YFP	Col-0 *rbohH-3 rbohJ-3*	AT3G05580	pLAT52:AUN1-YFP BASTA
rbohH-3 rbohJ-3 with AUN1[D94N]-YFP	Col-0 *rbohH-3 rbohJ-3*	AT3G05580	pLAT52:AUN1[D94N]-YFP BASTA
mri-1/MRI with AUN1-YFP	Col-0 *mri-1/MRI*	AT3G05580	pLAT52:AUN1-YFP BASTA
mri-1/MRI with AUN1[D94N]-YFP	Col-0 *mri-1/MRI*	AT3G05580	pLAT52:AUN1[D94N]-YFP BASTA

Tab. 2 List of transgenic lines used in this study.

Primer	Description	Primer Sequence (5' - 3')
ABD811	AUN1_H127A-R	GATCTTAGCATCTTCAGCGTTTCCTCTCAAGAG
ABD810	AUN1_H127A-F	CTCTTGAGAGGAAACGCTGAAGATGCTAAGATC
ABD779	AUN2-F2	ATACTAAACGTTTCCCCACTTGG
ABD778	AUN1-BPas2	GGGGACCACTTTGTACAAGAAAGCTGGGTTTCAAGACTTCCCCATTTTCGGTA
ABD777	AUN1-BPas1	GGGGACCACTTTGTACAAGAAAGCTGGGTTGCAAGACTTCCCCATTTTCGGTA
ABD776	AUN1-BPs	GGGGACAAGTTTGTACAAAAAAGCAGGCTTAATGATGACGAGTATGGAAGGGAT
ABD763	pMRI-R-SpeI	CACCACCGCAACTAGTCATATCTTCAG
ABD762	pMRI-F-SacI	GAAATAAGAGCTCATTAAATTCAAACGG
ABD747	Ds5-2	TCCGTTCCGTTTTCGTTTTTTAC
ABD744	pDONR-R	GTAACATCAGAGATTTTGAGACAC
ABD743	pDONR-F	TCGCGTTAACGCTAGCATGGATCTC
ABD739	MRI-BPas2	GGGGACCACTTTGTACAAGAAAGCTGGGTATTAGGACGTAGACTCAGGACCGG
ABD738	MRI-BPas1	GGGGACCACTTTGTACAAGAAAGCTGGGTAGGACGTAGACTCAGGACCGG
ABD737	MRI-BPs	GGGGACAAGTTTGTACAAAAAAGCAGGCTTAATGTTTTGTTGCGGTGGTGC
ABD736	820D05-R	CTGCATACTGGTTTGCGGG
ABD735	820D05-F	GTTCTATTCTTCGACCAAATGG
ABD731	AUN2-R1	CTTAGCATCCTCATGGTTCCC
ABD729	AUN1-R1	CTTCTCCATTGCAGTTTGCC
ABD728	AUN1-F1	CGATCTCATTTGCAGAGGCC
ABD727	SUP7-R1	CAAAAGGCTTGGTCTTGTTGG
ABD726	SUP7TaqIF	CCAAACTATGGAGGAGAGTTTGTC
ABD725	SUP19-XhoIR	TGGTAGCCGAATGTTCCCAAAACTC
ABD724	SUP19-F	GCATATGGAGCAGCCAAAGG
ABD688	VGA19-SpeI	GTATATTGTACTAGTCCGGACGTAGACTC
ABD687	VGA19-SalI	GTCGACATGTTTTGTTGCGGTGGTGC
ABD682	GT21229-R1	GGACCGGCCGGTTTAGAGTT

ABD681	GT21229-F1	TTCGGCTACCACGCTCCAGA
ABD614	LBgabi2	GGGCTACACTGAATTGGTAGCTC
ABD604	ANX2-R	TAAGATCATTAGCAGCCACGG
ABD603	ANX2-F	TTTAAGCAATGGATGGTCGAG
ABD600	LBa1	TGGTTCACGTAGTGGGCCATCG

Tab. 3 List of primers and primer sequences.

Donor Vector	Features	Plasmid Selection
pDONR207	contains attP-flanking sites	Gentamicin
pJet1.2	contains BglII-flanking sites	Ampicillin

Tab. 4 List of donor vectors, their features and selection markers.

Destination Vector	Features	Plasmid Selection Bacteria Plasmid Selection Plant
pABD35	pLAT52:GW-CFP, contains attL-flanking sites, 35S promoter from pB7CWG2 replaced with pLAT52	Spectinomycin BASTA
pABD34	pLAT52:GW-YFP, contains attL-flanking sites, 35S promoter from pB7YWG2 replaced with LAT52	Spectinomycin BASTA
pABD4 (ps779)	pACA9:TAP2(YFP), contains *Sal*I and *Spe*I sites	Kanamycin Hygromycin
pABD83	pMRI:GW-YFP, contains attL-flanking sites, pLAT52 promoter from pABD34 has been replaced with pMRI	Spectinomycin BASTA
pABD72	GST-GW-6hist/stop, contains GST and His-Tag for protein purification; contains a Tac promoter for IPTG mediated protein transcription	Carbenicillin

Tab. 5 List of destination vectors, their features and selection markers.

Expression Clone	Features	AGI code	Plasmid Selection Bacteria Plasmid Selection plant
pABD85	pMRI:MRI[R240C]-YFP from pABD83	AT2G41970	Spectinomycin BASTA
pABD49	pLAT52:MRI[R240C]-CFP from pABD35	AT2G41970	Spectinomycin BASTA
pABD47	pLAT52:MRI-CFP from pABD35	AT2G41970	Spectinomycin BASTA
pABD19	pACA9:MRI-YFP from pABD4	AT2G41970	Kanamycin Hygromycin
pCMF10	pLAT52:AUN1[H127A]-YFP from pABD34	AT3G05580	Spectinomycin BASTA
pCMF9	GST- AUN1[H127A]-6hist/stop	AT3G05580	Carbenicillin
pCMF8	GST- AUN1[D94N]-6hist/stop	AT3G05580	Carbenicillin
pCMF7	GST-AUN1-6hist/stop	AT3G05580	Carbenicillin
pCMF5	pLAT52:AUN1[D94N]-YFP from pABD34	AT3G05580	Spectinomycin BASTA
pCMF3	pLAT52:AUN1-YFP from pABD34	AT3G05580	Spectinomycin BASTA

Tab. 6 List of expression clones with features, AGI codes and selection markers.

2.9 SNP ratio mapping approach

In order to identify the *ipr7* and *ipr19* suppressor mutations, a SNP ratio mapping approach was carried out as described by Lindner et al. (2012). *ipr7* and *ipr19* mutants were backcrossed twice to *anx1 anx2* plants. In the backcrossed 1 (BC1) generation, only plants with elongated siliques were selected to be backcrossed to *anx1 anx2* a second time. As a result, the causative SNP will be enriched and segregates in a 1:1 ratio compared to an unlinked SNP, which would segregate in a 1:3 ratio. F1 plants from this second backcross showing elongated siliques were grown and genomic DNA was extracted with a DNeasy Plant Mini kit (Qiagen) and pooled, as described in Boisson-Dernier et al. (2015). With the pair-end Illumina HiSeq2000 platform, the Functional Genomics Center of the University of Zurich sequenced *ipr19/MRI* and *ipr7/AUN1* after preparation of an Illumina-adapted library. With NGM mapper (Sedlazeck et al., 2013), the raw sequencing data were mapped to the TAIR10 reference genome. Duplicate removal (Li et al., 2009) and overlap clipping (Barnett et al., 2011) were executed on unambiguously mapped reads with a mapping quality score greater than 20. The SNPs were then called with Freebayes (Garrison and Marth, 2012) with the lower threshold of three alternative reads per locus. A hidden Markov chain-based algorithm estimated the likelihood of a SNP given the read data on the assumption that the

SNPs were linked within each chromosome. Ensemble Variant Effect Predictor classified the SNPs into introgenic, intergenic, coding (synonymous and non-synonymous amino acid substitutions) and splice-site variants. The causative SNP should have a ratio very close to 0.5, as it segregates in a 1:1 ratio. Unlinked SNPs will have segregation ratios close to 0.25 due to their segregation in a 1:3 ratio. Also, SNPs in the vicinity of the causative SNP should have segregation ratios >0.25 as they cosegregate due to genetic linkage and thus were co-selected for.

2.10 Seed set analysis

8-15 green-yellowish siliques were harvested per plant and fixed in a 3:1 mixture of 96% EtOH : glacial acetic acid. After one day, the siliques were opened with a needle and the seeds per silique were counted.

2.11 *In vitro* pollen germination assays

Pollen germination medium (5mM KCl, 1mM $MgSO_4$, 0.01% H_3BO_3 (w/v), 5mM $CaCl_2$ and 10% Sucrose (w/v), dissolved in ddH_2O and adjusted to pH 7.5) was prepared as previously described (Boavida and McCormick, 2007; Franck et al., 2017). 1.5% low-melting agarose was added to half of the medium and boiled in a microwave until complete dissolution. 450µl of the hot medium were distributed evenly on a glass slide and left to solidify 3 minutes before being transferred to a moisture incubation box.

Freshly open flowers of 10-15cm high, untreated plants were harvested in a moisture incubation box and incubated at 22°C for 30min in order to allow re-hydration of the pollen. Subsequently, the flowers were gently brushed on the center of the glass slides with solidified medium to release pollen. The flowers were subsequently placed around the pollen with the pistil facing inwards in a circular manner. Per slide, pollen from 8-12 flowers was taken.

The slides were then transferred to a moisture incubation box and incubated for 35-45 min at 30°C before being transferred to 22°C for another 3-4 hours. Then, the flowers were gently removed from the slides and 80-100µl of liquid pollen germination medium was spread on top of the germinating pollen before a cover slip was applied. The pollen assays were imaged using a Leica DM5500 fluorescence microscope equipped with differential interference contrast (DIC) optics. Subcellular localisation of *AUN1-YFP* was investigated using the confocal laser-scanning microscope (CLSM) Leica TSC SP8.

Typically, three rounds of independent pollen germination assays were conducted per experiment. 200 pollen grains or more are counted per line per assay. The pollen grains are classified into three groups: bursting pollen grains, pollen grains that form PTs and pollen grains that do not match these two groups. The latter count as non-germinated pollen grains. Commonly, the germination and the bursting rate of each sample are determined. The germination rate is defined as $100\% \times \frac{number\ of\ germinated\ pollen\ grains}{total\ number\ of\ pollen\ grains}$. It determines the percentage of germinated pollen grains and is a measure for the quality of the pollen germination assay. Stress or pesticide treatment deteriorates the pollen quality, which is detrimental for experiments investigating fertilization-related phenotypes. Thus, if WT pollen depicts germination rates lower than 50%, the assays should be repeated with new, fresh

plants. The bursting rate is defined as $100\% \times \frac{number\ of\ burst\ pollen\ grains}{number\ of\ germinated\ pollen\ grains}$. It determines the percentage of burst pollen grains within the germinated pollen grains.

2.12 Calcium imaging in growing pollen tubes

The imaging of Ca^{2+} dynamics in growing PTs was conducted as described in Franck et al. (2017).

2.13 Aniline blue staining of pollinated pistils

WT flower buds with stamen prior to pollen release were emasculated by removing sepals, petals and stamen and allowed to recover for 2 days. Thereafter, nicely grown pistils with elongated papillae were pollinated with WT or mutant pollen, respectively. After 4 hours, the siliques were harvested and fixed in a 9:1 solution of 96% EtOH : glacial acetic acid overnight. The next day, the fixing solution was replaced with 70% EtOH for 5 min, 50% EtOH for 5 min and 30% EtOH for 5 min with occasional mild agitation. Thereafter, the EtOH was removed and replaced by 10% Chloral hydrate solution (in 24ml: 64g chloral hydrate, 16ml ddH$_2$O, 8ml glycerol) at 65°C for 5 min. The chloral hydrate was removed and the pistils were washed with sodium phosphate buffer (in 100ml: 9.3ml of 1M Na$_2$HPO$_4$, 6.8ml of 1M NaH$_2$PO$_4$, dissolved in ddH$_2$O; pH 8.0). Then, 5N NaOH was added and the pistils were incubated at 65°C for 10 min. The NaOH was removed and the samples were washed twice with sodium phosphate buffer. Before microscopy, the pistils were arranged parallel to each other on a glass slide and stained with 0.1% Methyl Blue before a cover slip was applied. The samples were imaged using the Leica DM5500 fluorescence microscope.

2.14 Root hair growth assays

For the solid medium assays, seedlings were grown vertically on half-strength MS plates with microagar for 5 days after germination. Subsequently, the roots were imaged with the stereomicroscope Leica MZ16F to analyse root hair length.

In the liquid growth medium assays, seedlings were grown vertically on half-strength MS plates with microagar for 4 days after germination. Thereafter, they were transferred to glass slides and the roots were covered in 1/10 MS medium. A cover slip was applied on top using 2 layers of parafilm on each end of the glass slide as spacer as to not squash the roots. The seedlings were transferred to an *in situ* hybridization dish covered in liquid 1/10 MS medium so the slides would not dry and allowed to recover vertically for 1.5 days. Thereafter, the root hairs were imaged with the CLSM Leica TCS SPE or the Leica DM5500 fluorescence microscope.

For ruthenium red staining, 4-day old seedlings were allowed to grow for 48h in liquid medium before 1 min treatment with 0.01% Ruthenium red, staining acidic pectins.

In root hair length analysis, only the mature root hairs were counted located 1.5–3.5 mm from the primary root tip.

2.15 Image analysis

Image analysis was conducted with the Leica LAS AF Lite software or the ImageJ/FiJi software (Schindelin et al., 2012, 2015).

2.16 Protein expression and GST-pulldown

2.16.1 Protein expression in *E.coli*

E. coli BL21 RIL cells (Chloramphenicol resistant) were used for protein expression and transformed with pCMF7, pCMF8 and pCMF9 by heat-shock transformation. These vectors contain a Tac promoter that can induce gene transcription by Isopropyl β-D-1-thiogalactopyranoside (IPTG) addition. The IPTG binds the Lac repressor and mediates its release form the *Lac* operon. Colonies of the transformed *RIL* lines were picked and inoculated at 37°C until an OD_{600} of 0.6-0.8 is reached with 100ml of Terrific Broth medium (For 1l medium: 12g Tryptone, 24g Yeast Extract, 4ml Glycerol, 900ml ddH2O. The medium is autoclaved and subsequently, 100ml phosphate buffer at pH 7.5 is added. The medium is then filter-sterilized.) A control sample (1ml) before induction was taken, immediately centrifuged at 4'000rpm for 15min at 4°C and then processed as described in chapter 2.16.2. Subsequently, the samples were induced with 0.2mM IPTG for 4-6 h. Thereafter, another 1ml of each sample was harvested as previously described for the control sample and processed as described in chapter 2.16.2. The remaining sample volume was then harvested at 4'000rpm for 15 min at 4°C and stored at -20°C for protein purification.

2.16.2 Protein detection

For verifying that the proteins were expressed, protein samples were resuspended in 100µl ddH$_2$O and 100µl 2x loading dye (50mM Tris/HCl (pH 6.8); 2% SDS; 10% Glycerol; 0.1% Bromophenol Blue; 100mM DTT) at 95°C for 10min. Thereafter, the proteins were separated on acrylamide gels. For the separation gel (5ml, 10%), 1.9ml ddH2O, 1.7 ml Rotiphorese Gel 30 (37,5 : 1, Roth), 1.3ml Tris (1.5M, pH 8.8), 0.05ml SDS (10%), 0.05ml Ammonium Persulphate (10%), and 2 µl Tetramethylethylenediamine were used. The stacking gel (1ml) was composed of 0.68ml ddH2O, 0.17ml Rotiphorese Gel 30 (37,5:1, Roth), 0.13ml Tris (1.5 M, pH 6.8), 0.01ml SDS (10%), 0.01ml Ammonium Persulphate (10%), and 1 µl Tetramethylethylenediamine. The PageRuler^{TM} Prestained Protein Ladder (Thermo Scientific) was used as marker. 20mA per gel were applied for 1h.
To visualize the proteins, the gels were stained with Coomassie (80mg Coomassie Brilliant Blue G250 and 1 l ddH$_2$O, agitated for 2 h. 3ml concentrated HCl were added subsequently). The protein gels were first boiled in H$_2$O for 1 min. This step was repeated three times. Subsequently, the gel was boiled in Coomassie for 1,5 min. The protein gel was destained by boiling it in H$_2$O for 1 min and repeating this last step as many times as required.

2.16.3 Protein purification by GST-pulldown

All steps were performed at 4°C. The pellets of the 100ml cultures were resuspended in 10ml binding buffer (50mM Tris (pH 7.5), 150mM NaCl, 1mM DTT) with an EDTA-free Protease Inhibitor Cocktail (1 tablet/50ml; Roche) and 1% TritonX-100. Thereafter, 100µg/ml lysozyme was freshly added to the samples and they were incubated on ice for 20-40 min. In each following step, namely the lysis, the washing and elution steps, 10-100µl of the respective supernatants were saved and mixed with an equal amount of 2x loading dye, whereafter they were boiled at 95°C for 10 min for protein detection, as previously described.

For lysis, the samples were sonicated twice at 60% for 1 min (Sonopuls, Bandolin) and centrifuged at 3'220 rpm for 15 min. The lysates were then added to 100µl equilibrated GSH-beads and incubated for 30 min under constant rotation. The samples were then centrifuged at 3'220rpm for 1 min, the supernatant was decanted and replaced with 15ml binding buffer and the equilibrated beads were resuspended. This washing step was repeated thrice whereafter the samples were centrifuged one more time. The supernatant was decanted after taking a sample for protein detection. Elution of the GST-tagged proteins was performed with 100ml elution buffer (50mM Tris (pH7.5), 150mM NaCl, 1mM DTT, 40mM reduced Glutathione). The samples were incubated for 15 min and subsequently centrifuged at 500g for 3 min. The supernatant was saved and 10µl were separated for protein detection. These elution steps were repeated thrice. Additionally, 50µl of the GSH-beads fraction was saved. The beads were resuspended in an equal amount of 2x loading dye and ddH$_2$O and boiled at 95°C for 10 min. The boiled protein samples were then processed as previously described in chapter 1.16.2.

3. RESULTS

3.1 MARIS, a positive component of pollen tube and root hair growth

3.1.1 MRI is expressed in both pollen and root hairs

At the time I joined the MRI project, part of the experiments had been conducted already. Thus, in the following pages, I will highlight my contributions to the characterization of MRI in context of the complete experimental approach.

After identifying MRI as the gene targeted by the *ipr19* mutation, we were interested in the expression potential of MRI (Fig. 7). Therefore, we constructed a phylogenetic tree of *Arabidopsis* RLCK-VIII proteins (see figure description for details). We then combined this phylogenetic tree with relative gene-expression data of these RLCK-VIII proteins according to the Genevestigator microarray database. The underlying expression data was based on RNA-seq (Loraine et al., 2013) or Affymetrix *Arabidopsis* ATH1 arrays (Honys and Twell, 2004; Becker et al., 2013) for *Cr*RLK1L related pathways in tip-growing cells. We also analysed the protein sequence of the *Arabidopsis* RLCK-VIII proteins and discovered that the R240 is part of a very conserved STR motif in all RLCK-VIII proteins (Fig. 8).

To our surprise, apart from showing strong expression in pollen, *MRI* also depicted expression in root tissue. This was very intriguing, as in the root, there are tip-growing unicellular systems very similar to PTs, namely the root hairs (RHs).
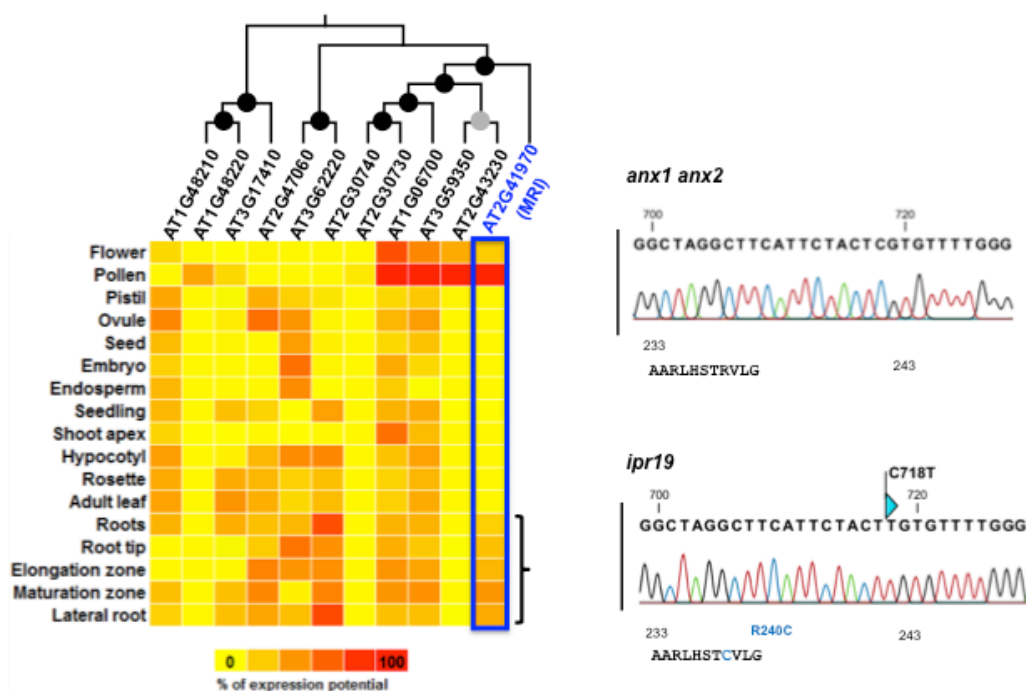
Fig. 7 Phylogenetic tree of the *Arabidopsis* RLCK-VIII family with relative expression levels and representation of the *ipr19* mutation. **Left:** Phylogenetic tree of the *Arabidopsis* RLCK-VIII family combined with relative gene-expression data. Multiple alignments of *Arabidopsis thaliana* RLCK-VIII proteins were made in ClustalW2.0 and with MEGA6, the phylogenetic tree was reconstructed under usage of the protein sequence parsimony method (Bootstrap test, 1'000 replicates) (Boisson-Dernier et al., 2015). The black and grey circles indicate bootstrap values of more than 900 and between 800 and 900, respectively. Thereafter, the tree was combined with the relative gene expression data of *Arabidopsis* RLCK-VIII family members in various plant tissues according to the Genevestigator microarray database with the Meta-Profile Analysis tool Anatomy Profile (Hruz et al., 2008). Blue color highlights *MRI*. **Right:** Representation of the *ipr19* mutation and the resulting R240C amino acid substitution. Shown are spectra from the Sanger sequencing reactions of the *AT2G41970* cDNA

amplified from *anx1 anx2* (*Upper*) or *ipr19* (*Lower*) flowers. Adapted from Boisson-Dernier et al. (2015).

Fig. 8 The conserved STR motifs of *Arabidopsis* RLCK-VIII protein sequences. Multiple alignment done with ClustalW2.0. Adapted from Boisson-Dernier et al. (2015).

3.1.1.1 Root hair growth is similar to pollen tube growth

RHs exist in order to maximize the root surface and thus the interaction possibilities with the soil and microorganisms within the soil. It is thought that their function is the facilitation of water and nutrient uptake, as well as anchoring the plant firmly in the ground. RH growth rates typically account to 1μm/min or more (Ketelaar et al., 2003; Grierson et al., 2014). Such high growth rates require strict growth regulations.

Just as in PTs, the CWI has to be closely coordinated with the internal growth machineries. Steady RH growth, like PT growth, requires a tip-focussed Ca^{2+} gradient (Wymer et al., 1997, Bibikova et al., 1997, Felle and Hepler et al., 1997). If this gradient is disrupted, e.g. by chemical treatment with verapamil, a putative Ca^{2+} channel blocker, RH growth is stalled (Wymer et al., 1997). Foreman et al. (2003) discovered that a tip-focussed ROS gradient is also important for RH growth. Disruption of this gradient compromises the Ca^{2+} gradient and leads to problems in RH elongation. Furthermore, pH maintenance must be tightly regulated, as extra- and intracellular pH changes were shown to interrupt RH growth (Bibikova et al., 1998). For a long time, there was no evidence that a pH gradient is required for RH growth, unlike for PT growth (Herrmann and Felle, 1995; Parton et al., 1997; Bibikova et al., 1998). However, Monshausen et al. (2007) could demonstrate that RH growth is tightly associated with oscillatory pH changes at the surface in the RH apex region. Also, their results point towards a close collaboration between pH regulation of the RH tip apoplastic region and ROS production.

3.1.1.2 The CWI pathway in root hairs

Arabidopsis thaliana RHs depict a similar CWI system as PTs. A *Cr*RLK1L-family member called FERONIA (FER), after an Etruscan deity of fertility, governs the RH CWI pathway (Fig. 9). *FER* is the closest homologue of the pollen- expressed *ANX1/2* and fittingly also the wife of Anxur in Etruscan mythology. In contrast to ANX1/2, FER is ubiquitously expressed in the plant and has a plethora of functions in cell morphology, fertilization, pathogen attack, hormone signaling, and abiotic stress responses (Franck et al., 2017). Knock-out mutants of *FER*, among other phenotypes, are unable to form intact RHs (Duan et al., 2010). Instead, *fer* RHs burst after forming little bulges, similarly to *anx1 anx2* pollen.
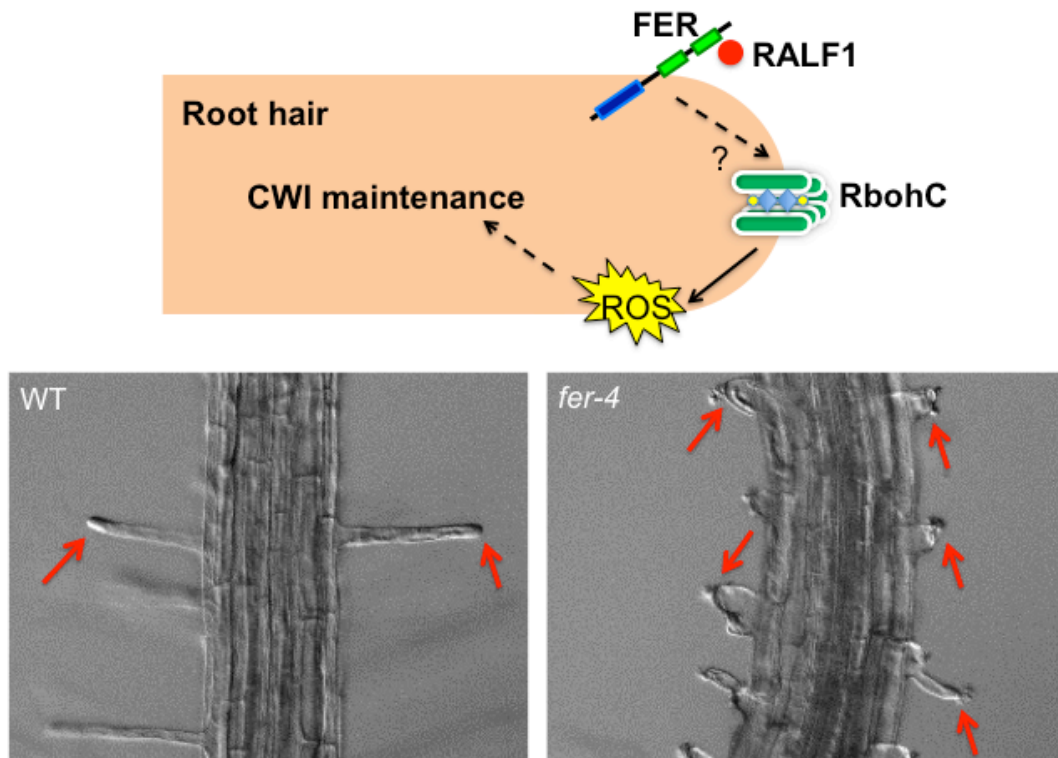
Fig. 9 The role of FER in RH growth. **Top:** Schematic representation of the RH CWI pathway governed by *Cr*RLK1L FER and its ligand RALF1. FER putatively triggers activation of ROS-producing NADPH oxidase RbohC that positively regulates CWI maintenance. **Bottom:** Roots of WT and *fer-4* seedlings. While the WT RHs are intact, *fer-4* root hairs are burst, indicated by red arrows.

FER has a ligand called Rapid Alkalinization Factor 1 (RALF1) that binds to the FER ectodomain (Haruta et al., 2014). Upon RALF1 treatment, root and hypocotyl elongation is inhibited in WT seedlings (Bergonci et al., 2014; do Canto et al., 2014). *fer* roots are insensitive to RALF1 treatment (Haruta et al., 2014). It was proposed that RALF1 acts as a regulator of cell elongation by binding to FER, which in turn activates signaling that leads to the phosphorylation of proton pump AHA2. Consequently, AHA2 would be less active, the extracellular matrix would increase in pH and root elongation would be inhibited.

Interestingly, just as in the ANX-dependent CWI pathway, a NADPH oxidase is thought to act downstream of FER, namely RbohC/Root Hair Defective 2 (RHD2), a close homologue of RbohH/J in PTs (Foreman et al., 2003). *rhd2* mutants have very short RHs that lack the tip-focussed Ca^{2+} and ROS gradients required for RH growth. Thus, at close examination, *rhd2* mutant RHs appear short and stunted because they eventually burst, just like *fer* RHs.

The finding, that MRI is expressed in both RHs and PTs is very intriguing, as the CWI pathways are so similar in these two cell types. Thus, we figured that MRI putatively could play a role in both the PT and the RH CWI pathway. If so, this would be the first time a common CWI regulator would be discovered for PTs and RHs.

With this information, we started with the phenotypic characterization of *ipr19* by first investigating the seed set and PT growth behavior and ultimately also examining the RHs.

3.1.2 Phenotypic characterization of *ipr19*

As we discovered *ipr19* due to elongated siliques in the M1 generation compared to the male sterile *anx1-2 anx2-2* plants, I compared the seed set of the original suppressor mutant *anx1-2 anx2-2 ipr19/MRI* to wild type (WT) and *anx1-2 anx2-2* plants. This experiment

should reveal the extent of seed set rescue. Henceforth, *anx1-2 anx2-2 ipr19/MRI* plants will be referred to as *ipr19*, unless stated differently. Also, the term "WT" corresponds to "WT-Columbia 0", unless differently specified. The error bars always correspond to the standard deviation, unless differently specified. While WT plants exhibit an average of 48.7 seeds per silique, *anx1-2 anx2-2* plants depict 0.8 seeds per silique (Fig. 10a). In contrast, *ipr19* shows a strong seed set rescue of 43.5 seeds per silique on average. This indicates that *ipr19* can rescue the *anx1-2 anx2-2* male sterility *in vivo*. A bigger seed set hints that a larger number of ovules are successfully fertilized. This might originate from a reduction in *anx1-2 anx2-2* precocious pollen bursting, allowing for PT growth.
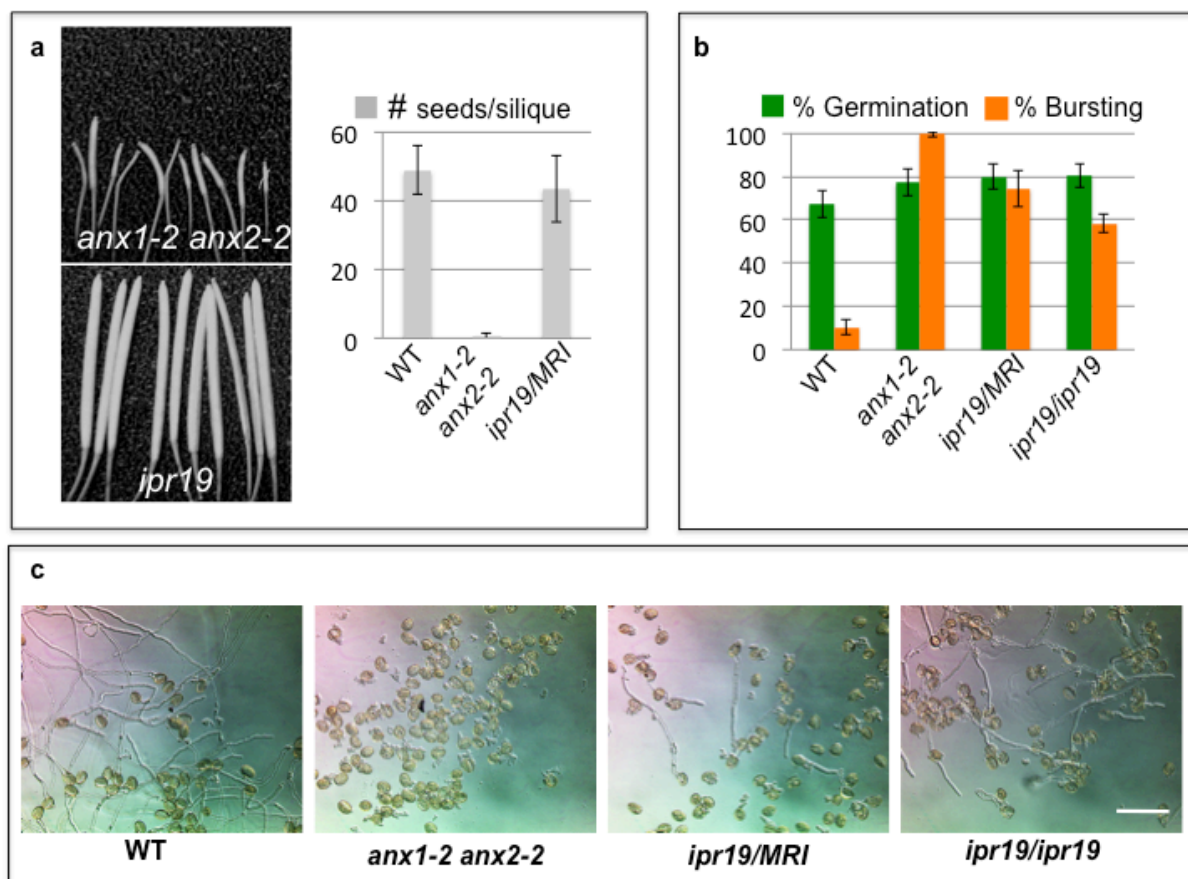
Fig. 10 The *ipr19* mutation rescues the *anx1 anx2* male sterility. **a:** Seed set rescue of *ipr19* plants compared to WT and *anx1-anx2*. The number of siliques investigated per line is>10. **b:** Germination and bursting rate of *ipr19/MRI* and *ipr19/ipr19* pollen from three independent pollen germination assays. WT and *anx1 anx2* are used as controls. **c:** Representative images of the pollen germination assay. Note, how compared to *anx1 anx2* pollen, the *ipr19/MRI* and *ipr19/ipr19* pollen are able to form PTs. Adapted from Boisson-Dernier et al. (2015). Scale bar: 100µm.

To test this, we conducted 3 independent *in vitro* pollen germination assays to investigate the PT growth behavior of *ipr19* and homozygous *ipr19* plants compared to WT and *anx1-2 anx2-2* plants. WT pollen germinated on average at 67.2% with a bursting rate of 10.4% (Fig. 10b and 10c). In comparison, *anx1-2 anx2-2* pollen depicts a germination rate of 79.9% with a bursting rate of 99.4%. *ipr19* pollen had a germination rate of 79.9% and burst on average at 74.3%. Homozygous *ipr19* showed a germination rate of 80.2% with a bursting rate of 58.4%. These results show that both *ipr19* and homozygous *ipr19* pollen depict a strongly reduced pollen bursting rate compared to *anx1-2 anx2-2* pollen. The increased seed set size of *ipr19* is due to a reduction in *anx1-2 anx2-2* precocious pollen bursting, allowing for the formation of more PTs that consequently fertilize more ovules. Also, this confirmed that the *ipr19* really is a suppressor mutant of *anx1-2 anx2-2*.

Next, as we previously had discovered that MRI shows expression in root tissue, I examined the RHs of 4-days old WT, *fer-4* and *ipr19* seedlings, vertically grown on microagar plates under a binocular. WT RHs reached an average length of 251.7µm while *fer-4* RHs were 92µm long (Fig. 11). Interestingly, *ipr19* RHs had an average length of only 46.7µm, which is even shorter than in *fer-4* mutants. This indicates that, like *fer-4* plants, *ipr19* plants are clearly impaired in RH growth.
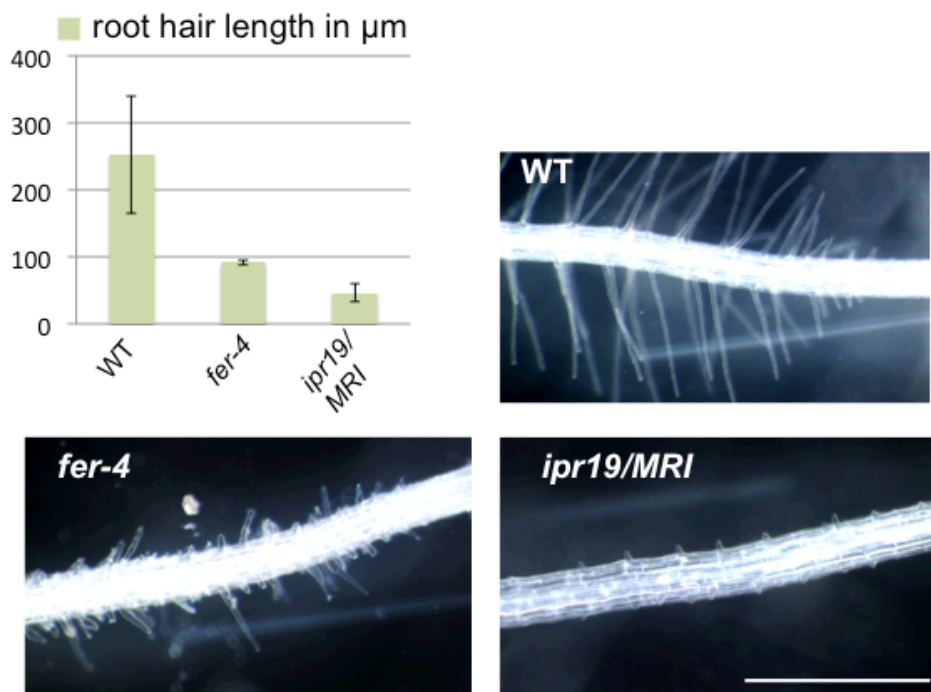
Fig. 11 Root hair phenotyping of the *ipr19* mutant. Root hair length of 4-day old WT, *fer-4* and *ipr19/MRI* seedlings. The number of root hairs investigated is >130 per line from >9 individual seedlings each. Adapted from Boisson-Dernier et al. (2015). Scale bar: 2mm.

However, this experiment did not show whether the short *ipr19* RHs were burst like *fer-4* RHs or intact like WT RHs. To test this, we grew WT, *fer-4* and *ipr19* seedlings vertically on microagar until 4 days after seed germination. Then, we transferred them to glass slides covered in liquid 1/10 MS medium and allowed them to recover for 1.5 days (see Materials and Methods). Thereafter, we imaged the RHs under a confocal microscope.

Interestingly, we found that *ipr19* roots only form little RH bulges instead of elongating RHs. However, the RH bulges clearly were intact and not burst like *fer-4* RHs (Fig. 12). This was very intriguing, as the RH bulges reminded us of growth-impaired *ANX1/2* over-expressing PTs with wide tips from CW material over-accumulations. Using ruthenium red for staining pectins, I could show that indeed, the growth- arrested RH bulges in *ipr19* originate from pectinuous over-accumulations of CW material at the RH tip. Likely, the balance between exo- and endocytosis had been shifted towards exocytosis in these RHs, as known from ANX1/2 over-expressing PTs (Boisson-Dernier et al., 2013). Consequently, normal RH growth is impossible and the RHs remain stunted.

This was a very interesting finding as it confirms that indeed, the *ipr19* mutation is able to rescue *anx1-2 anx2-2* pollen bursting while at the same time it strongly inhibits RH growth. Thus, MRI might have a function in both the PT and the RH CWI pathway. The CW material over-accumulations in the *ipr19* RH bulges indicate that the CWI maintenance pathway in RHs is over-activated. This allows for further investigation regarding the type of suppressor

mutation *ipr19* constitutes. However, first, it was key to confirm whether the *ipr19* mutation really corresponds to *MRI[R240C]* as predicted by the SNP-ratio mapping.
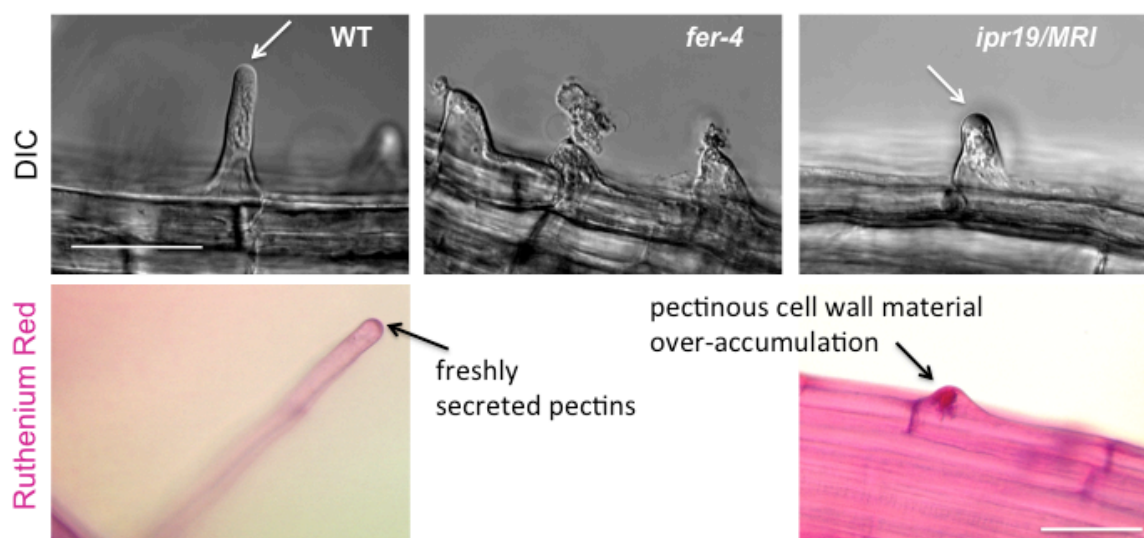
Fig. 12 *ipr19* mutant RHs show pectinuous CW material over-accumulations. **Top:** RH imaging of WT, *fer-4* and *ipr19/MRI* root hairs with DIC. White arrows point towards a normal RH tip in WT and a RH tip with CW material over-accumulations in an *ipr19/MRI* seedling, respectively. Scale bar: 20µm. **Bottom:** Ruthenium red staining reveals freshly secreted pectins at the tip of a WT RH and a CW material over-accumulation at the tip of an *ipr19/MRI* RH (black arrows) in 4-day old seedlings. Adapted from Boisson-Dernier et al. (2015). Scale bar: 100µm.

3.1.3 *MRI[R240C]* is the *ipr19* mutation

To assess this, we cloned *MRI* and *MRI[R240C]* without stop-codon into *p*ACA9:GW-YFP and *p*LAT52:GW-CFP constructs. Both LAT52 and ACA9 promoters drive expression in pollen (Twell et al., 1989; Schiøtt et al., 2004). Subsequently, *anx1-1/anx1-1 anx2-1/ANX2* plants were transformed with *p*LAT52:MRI-CFP and *p*LAT52:MRI[R240C]-CFP by floral dipping. Transformants were pre-selected by growing the seeds on ½ MS plates with the herbicide BASTA and were subsequently screened for fluorescence in pollen grains in the T1 generation. A strong CFP-signal indicates strong expression in pollen.

We chose *anx1-1* homozygous *anx2-1* heterozygous plants because *anx1-1 anx2-1* double homozygous plants are male sterile and produce very few seeds. Consequently, it would be strenuous to transform with this line. In contrast, *anx1-1/anx1-1 anx2-1/ANX2* plants exhibit a WT-like seed set. I selected the T1 generation for fluorescence in pollen grains since this would indicate that the respective constructs are expressed and additionally, I genotyped for *anx2-1/ANX2* plants. I chose three lines with good fluorescence for MRI-CFP and MRI[R240C]-CFP, respectively. In the T2 generation, I genotyped 32, 22 and 29 plants, respectively, of the 3 MRI-CFP transformed lines for ANX2. Out of 88 genotyped MRI-CFP transformed plants, 50 were *ANX2/ANX2* and 33 *anx2-1/ANX2*. No *anx2-1* homozygous plant could be obtained. In contrast, when I genotyped 31, 27 and 30 plants of the 3 MRI[R240C]-CFP transformed lines for ANX2, respectively, I obtained 32 *ANX2/ANX2*, 44 *anx2-1/ANX2* and 12 *anx2-1/anx2-1* plants. This indicates that MRI[R240C]-CFP, but not MRI-CFP, might be able to rescue the *anx1-1 anx2-1* pollen bursting phenotype.

I next investigated the seed set of 11 of the 12 *anx1-1 anx2-1 MRI[R240C]-CFP* triple homozygous plants. If MRI[R240C] indeed was the *ipr19* causative mutation, I would see a seed set rescue in these lines. In all 10 lines, the seed set values ranged between 11.4 and 17.4 seeds per silique, compared to less than one seed per silique in *anx1-2 anx2-2* plants

(Fig. 13). This indicates that all $MRI^{[R240C]}$-CFP lines homozygous for *anx1-1 anx2-1* exhibit an elevated seed set compared to non-transformed *anx1-2 anx2-2* plants. Thus, MRI$^{[R240C]}$ is capable of rescuing the *anx1-1 anx2-1* sterility *in vivo*, albeit to a lower extent than the original *ipr19* mutant.

In a pollen germination assay, we further investigated the PT growth behavior of 3 representative lines of the 11 *anx1-1 anx2-1* $MRI^{[R240C]}$-CFP lines compared to untransformed *anx1-1 anx2-1* pollen (Fig. 13). We wanted to know whether the elevated seed set in these lines originates from the ability to produce PTs. We could show that *anx1-1 anx2-1* $MRI^{[R240C]}$ pollen is capable of producing PTs, unlike precociously bursting *anx1-1 anx2-1* pollen. Thus, the observed seed set rescue apparently originates from a higher number of pollen producing PTs in the $MRI^{[R240C]}$-CFP transformed *anx1-1 anx2-1* lines.

In summary, these results indicate that $MRI^{[R240C]}$ really is the *ipr19* causative mutation and that *MRI* acts downstream of *ANX1/2* in the PT CWI maintenance pathway.
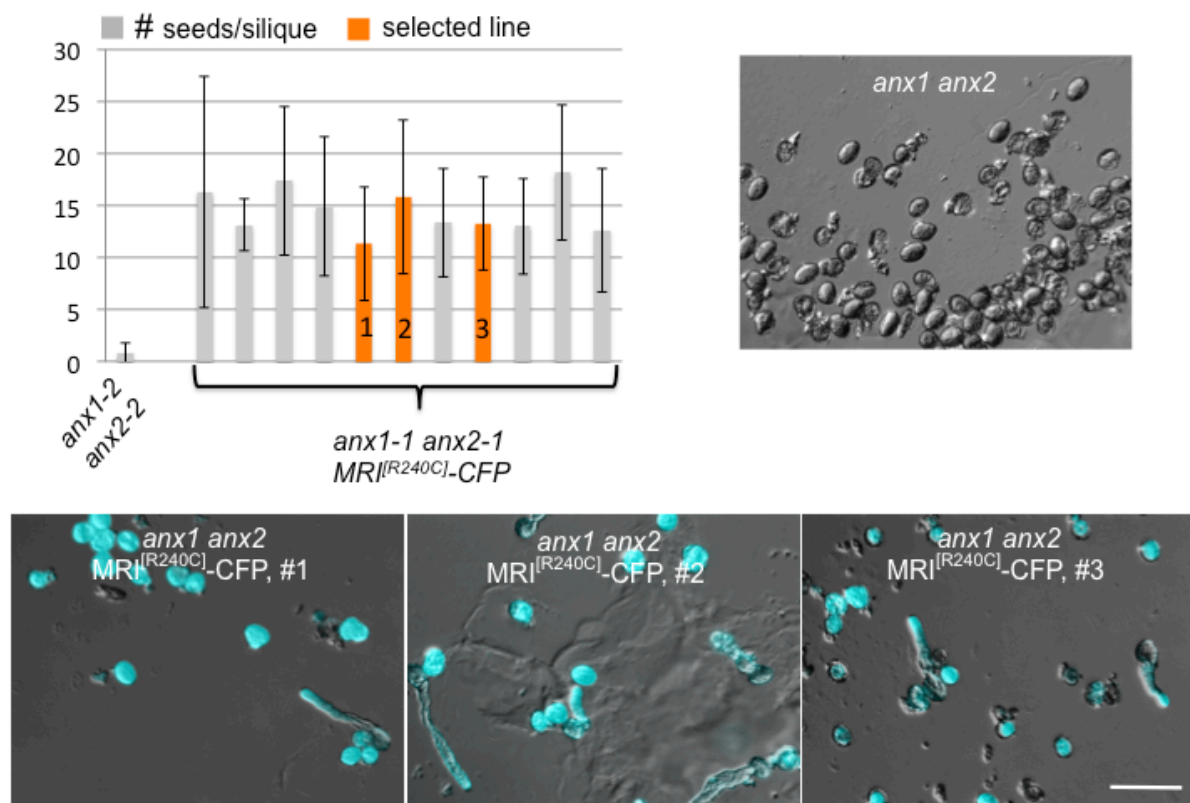
Fig. 13 $MRI^{[R240C]}$ is the *ipr19* mutation. **Top left:** Seed set analysis of 10-12 siliques per triple homozygous *anx1-1 anx2-1* $MRI^{[R240C]}$ plant and *anx1-2 anx2-2* control plant. The lines selected for pollen germination assays are marked in orange. **Top right:** Representative image of *anx1 anx2* pollen as control in a pollen germination assay. **Bottom:** One representative image per orange *anx1-1 anx2-1* $MRI^{[R240C]}$ line in pollen germination assays. Note, how PTs can be found in these lines compared to 100% bursting in *anx1 anx2* pollen germination assays. Adapted from Boisson-Dernier et al. (2015). Scale bar: 80µm.

3.1.4 MRI acts downstream of FER in root hair growth

As previously described, *ipr19* plants not only depicted elongated siliques compared to *anx1-1 anx2-1* plants but also showed stunted RHs with CW material over-accumulations at the tip. After we demonstrated that $MRI^{[R240C]}$-CFP can partially rescue the *anx1-1 anx2-1* pollen bursting and that MRI is downstream of *ANX1/2*, we were interested if $MRI^{[R240C]}$ could also rescue the RH bursting in *fer-4* plants. To test this, we cloned the promoter of MRI (*p*MRI)

and exchanged it with the *LAT52* promoter of the *p*LAT52:MRI[R240C]-YFP construct. This was necessary as LAT52 is a pollen-specific promoter and does not drive expression in RHs. We then transformed *fer-4* plants with the *p*MRI:MRI[R240C]-YFP construct and screened for transformants in the T1 generation by pre-selecting on antibiotic plates with BASTA and subsequently checking for fluorescence in RHs. In most of these lines, we could observe elongated, intact RHs. Compared to the short, burst RHs of *fer-4* control plants, most of the *fer-4* seedlings transformed with MRI[R240C]-YFP exhibited partial rescue of RH bursting (Fig. 14). This was further confirmed in the T3 generation in homozygous MRI[R240C]-YFP transformed *fer-4* lines (Fig. 15). It indicates that MRI acts downstream of both ANX1/2 and FER and that MRI[R240C] is capable of partially rescuing the *fer-4* bursting RH phenotype. Also, it shows that the *MRI* promoter is sufficient to drive expression in RHs, confirming the microarray data shown previously (Fig. 7).
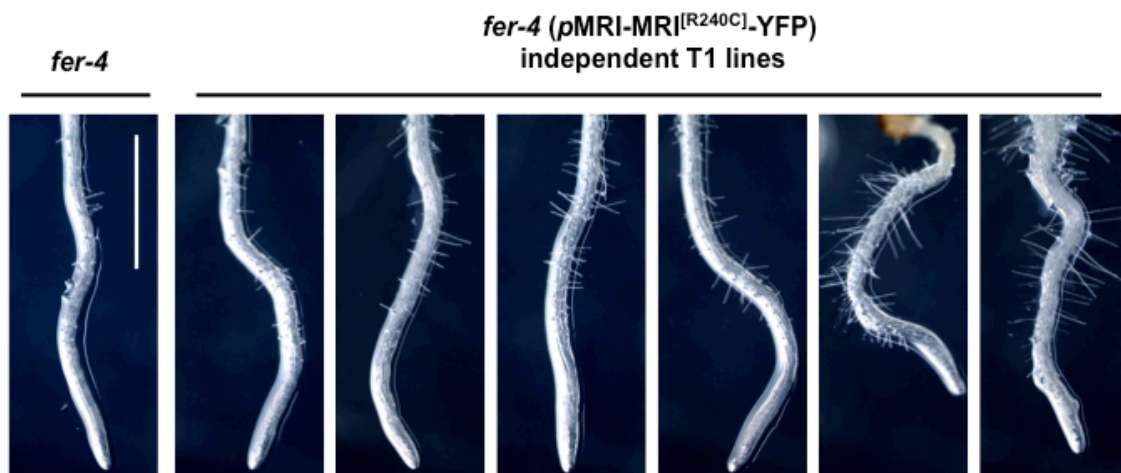
Fig. 14 MRI[R240C]-YFP can rescue *fer-4* RH bursting (T1 generation). Representative images of roots of *fer-4* seedlings and roots of *fer-4* T1 lines transformed with MRI[R240C]-CFP. The extent of RH bursting rescue increases from left to right. Adapted from Boisson-Dernier et al., (2015). Scale bar: 1mm.
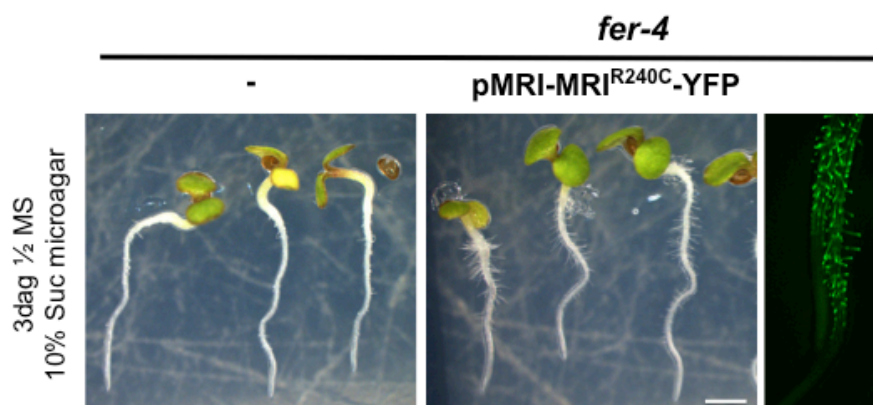
Fig. 15 MRI[R240C]-YFP can rescue *fer-4* RH bursting (T3 generation). Representative images of untransformed *fer-4* seedlings and *fer-4 MRI[R240C]-YFP* seedlings. YFP-expression in RHs of MRI[R240C] transformed seedlings. Scale bar: 1mm.

3.1.5 MRI is a positive regulator of both root hair and pollen tube growth

We next wanted to know if MRI is a positive or a negative regulator of the ANX1/2 and FER-dependent CWI maintenance pathways. Until now, MRI could still have either of the two functions. To elucidate this, we planned on using knock-out mutants for *MRI* and screen them for PT growth behavior and RH growth phenotypes.
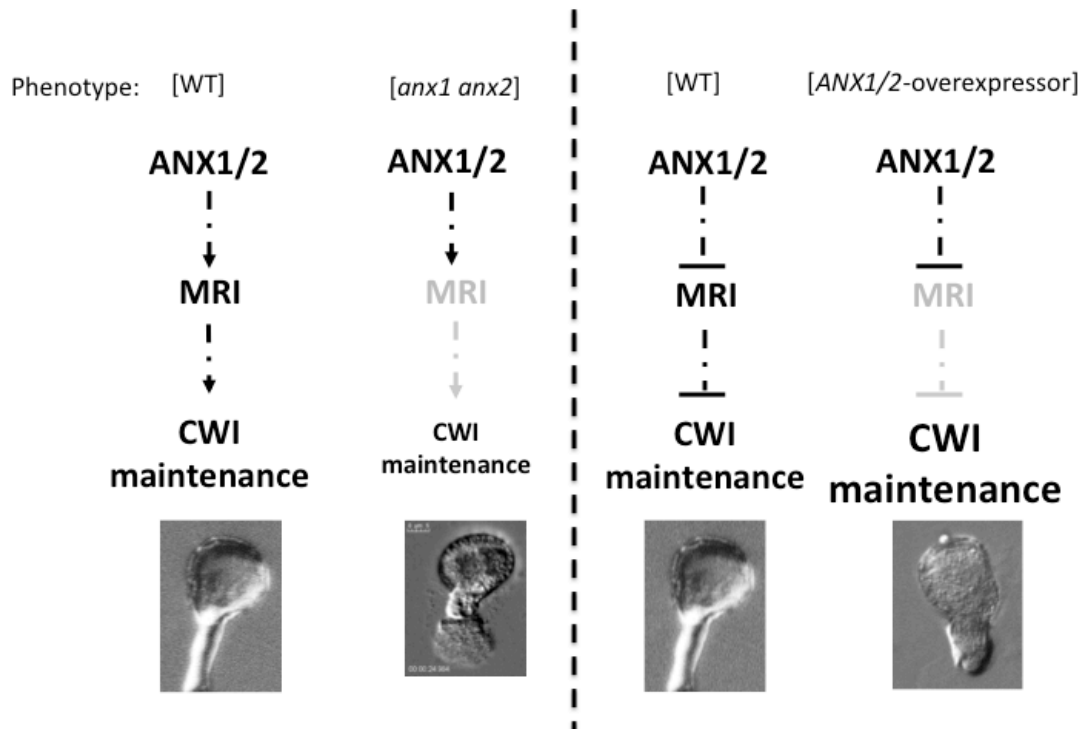
Fig. 16 Schematic representation of the expected outcomes of knocking-out *MRI* if MRI was a positive or negative regulator.

As we saw, ANX1/2 and FER act upstream of MRI. Assuming that MRI is a positive regulator of the respective pathways, ANX1/2 or FER would positively regulate MRI, which in turn would activate the CWI maintenance machinery in order to sustain tip-growth (Fig. 16). Consequently, if MRI is disrupted, it could no longer activate the CWI maintenance machinery and as a result, the tip-growing cell would burst. However, if MRI was a negative regulator of the ANX1/2 and FER-dependent CWI pathways, ANX1/2 or FER would inhibit MRI, which would inhibit CWI maintenance. If now MRI was disrupted, the CWI maintenance machinery would no longer be inhibited and thus be over-activated. Consequently, PTs and RHs should be inhibited in growth, possibly depicting pectinuous CW material over-accumulations.

To investigate which scenario corresponds to reality, two lines with a disrupted *MRI* gene were acquired, knock-out line *mri-1* and knock-down line *mri-2* (Boisson-Dernier et al., 2015) (Fig. 17a). While *mri-1,* alias CSHL_GT21229, is ecotype Landsberg *erecta (*L*er)* and disrupted by a *Ds* transposon, *mri-2* (GABI_820D05) is a T-DNA insertional line from ecotype Columbia-0 (Col-0). We were capable of retrieving homozygous *mri-2* plants but could not isolate homozygous *mri-1* plants albeit 235 F1 plants of *mri-1/MRI* were genotyped for *MRI*.

3.1.5.1 *mri-1/MRI* and *mri-2* plants have a reduced seed set size

First, we checked the seed set size of WT, *mri-1/MRI* and *mri-2* plants. While WT plants exhibited an average seed set of 53.5 seeds per silique, *mri-1/MRI* siliques contained 38.5 seeds on average and in *mri-2* siliques, 31.5 seeds were found (Fig. 17b). This indicates that in both lines with *MRI* disruption, the seed production is mildly decreased. To confirm that this was due to an exclusively pollen-derived defect, we next conducted transmission efficiency analysis.
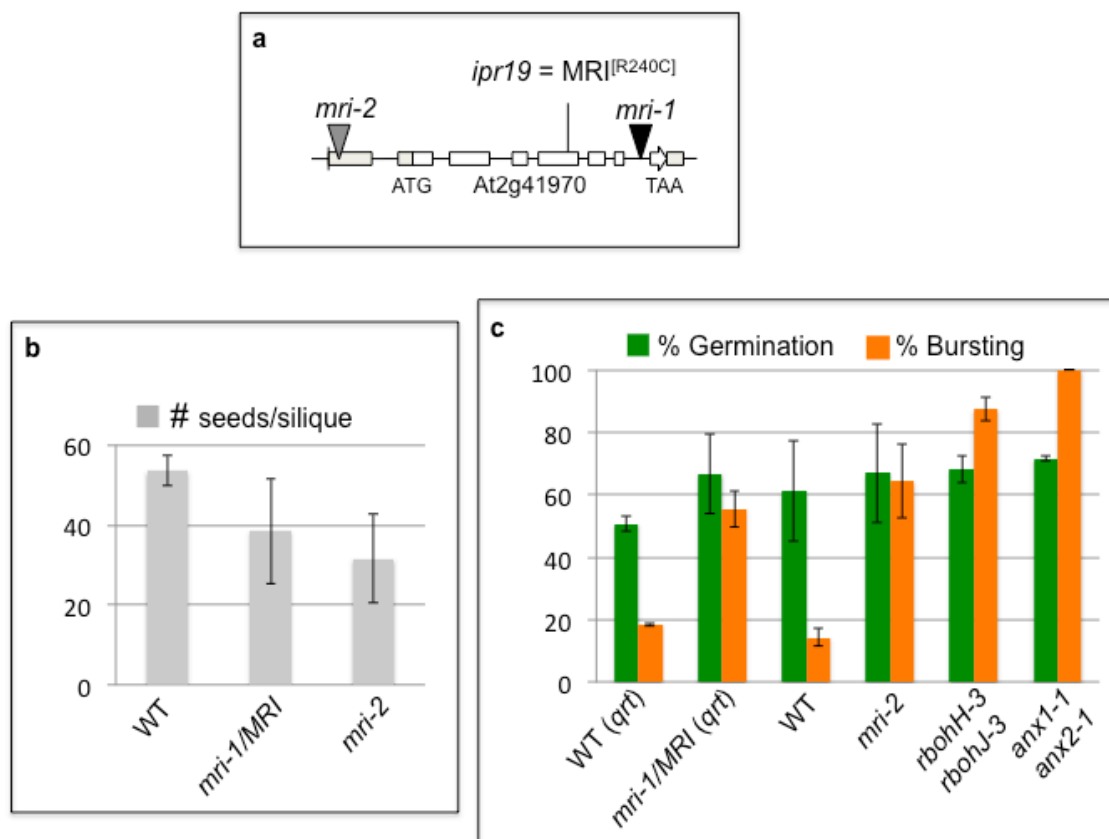
Fig. 17 *MRI* disruption causes pollen bursting. **a:** Representation of the *AT2G41970* locus with introns, exons, and positions of the mutant. Adapted from Boisson-Dernier et al. (2015). **b:** Seed sets of WT, *mri-1* and *mri-2* plants. Data originates from 13 siliques per line. **c:** Germination and bursting rate of WT (*qrt*), *mri-1/MRI (qrt),* WT, *mri-2*, *rbohH-3 rbohJ-3* and *anx1-1 anx2-1* pollen. Data originates from 3 independent pollen germination assays.

3.1.5.2 The seed set reduction in *mri-1/MRI* and *mri-2* originates from an exclusively male defect

Therefore, we backcrossed a *mri-1/MRI* line that was outcrossed 4 times with Col-0 to WT and conducted transmission efficiency analysis on the F1 generation. The transmission efficiency of an allele is defined as $\frac{number\ of\ progeny\ carrying\ the\ desired\ allele}{number\ of\ progeny\ that\ does\ not\ carry\ the\ desired\ allele} \times 100\%$. In our case, *mri-1* is the desired allele. Normally, half of the F1 progeny carries the desired allele and thus, the transmission efficiency will be 100%. However, if *mri-1* confers a reproductive defect on the pollen side, the transmission efficiency will be less than 100% if *mri-1/MRI* is used as pollen donor. If *mri-1* additionally confers a reproductive defect on the female side, the transmission efficiency will also be reduced if *mri-1/MRI* is used as pollen recipient.

When I used *mri-1/MRI* as female recipient and pollinated with WT pollen, out of 181 genotyped F1 plants, 92 were *MRI/MRI* and 89 *mri-1/MRI.* Thus, the transmission efficiency accounted to 96.7%. However, when *mri-1/MRI* pollen was used on WT stigmas, not a single plant out of 1'005 F1 plants carried the BASTA resistance of the *mri-1* allele. Thus, the transmission efficiency was 0%. We then conducted the same experiment for *mri-2/MRI* plants. When *mri-2/MRI* stigmas were pollinated by WT pollen, 50 plants of the resulting F1 generation had the genotype *MRI/MRI* and 46 were *mri-2/MRI.* Thus, the transmission efficiency was 92%. When the roles were reversed and *mri-2/MRI* was used as pollen donor for WT stigmas, 152 F1 plants were *MRI/MRI* and 82 plants *mri-2/MRI*, resulting in a transmission efficiency of 53.9%. Thus, whenever *mri/MRI* was used as female recipient, the transmission efficiency shows that *mri* is normally transmitted. However, when *mri/MRI* pollen is used, the transmission efficiency drastically decreases to ~50% for *mri-2/MRI* or even 0% for *mri-1/MRI*. Thus, the observed seed set reduction in *mri-2* and *mri-1/MRI* truly originates from an exclusively pollen derived defect. Also, the transmission efficiency of 0% is the explanation for the observed absence of homozygous *mri-1* plants in the *mri-1/MRI* progeny. Ultimately, this indicates that *mri-1* is a stronger allele than *mri-2.*

3.1.5.3 Disruption of *MRI* triggers pollen bursting

To investigate the nature of this pollen-derived defect in *mri-2* and *mri-1/MRI* plants, we conducted *in vitro* pollen germination assays to investigate PT growth behavior. As *mri-1/MRI* originally is ecotype L*er* and L*er* pollen is known to be difficult to cultivate *in vitro*, we outcrossed the original *mri-1/MRI* line from L*er* as female recipient four times with a Col-0 WT line with a *quartet* (*qrt*) background as pollen donor. The outer wall of the four meiotic products of *qrt* pollen is fused and thus, the individual grains do not separate but are released in a tetrad (Preuss et al., 1994). This facilitates analysis of *in vitro* pollen germination assays in the case of *mri-1/MRI* plants, as we expect 2 pollen grains to behave WT-like and 2 pollen grains to have a mutant phenotype per tetrad.

We conducted 3 independent pollen germination assays on *mri-1/MRI (qrt),* WT-Col0 (*qrt*), *mri-2/mri-2*, WT, *anx1-2 anx2-2* and *rbohH-3 rbohJ-3* plants. WT-Col0 (*qrt*) pollen had a germination rate of 50.8% and a bursting rate of 18.5% (Fig. 17c and 18). In comparison, *mri-1/MRI (qrt)* pollen germinated at 66.8% and burst at 55.5%. WT pollen depicted a germination rate of 61.1% and a bursting rate of 14.4% and *mri-2* pollen showed germination and bursting rates of 66.9% and 64.3%, respectively. The bursting controls *anx1-2 anx2-2* and *rbohH-3 rbohJ-3* had germination rates of 71.6% and 68.1% with bursting rates of 100.0% and 87.4%, respectively.

These results show that *mri-1/MRI* and *mri-2* depict a similar pollen bursting phenotype as *anx1-2 anx2-2* and *rbohH-3 rbohJ-3* plants, albeit to a lower extent. This indicates that the reduced seed set in *mri-1/MRI* and *mri-2* originates from precocious bursting of PTs that consequently fail to fertilize the ovules. Also, this points towards MRI being a positive component in the PT CWI maintenance pathway as its disruption triggers the same phenotype as the disruption of *ANX1/2*.
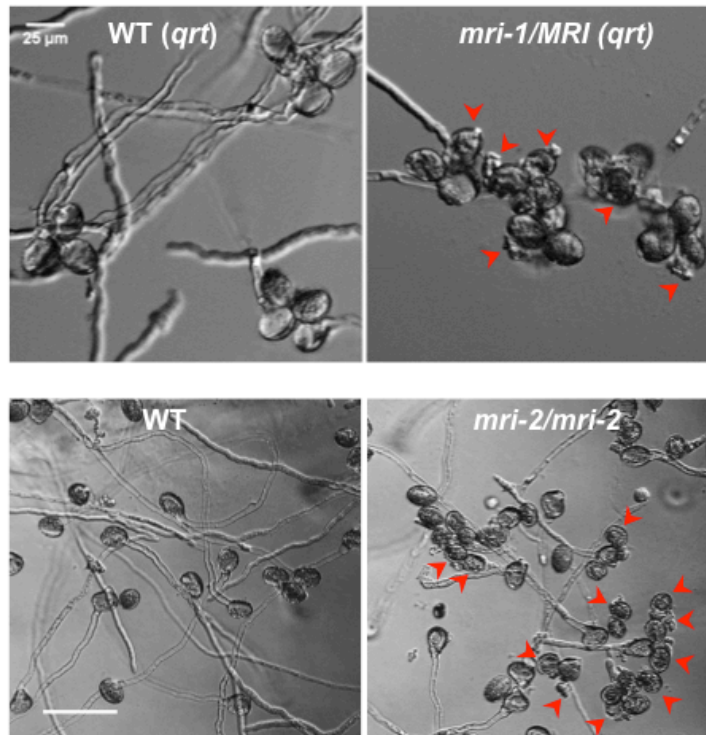
Fig. 18 Representative images of *in vitro* pollen germination assays of WT (*qrt*), *mri-1/MRI* (*qrt*), WT and *mri-2* pollen. Red arrowheads indicate bursting pollen grains, discharging their cytoplasm into the pollen germination medium. Adapted from Boisson-Dernier et al. (2015). Scale bar: 25µm.

To confirm that the observed pollen bursting phenotype really originates from the disruption of *MRI*, I assessed whether we could complement the *mri-1/MRI* phenotype. Therefore, I transformed *mri-1/MRI* plants with *p*ACA9:MRI-YFP. In the T1 generation, I selected 4 independent transgenic lines with good fluorescence in pollen and conducted pollen germination assays on them. I compared the germination and bursting rates of these 4 lines to the bursting rate of *mri-1/MRI* (Fig. 19a). They had germination rates between 61.3% and 70.4% and their pollen bursting rates ranged between 30.0% and 38.7%, which was significantly lower than the bursting rate of *mri-1/MRI* pollen ($P < 0.001$ for all lines, Student's *t* test). Furthermore, we were able to identify 29 homozygous *mri-1/mri-1* individuals out of 90 genotyped plants in the subsequent generation, indicating that MRI-YFP is functional. This was very convenient as we wanted to have a second homozygous *mri* allele for further experiments in RHs.

By using FM4-64 staining to visualize the plasma membrane, we could further confirm that the YFP-signal in growing *mri-1/MRI* PTs transformed with *p*ACA9:MRI-YFP uniformly localizes to the plasma membrane (Fig. 19b).

Thus, I could show that the MRI-YFP construct is functional and that the disruption of *MRI* really is responsible for the observed pollen bursting phenotype. Also, this demonstrated that MRI is anchored to the PT plasma membrane.
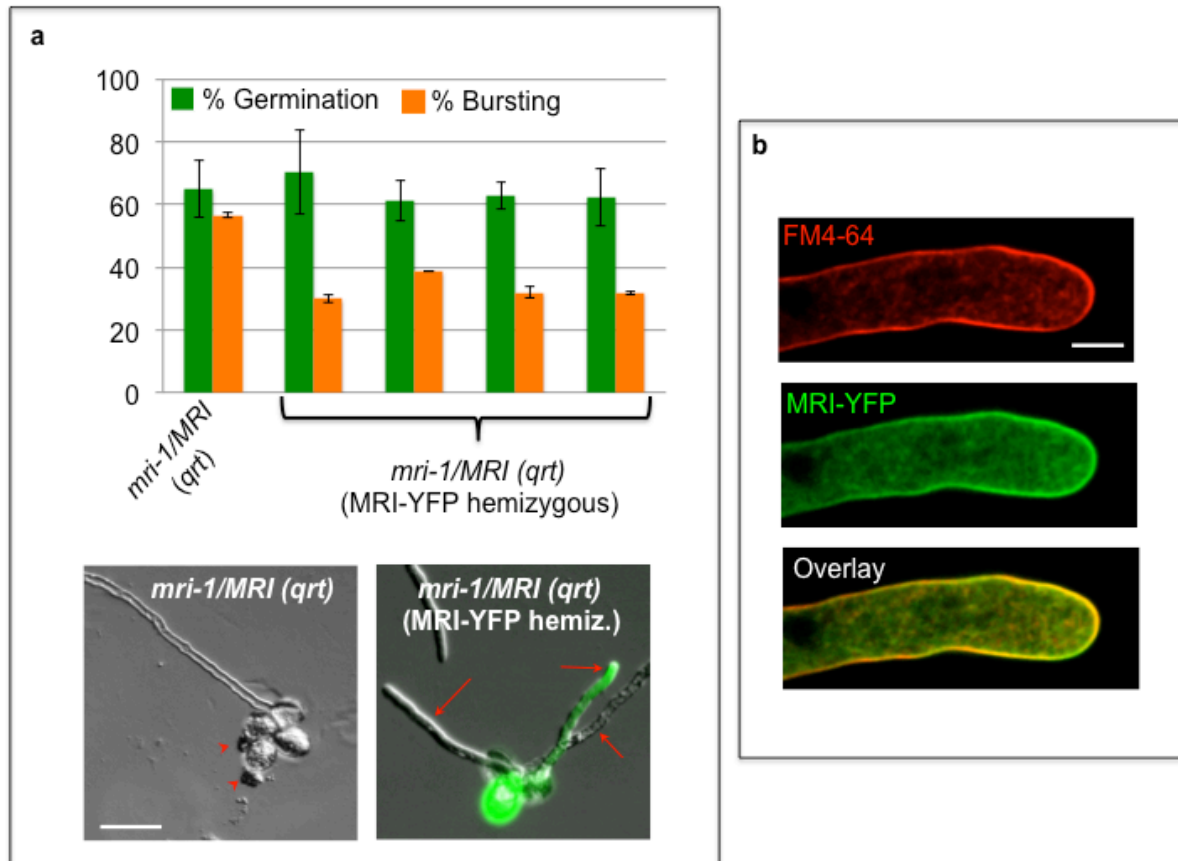
Fig. 19 *MRI-YFP* complements *mri-1/MRI* pollen bursting and reveals MRI localization. **a: (Top)** Germination and bursting rates of 4 independent *mri-1/MRI* T1 lines transformed with MRI-YFP (2 technical replicates each line) and untransformed *mri-1/MRI* pollen (3 technical replicates). 55-87 tetrads were counted per line. **(Bottom)** Representative images of an *mri-1/MRI* quartet and an *MRI-YFP* hemizygous *mri-1/MRI* quartet. Red arrowheads indicate bursting pollen grains while red arrows indicate PTs. Scale bar: 50µm. **b:** FM4-64 staining of the PT plasma membrane reveals that MRI-YFP is localized uniformly at the latter. Adapted from Boisson-Dernier et al. (2015). Scale bar: 5µm.

3.1.5.4 Disruption of *MRI* triggers root hair bursting

Since *MRI* disruption triggers pollen bursting, we were interested whether it has a similar effect on RH growth. Therefore, we could make use of the *p*ACA9:MRI-YFP complemented *mri-1/MRI* lines from the *mri-1* pollen bursting complementation experiment. As *p*ACA9 drives expression in pollen, it would complement the pollen bursting phenotype of *mri-1/MRI* plants without being expressed in RHs. We chose one of the four *p*ACA9:MRI-YFP complemented *mri-1/MRI* T1 lines. As the *mri-1* allele confers kanamycin resistance, it could easily be selected for on selection plates. Out of 69 kanamycin-resistant T2 plants, genotyping revealed that 43 plants were *mri-1/MRI* and 26 were *mri-1/mri-1*. This suits the expected 2:1 ratio for *mri-1/MRI* : *mri-1/mri-1* plants. We chose three independent T2 lines homozygous for *mri-1* and MRI-YFP to be further investigated. First, I conducted RH length measurements of 5-day old *mri-1 (p*ACA9:MRI-YFP)*, mri-2, fer-1 (*L*er), fer-4* (Col-0), WT (L*er*) and WT seedlings vertically grown on ½ MS plates with microagar.

I found that WT seedlings reached an average RH length of 0.23mm while *fer-4* RHs only became 0.06mm long (Fig. 20). *mri-2* seedlings arrived at 0.09mm average RH length. WT (L*er*) seedlings depicted RHs of 0.21mm length and *fer-1* RHs were on average 0.07mm long. I pooled the RH data for the three *mri-1 MRI-YFP* double homozygous lines and obtained an average RH length of 0.15mm. These results show that both *mri-1* and *mri-2* plants have significantly shorter RHs than WT/ WT (L*er*) plants. Compared to *fer-4* RHs, *mri-*

2 RHs are almost as short, compared to *fer-1* RHs, *mri-1* RHs appear to be longer. Interestingly, while *mri-1* appears to be the stronger allele, its RH length impairment appears to be milder than that of *mri-2*. This was surprising, and thus we checked the expression potential of the *ACA9* promoter. We detected that unfortunately, the pollen-preferential promoter also drives weak expression in RHs. Thus, we screened the *mri-1 MRI-YFP* lines for fluorescence in RHs, which would indicate that MRI-YFP is expressed there. However, we could not detect fluorescence in the RHs of any of these lines. Thus, it might be possible that MRI-YFP is expressed in RHs to very low, undetectable levels, which potentially is sufficient to partially complement the *mri-1* RH phenotype.
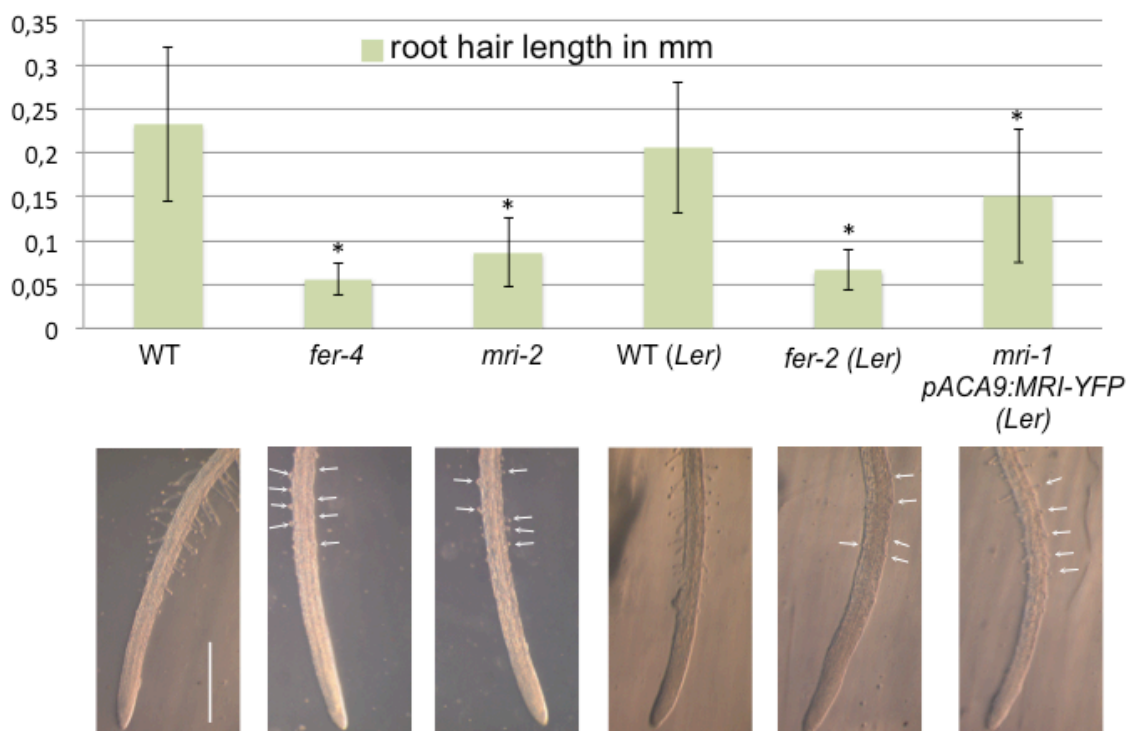
Fig. 20 *mri* mutants have shorter RHs. RH length measurements of 4-day old WT (n=160 from 29 individuals), *fer-4* (n=84 from 19 individuals), *mri-2* (n=133 from 28 individuals), WT (L*er*) (n=101 from 18 individuals), *fer-1* (n=104 from 24 individuals) and *mri-1 MRI-YFP* (n=149 from 29 individuals) seedlings. The RH data was pooled for the three *mri-1 MRI-YFP* double homozygous lines. White arrows indicate shorter RHs. Asterisks denote significant differences compared to the appropriate control (P<0.001, two-tailed unpaired Student's *t* test). Adapted from Boisson-Dernier et al. (2015).

In order to test our hypothesis that the *ACA9* promoter also drives expression in RHs, we transformed *mri-1/MRI* plants with *p*LAT52:MRI-YFP and retrieved homozygous *mri-1* plants in the T2 generation. In the T3 generation, we then monitored RH growth in double homozygous *mri-1 MRI-YFP* plants compared to *mri-2, fer-4* and WT plants (Fig. 20). As can be seen, the *mri-1 MRI-YFP* seedlings phenocopy *mri-2* roots. The MRI-YFP construct indeed only complements the pollen phenotype of *mri-1* mutants and not the RH phenotype, indicating that the milder RH phenotype of *p*ACA9:MRI[R240C]-YFP complemented *mri-1* plants indeed originates from undetectable expression of the *ACA9* promoter in RHs.

To test whether the short RHs of *mri-2* are intact or burst, I conducted a liquid medium RH assay (Fig. 21). With DIC mircroscopy, we found that *mri-2* RHs are short because they are burst just as *fer-4* RHs.

Taken together, these results indicate that MRI is a positive component of both the ANX1/2-dependent CWI pathway in pollen and the FER-dependent CWI pathway in RHs, as the disruption of MRI causes integrity loss in both PTs and RHs.
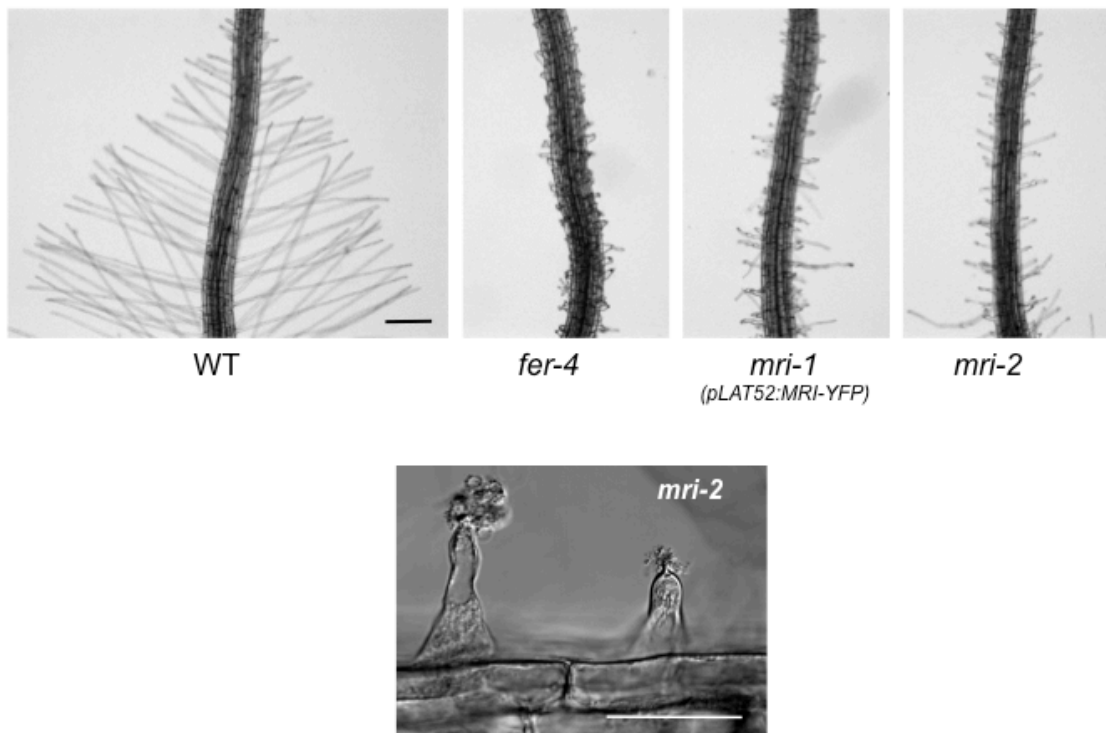
Fig. 21 *mri* mutant RHs are shorter due to precocious bursting. **Top:** Representative images of WT, *fer-4, mri-1 MRI-YFP* and *mri-2* roots. Scale bar: 200µm. **Bottom:** Bursting *mri-2* RHs. Adapted from Boisson-Dernier et al. (2015). Scale bar: 20µm.

3.1.5.5 Over-expression of MRI and MRI[R240C] has a growth inhibitory effect

If MRI is a positive regulator of CWI maintenance, then MRI[R240C] might be a dominant positive form of MRI since it is able to restore PT growth in the absence of ANX1/2 and normal RH growth in the absence of FER.

To confirm that MRI really is a positive regulator of the CWI maintenance pathway and to test whether MRI[R240C] is a dominant positive MRI form in pollen, we decided to transform WT plants with *p*LAT52:MRI-CFP and *p*LAT52:MRI[R240C]-CFP. If MRI was a positive regulator, over-expression should trigger a slight over-activation of the CWI pathway. As a result, PTs would be inhibited in growth. In this case, *MRI[R240C]* expression in addition to native MRI should trigger a stronger over-activation of the CWI pathway with similar results for PT growth.

In the T1 generation, we selected three lines hemizygous for *MRI-CFP* and three lines hemizygous for *MRI[R240C]-CFP*, respectively, by fluorescence in pollen grains. Then, we chose one representative line each and conducted 2 independent *in vitro* pollen germination assays. We were interested in the ratio between fluorescent and non-fluorescent PTs in these lines, as in case of CWI maintenance pathway over-activation, the ratio between fluorescent and non-fluorescent PTs should differ from the expected 1:1. There should be more non-fluorescent PTs than fluorescent ones, as the fluorescent pollen grains would be inhibited in growth so strongly that they would not even germinate.

For WT transformed with *MRI-CFP*, we investigated 452 pollen grains that formed PTs and found 156 fluorescent PTs and 296 non-fluorescent ones. This significantly diverges from the expected 1:1 ratio (P = 0.0022, two-tailed Fisher's exact test, n = 330). Even more strikingly, when we checked fluorescence in WT PTs transformed with *MRI[R240C]-CFP*, we found that only 2 out of 320 PTs were fluorescent, which was even more strongly divergent from the expected 1:1 ratio (P < 0.0001, two-tailed Fisher's exact test, n = 240). These two

PTs had a bulge-like appearance: they were very short with a wide tip, reminding of CW material over-accumulations in *ANX1/2* over-expressing PTs or *ipr19* RHs (Fig. 22). In the CFP-channel, we could detect that the plasma membrane was invaginated in these PTs. This indicates that expression of *MRI[R240C]-CFP* in a WT background has a strong growth inhibitory effect on pollen. Thus, additional expression of both *MRI-CFP* and *MRI[R240C]-CFP* in presence of native MRI over-activates the CWI pathway in PTs, resulting in lower germination of transformed pollen grains. Also, *MRI[R240C]-CFP* is obviously a dominant positive form of MRI since its growth inhibitory effect is even stronger than that of *MRI-CFP*. In summary, these results demonstrate that MRI indeed is a positive regulator of the CWI maintenance pathway in pollen.
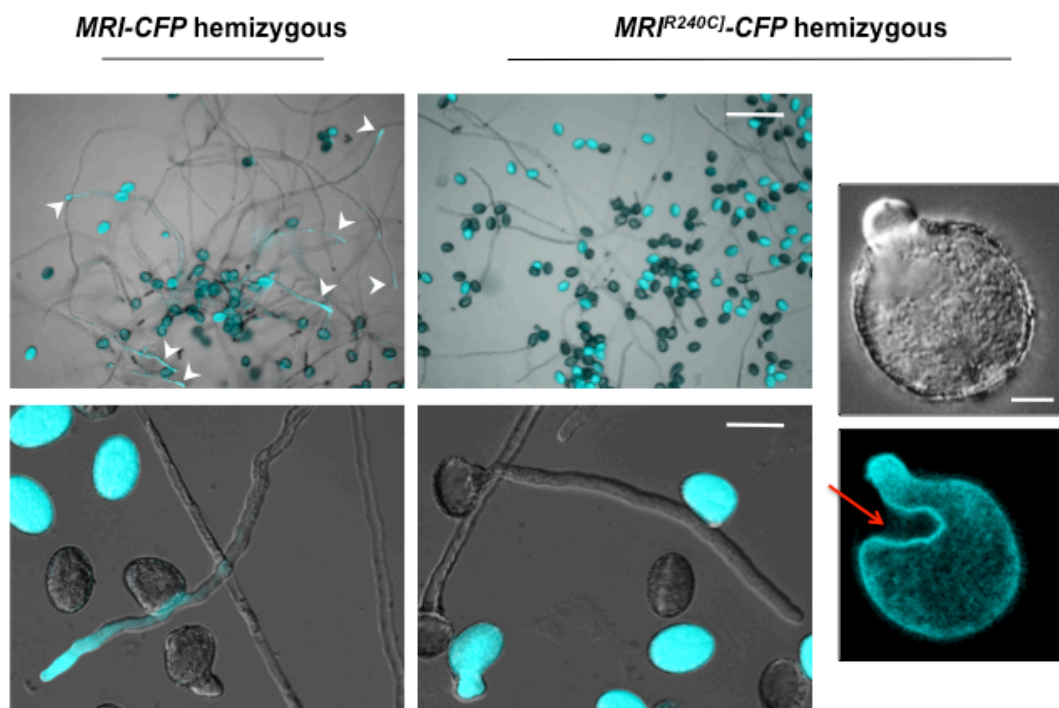
Fig. 22 *MRI[R240C]-CFP* expression in WT background over-activates the CWI pathway in pollen. Representative images of WT pollen hemizygous for MRI-CFP and WT pollen hemizygous for MRI[R240C]-CFP. White arrowheads point towards fluorescent PTs. The red arrow points out a plasma membrane invagination. Adapted from Boisson-Dernier et al. (2015). Scales bars: (Left top) 100µm, (Left bottom) 30µm. (Right top) 5µm.

3.1.6 MRI acts downstream of RbohH/J in pollen tubes

Since we could previously show that MRI acts downstream of ANX1/2 in PTs, we were now interested if this was also true for RbohH/J. To test this, we transformed *rbohH-3 rbohJ-3* plants with *p*LAT52:MRI-CFP and *p*LAT52:MRI[R240C]-CFP and screened for fluorescence in pollen grains and silique elongation in the T1 as *rbohH-3 rbohJ-3* plants are partially male sterile. None of the 32 CFP-fluorescent *rbohH-3 rbohJ-3* plants transformed with MRI-CFP exhibited elongated siliques. I selected three lines with good fluorescence and analysed the seed set compared to untransformed *rbohH-3 rbohJ-3* plants. While *rbohH-3 rbohJ-3* mutants exhibited 7.2 seeds per silique, the seed set of the three transformant lines was 8.5, 8.8 and 9.4, respectively. In contrast, out of 32 MRI[R240C]-CFP transformed *rbohH-3 rbohJ-3* plants, all depicted elongated siliques. I selected three representative lines and analysed the seed set. These lines reached values of 30.3, 23.0 and 28.6 seeds per silique, respectively.

Thus, it appeared that MRI[R240C]-CFP, but not MRI-CFP, could rescue the seed set of *rbohH-3 rbohJ-3* plants *in vivo*.
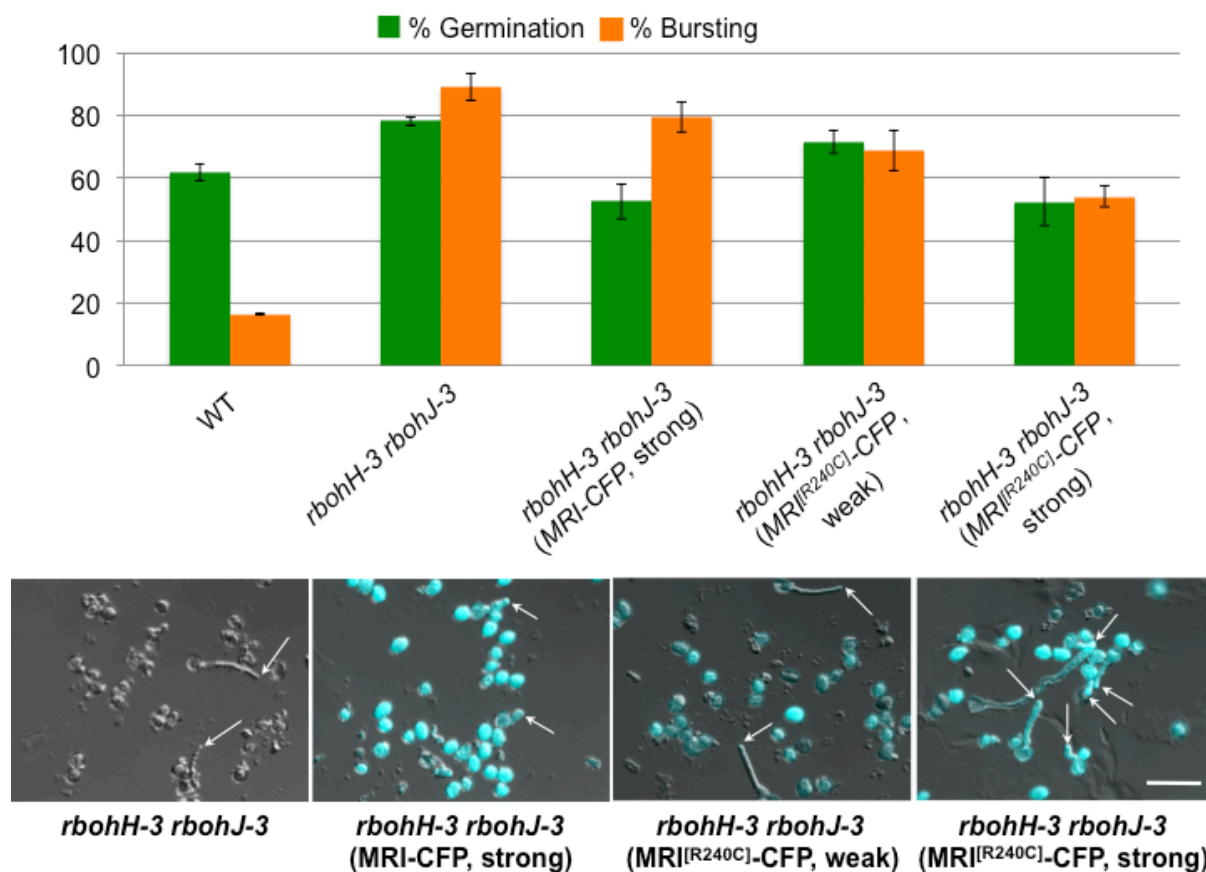
Fig. 23 MRI acts downstream of RbohH/J in PT growth. Germination and bursting rates of WT (2 technical replicates), *rbohH-3 rbohJ-3* (2 technical replicates)*, rbohH-3 rbohJ-3* strongly expressing MRI-CFP (3 technical replicates), *rbohH-3 rbohJ-3* weakly expressing MRI[R240C]-CFP (2 technical replicates) and *rbohH-3 rbohJ-3* strongly expressing MRI[R240C]-CFP (5 technical replicates). Corresponding representative images below with white arrows indicating PTs. Adapted from Boisson-Dernier et al. (2015). Scale bar: 80µm.

To assess whether this was due to a reduction in precocious pollen bursting, I conducted pollen germination assays on WT, *rbohH-3 rbohJ-3*, a strong and a weak MRI[R240C]-CFP expression line and a strong MRI-CFP expression line in the T2 generation. The three selected MRI[R240C]-CFP/MRI-CFP transformed lines were homozygous for their respective construct. The strong and the weak MRI[R240C]-CFP expressing lines had seed sets of 25.6 and 32.2, respectively, while the strongly MRI-CFP expressing line exhibited 4.6 seeds per silique. All seed set data described is derived from >11 siliques. In a pollen germination assay, WT pollen germinated at 61.7% and burst at 16.5% (Fig. 23). *rbohH-3 rbohJ-3* pollen had a germination rate of 78.1% and a bursting rate of 89.1%. The strong MRI-CFP expression line accounted to 52.6% of germination and 79.6% of bursting. Moreover, the weak MRI[R240C]-CFP suppressor line showed 71.6% of germination with a bursting rate of 68.6%. The strong MRI[R240C]-CFP suppressor had a germination rate of 52.4% and a bursting rate of 53.9%.

These results indicate that MRI[R240C]-CFP, but not MRI-CFP, is capable of rescuing the *rbohH-3 rbohJ-3* pollen bursting phenotype. The stronger the expression of the MRI[R240C]-CFP, the lower the pollen bursting rate and the higher the seed set. Also, this indicates that MRI acts downstream of ANX1/2 and RbohH/J in PT CWI maintenance.

3.1.7 Summary

In summary, we could show that MRI is a positive component of CWI maintenance pathway in both PTs and RHs. Disruption of *MRI* triggers bursting in these cell types. MRI is a receptor-like cytoplasmic kinase that localizes uniformly to the PT plasma membrane. It acts downstream of ANX1/2 and RbohH/J in PTs and downstream of FER in RHs (Fig. 24). Also, MRI[R240C] is a dominant, over-active form of MRI that is capable of rescuing *anx1 anx2* and *rbohH-3 rbohJ-3* male sterility as well as *fer* RH bursting. *MRI*[R240C] expression in WT background triggers a strong inhibition of tip-growth, resulting in CW material over-accumulations and plasma membrane invaginations.
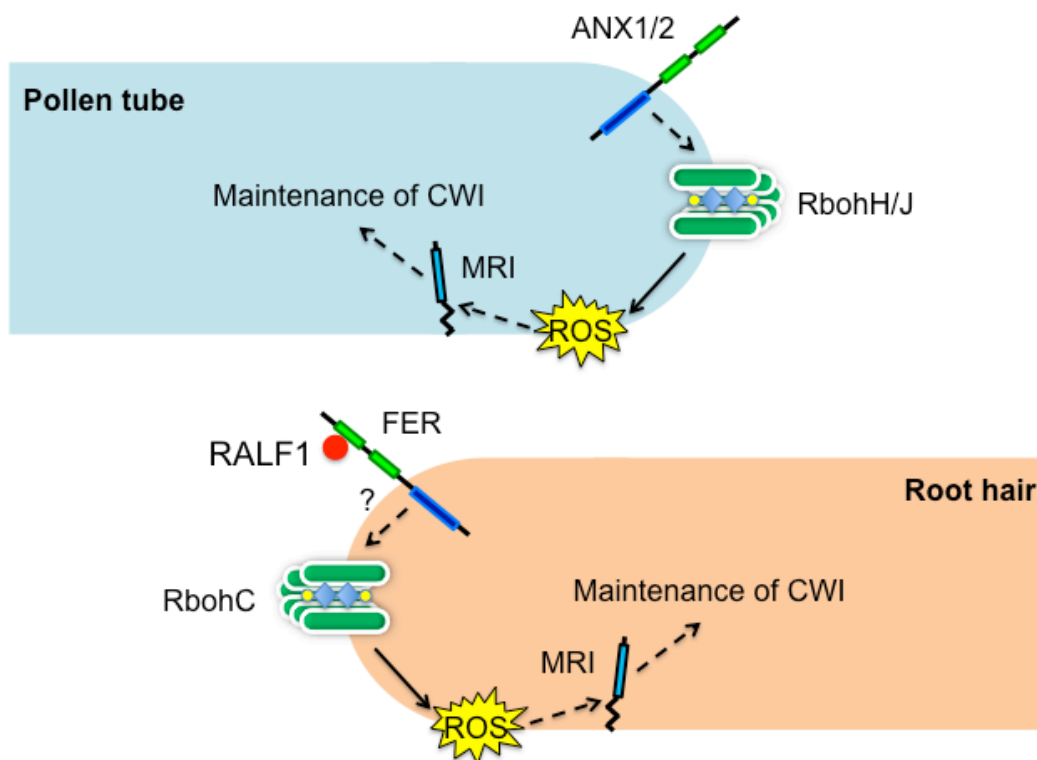
Fig. 24 Schematic representation of the role of MRI in PT and RH growth.

3.2 ATUNIS1/2, negative components of pollen tube and root hair growth

After learning that the *ipr*7 mutation was situated in *AUN1*, we were interested in the expression potential of the gene (Fig. 25). Therefore, we constructed a phylogenetic tree of *Arabidopsis* TOPP proteins (see figure description for details). We then combined this phylogenetic tree with relative gene-expression data of the TOPP proteins in various plant tissues according to the Genevestigator microarray database with the Meta-Profile Analysis tool Anatomy Profile (Hruz et al., 2008).
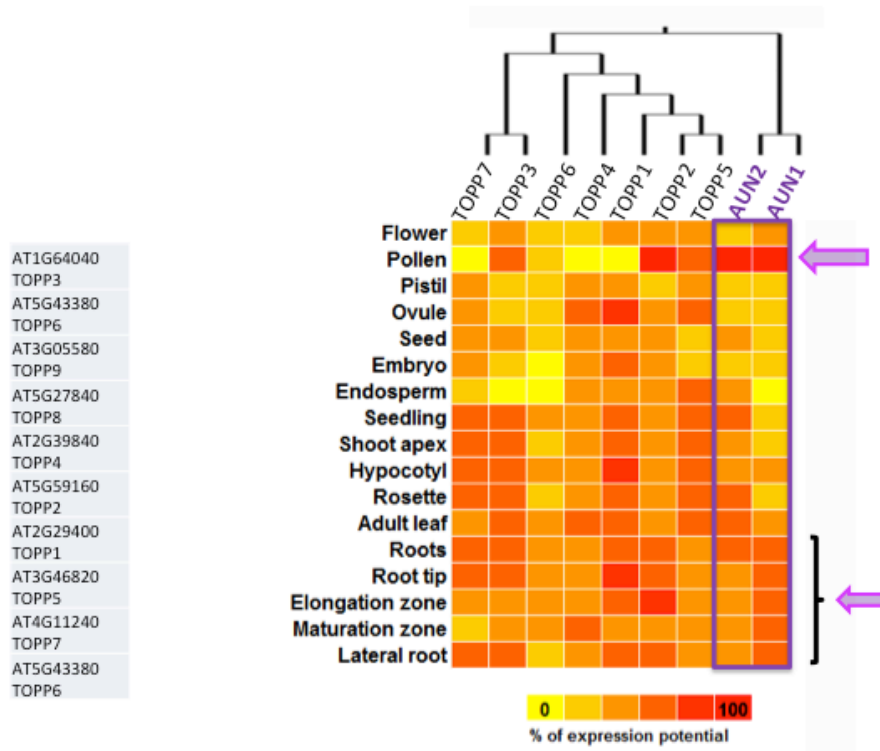
Fig. 25 Phylogenetic tree of the *Arabidopsis* TOPP family combined with relative gene-expression data. Multiple alignments of *Arabidopsis thaliana* TOPP proteins were made in ClustalW2.0 and with MEGA7, the phylogenetic tree was reconstructed under usage of the protein sequence parsimony method (Bootstrap test, 1'000 replicates) (Boisson-Dernier et al., 2015). Thereafter, the tree was combined with the relative gene expression data of *Arabidopsis* TOPP family members in various plant tissues according to the Genevestigator microarray database with the Meta-Profile Analysis tool Anatomy Profile (Hruz et al., 2008). Purple color highlights *AUN1/2*.

Interestingly, we found that although *AUN1* is preferentially pollen-expressed, it also shows mild expression in root tissue. Additionally, Jakoby et al. (2008) discovered that AUN1 is amongst the 5% of most highly expressed genes in trichomes. This was very intriguing since we previously discovered the role of MRI in RH growth control and could potentially have found yet another gene with roles in both RH and PT growth. Even more interestingly, we found that *AUN1* has a very close homologue, *TOPP8* (*AT5G27840*). *TOPP8* and *AUN1* share 89.8% identity at the amino acid level. We named the gene *ATUNIS2* (*AUN2*). With a percentage of sequence similarity this high, at least partial functional redundancy of the two genes could be expected. Another interesting detail is the predicted position of the *ipr*7 mutation. The D94 is very conserved in all *Arabidopsis* TOPP proteins (Fig. 26) and located in the conserved core catalytic domain. It is widely known that mutations in the catalytic core region of protein phosphatases can result in dominant negative forms of the protein phosphatases (Jurczak et al., 2010; Qin et al., 2014). Thus, we figured that AUN1[D94N] might be dominant negative form of AUN1. This would mean that the phosphatase still binds its

substrate but would no longer be able to remove the phosphate group from it. Thus, the inactive phosphatase would trap the substrate and block it from interaction with active phosphatases. Also, by not releasing the substrate, the inactive phosphatase would prevent it from interacting with downstream components. With this information, I started with the phenotypic characterization of the original *ipr7* mutant.
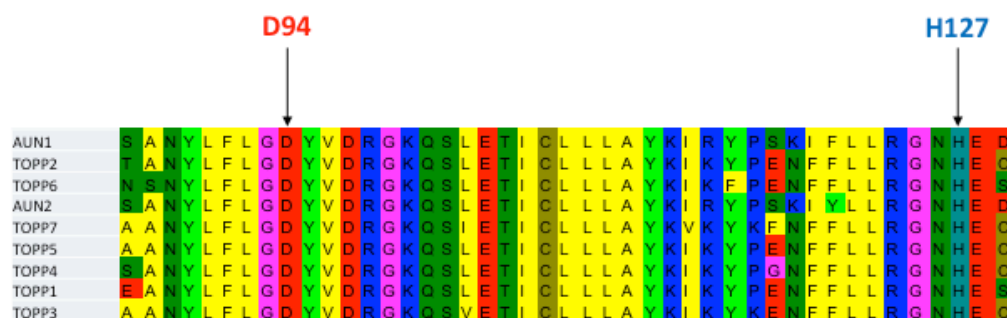
Fig. 26 Protein alignment of the *Arabidopsis* TOPP family with the conserved D94 and H127 residues.

3.2.1 *ipr7* phenotypic characterization

To determine the extent of seed set rescue, I first checked the seed set of the original suppressor mutant *ipr7* in comparison to WT and *anx1-2 anx2-2* plants. Henceforth, *ipr7* refers to *anx1-2 anx2-2 ipr7/AUN1* plants unless stated differently. A normal WT silique contains 52.0 seeds on average while the male sterile *anx1-2 anx2-2* plants produce only 2.9 seeds per silique (Fig. 27a). *ipr7* plants exhibit 8.0 seeds per silique, which represents a slight rescue of the *anx1-2 anx2-2* male sterility *in vivo*. Homozygous *ipr7* plants depict a stronger seed set rescue of 14.9 seeds per silique. Since the *anx1 anx2* male sterility originates from precocious PT bursting, I next conducted *in vitro* pollen germination assays to investigate pollen germination and PT growth behavior.

While in 3 independent pollen germination assays, *anx1-2 anx2-2* pollen germinated on average at 64.5% and burst at 99.7%, *ipr7* pollen exhibited a germination rate of 68.4% and a bursting rate of 89.2% (Fig. 27b). Interestingly, *ipr7* homozygous pollen did not behave substantially different to that (germination rate 63.5% and bursting rate 90.2%, respectively). This indicates that the *ipr7* mutation rescues *anx1-2 anx2-2* pollen bursting significantly by decreasing the bursting rate from ~100% to ~89% (*P= 0.0014,* unpaired Student's *t* test). Thus, the observed mild seed set rescue is due to a reduction of precocious pollen bursting, enabling more PTs to fertilize ovules.

Ultimately, I also monitored RH growth in homozygous *ipr7* plants, as we previously had discovered a RH phenotype in *ipr19* plants and *AUN1* shows RH expression. Surprisingly, we indeed found a difference between *anx1-2 anx2-2* and *ipr7* RH length (Fig. 28). As *ANX1/2* are not expressed in RHs and *anx1 anx2* plants do not exhibit a RH phenotype (Boisson-Dernier et al., 2015), the *anx1-2 anx2-2* mutant can be regarded as WT in this case. An average *anx1-2 anx2-2* RH measures 506.9µm whereas an *ipr7* RH only accounts to 285.0µm on average. This indicates that the *ipr7* mutation causes growth inhibition of RHs, a phenomenon we previously observed even stronger in the *ipr19* mutant, where we found little bulges only instead of RHs. This was a good indication that *AUN1/2* might play a role in the FER-dependent RH CWI pathway as well.

Taken together, we observed that the *ipr7* mutation is capable of mildly rescuing the pollen bursting-mediated seed set phenotype of *anx1-2 anx2-2* plants and that it triggers growth inhibition in RHs.
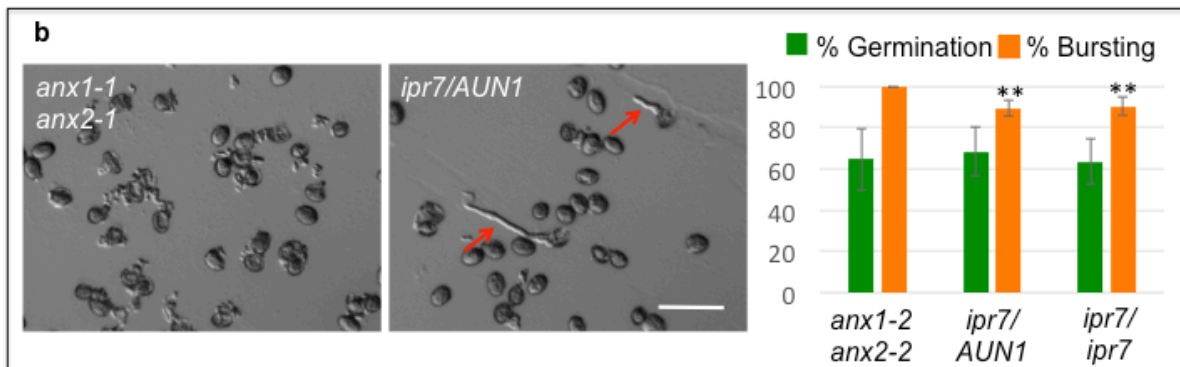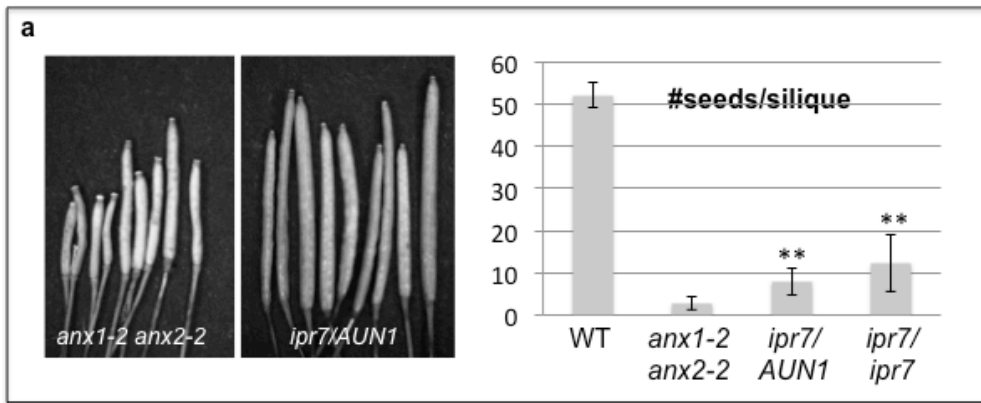
Fig. 27 The *ipr7* mutantion weakly rescues *anx1 anx2* male sterility **a:** Seed set analysis of WT, *anx1-2 anx2-2, ipr7/AUN1* and *ipr7/ipr7* siliques. Asterisks denote a significant increase in seed set compared to *anx1 anx2* (*P<0.001* in both lines, Student's *t* test). **b:** Germination and bursting rates of *anx1-2 anx2-2, ipr7/AUN1* and *ipr7/ipr7* pollen. Data originates from 4 independent pollen germination assays. Asterisks denote a significant reduction in pollen bursting compared to *anx1 anx2* (*P<0.0061* in both lines, Student's *t* test). Representative images of *anx1-2 anx2-2* and *ipr7/AUN1* pollen germination assays. Red arrows indicate PTs. Scale bar: 80μm.
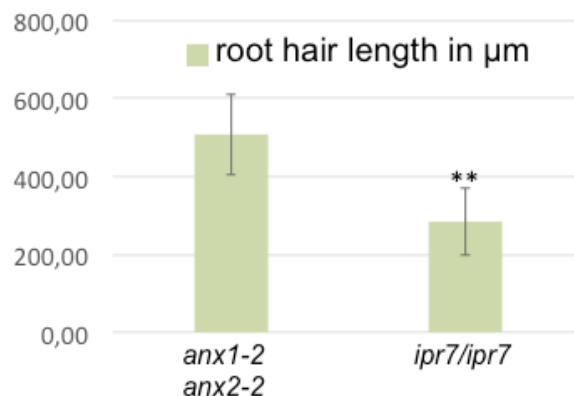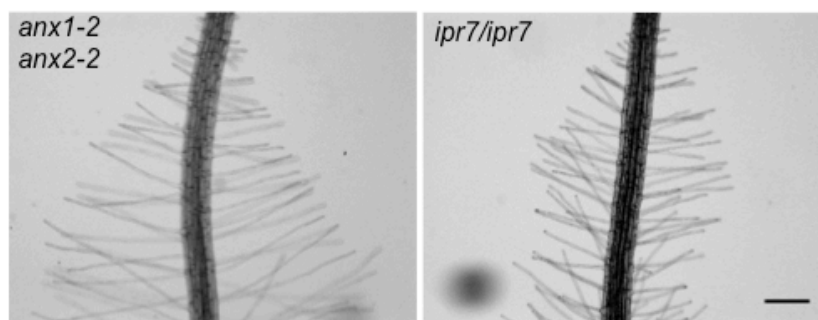
Fig. 28 *ipr19* RHs are shorter than *anx1 anx2* RHs. **Top:** Representative images of an *anx1-2 anx2-2* and an *ipr7/ipr7* root. Scale bar: 200μm. **Bottom:** Root hair length of *anx1-2 anx2-2* seedlings (n=97

rhs from >9 individual seedlings) compared to *ipr7* homozygous seedlings (n=118 rhs from >11 individual seedlings). Asterisk denotes a significant decrease in RH length (*P<0.0001*, unpaired Student's *t* test).

3.2.2 *AUN1*[D94N] is the *ipr7* mutation

We had not investigated yet if the D94N substitution in AUN1 really was the *ipr7* mutation responsible for the observed phenotypes. To elucidate this, I cloned *AUN1* and *AUN1*[D94N] without stop codon into *p*LAT52:GW-YFP and transformed *anx1-1/anx1-1 anx2-1/ANX2* plants with the two constructs. Transformants were pre-selected by growing the seeds on BASTA plates and were subsequently screened for fluorescence in pollen grains in the T1 generation. A strong YFP- signal indicates strong expression in pollen. By genotyping for *ANX2* in the T2 generation of selfed transformants, transformed double homozygous *anx1-1 anx2-1* plants can be identified. If any are obtained, this is a very strong indication that the constructs *p*LAT52:AUN1-YFP and/or *p*LAT52:AUN1[D94N]-YFP are capable of rescuing the *anx1 anx2* male sterility phenotype. The T2 generation was screened to be homozygous for *AUN1-YFP* and *AUN1*[D94N]-YFP, respectively.

In the T2 generation of homozygous *AUN1-YFP* transformed *anx1-1/anx1-1 anx2-1/ANX2* plants, 2 independent lines were selected and a total of 141 plants was genotyped for ANX2. No *anx1-1 anx2-1* double homozygous plant could be retrieved. In the T2 progeny of homozygous *AUN1*[D94N]-YFP transformed plants, however, 127 plants from 2 independent lines were genotyped for ANX2 and 3 double homozygous *anx1-1 anx2-1* plants could be retrieved. This indicates that AUN1[D94N]-YFP, but not AUN1-YFP, is able to rescue the *anx1-1 anx2-1* male sterility phenotype. The T3 generation of two of these three plants was further investigated in a seed set analysis and in pollen germination assays. The two *anx1-1 anx2-1 AUN1*[D94N] triple homozygous plants will be referred to as *anx rescue line 1* and *2* (*arl1* and *arl2*) from here on.

First, I checked the seed set of *arl1* and *arl2* compared to WT and *anx1-1 anx2-1* (Fig. 29a)*. WT siliques exhibited an average of 50.1 seeds per silique and *anx1-1 anx2-1* plants depicted 1.3 seeds per silique on average. In comparison, *arl1* and *arl2* had increased seed sets of 19.5 and 19.4 seeds per silique, respectively. This is reminiscent of the previously reported ~14 seeds/silique in the homozygous *ipr7* mutant. Thus, AUN1[D94N]-YFP is capable of partially rescuing the *anx1-1 anx2-1* male sterility.

Next, I conducted three independent pollen germination assays on *anx1-1 anx2-1*, *arl1* and *arl2* pollen to confirm that this seed set rescue is due to a decrease in precocious pollen bursting (Fig. 29b and 29c). While *anx1-1 anx2-1* pollen germinated at 65.5% and burst at 100%, *arl1* pollen had an average germination rate of 75.2% with a bursting rate of 85.4%. *arl2* depicted an average germination rate of 71.2% and a bursting rate of 87.2%, respectively. Thus, both *arl*s show a reduction of pollen bursting of ~13-15%, very similar to the observed ~11% bursting rate reduction in the original *ipr7* mutant. This indicates that AUN1[D94N]-YFP is sufficient to replicate the *ipr7* original phenotype and that *AUN1*[D94N] corresponds to the *ipr7* mutation. Also, it shows that *AUN1*[D94N] acts downstream of ANX1/2.
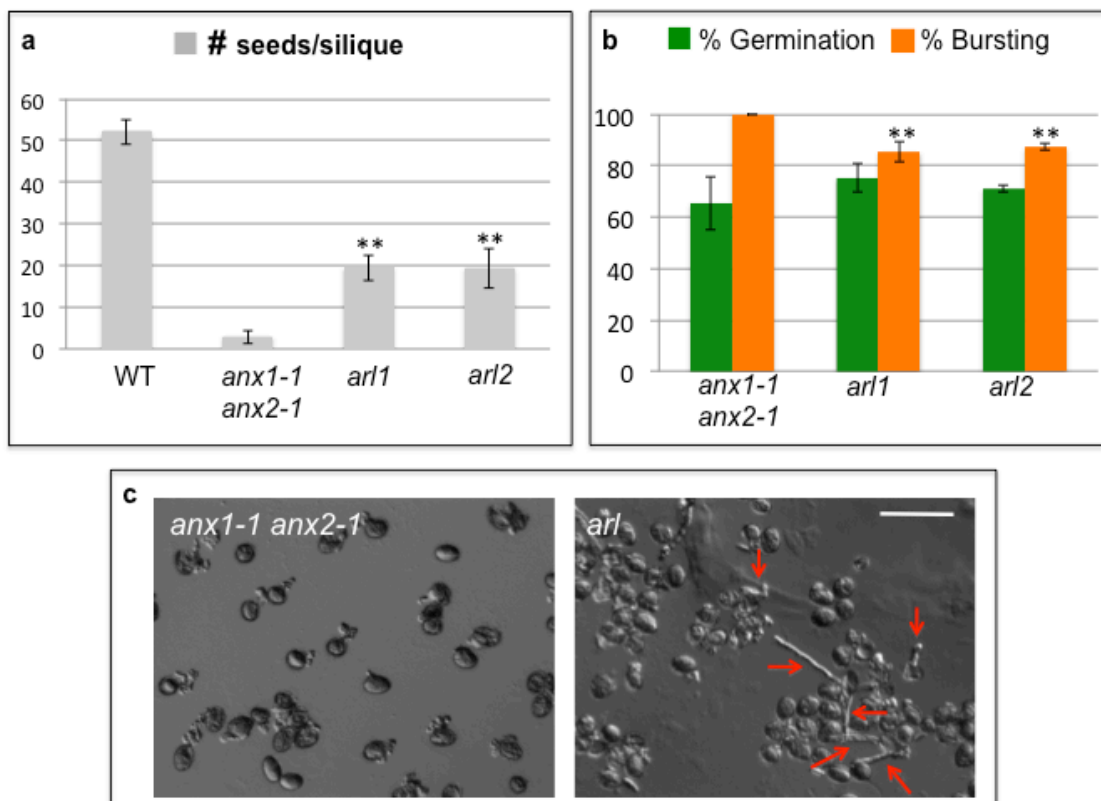
Fig. 29 *AUN1*[D94N] corresponds to the *ipr7* mutation. **a:** Seed set analysis of WT, *anx1-1 anx2-1*, *arl1* and *arl2*. Asterisks denote significant decreases in seed set compared to *anx1-1 anx2-1* (*P<0.001* in both lines, Student's *t* test). **b:** Germination and bursting rates of *anx1-1 anx2-1*, *arl1* and *arl2*. Asterisks denote significant decreases in pollen bursting compared to *anx1-1 anx2-1* (*P<0.0029* in both lines, Student's *t* test). **c:** Representative images of *anx1-1 anx2-1* and *arl* pollen germination assays. Red arrows point out PTs. Scale bar: 80µm.

3.2.3 *AUN1/2* are negative regulators of pollen tube and root hair growth

3.2.3.1 Disruption of *AUN1/2* triggers growth inhibition in pollen tubes

We next wanted to know, what type of regulator AUN1 is. As previously introduced, we assumed AUN1 might be a negative regulator. In this scenario, ANX1/2 would negatively regulate AUN1 that in turn inhibits CWI maintenance (Fig. 30). Lack of AUN1 would then result in an over-activation of the CWI maintenance machinery due to loss of AUN1-mediated negative regulation. Consequently, PT growth would be inhibited. To test this, we ordered t-DNA insertion knock-out lines for *AUN1* and *AUN2*, namely *aun1-1* (*SALK_045433C*) and *aun2-1 (SALK_137888)* (Fig. 31). When I checked the seed set, I found that the number of seeds per silique is WT-like in *aun1-1* and *aun2-1* plants. Also, when I conducted pollen germination assays on the two single mutants, *aun2-1* pollen behaved completely WT-like and also for *aun1-1* pollen, I could not observe a phenotype. This was not too surprising, as *AUN1* and *AUN2* show such a high degree of homology that we expected at least partial functional redundancy. Consequently, I crossed the two single mutant lines in search for an *aun1-1 aun2-1* double homozygous plant. In the F2 generation, out of 100 genotyped plants, I did not obtain a double homozygous plant. However, I proceeded to the F3 with an *aun1-1/AUN1 aun2-1/aun2-1* plant and selfed it. Out of 94 F3 plants, we found 18 *aun1-1 aun2-1* double homozygous plants, 56 *aun1-1/AUN1 aun2-1/aun2-1,* and 20 *AUN1/AUN1 aun2-1/aun2-1* plants which corresponds to the expected

mendelian segregation ratio of 1:2:1 (*aun1-1/aun1-1 : aun1-1/AUN1 : AUN1/AUN1*) (*P=0.171*, Chi^2-Test).
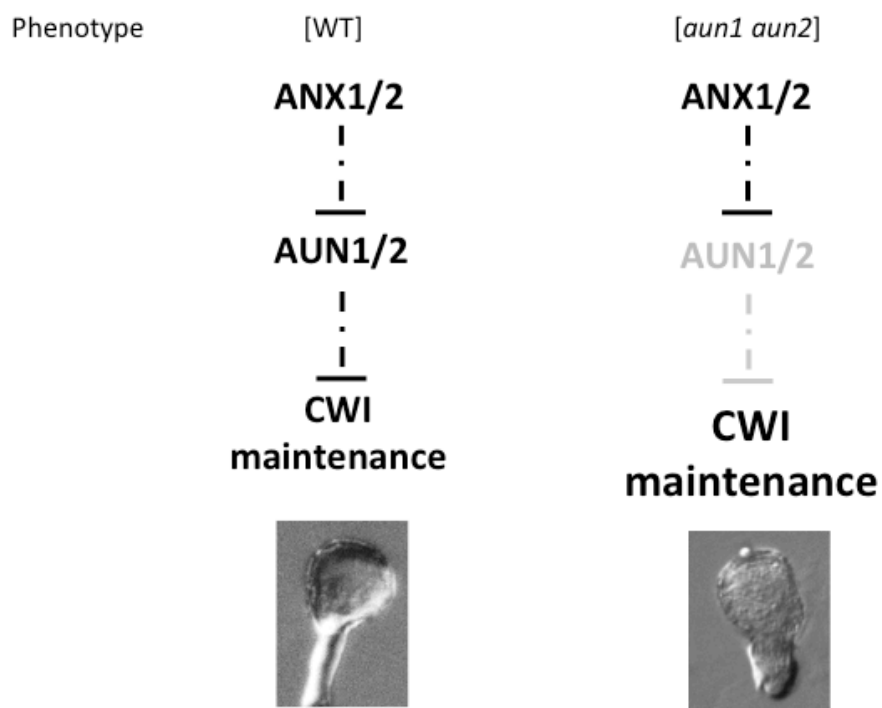
Fig. 30 Schematic representation of the expected outcome of knocking-out *AUN1* and/or *AUN2.*
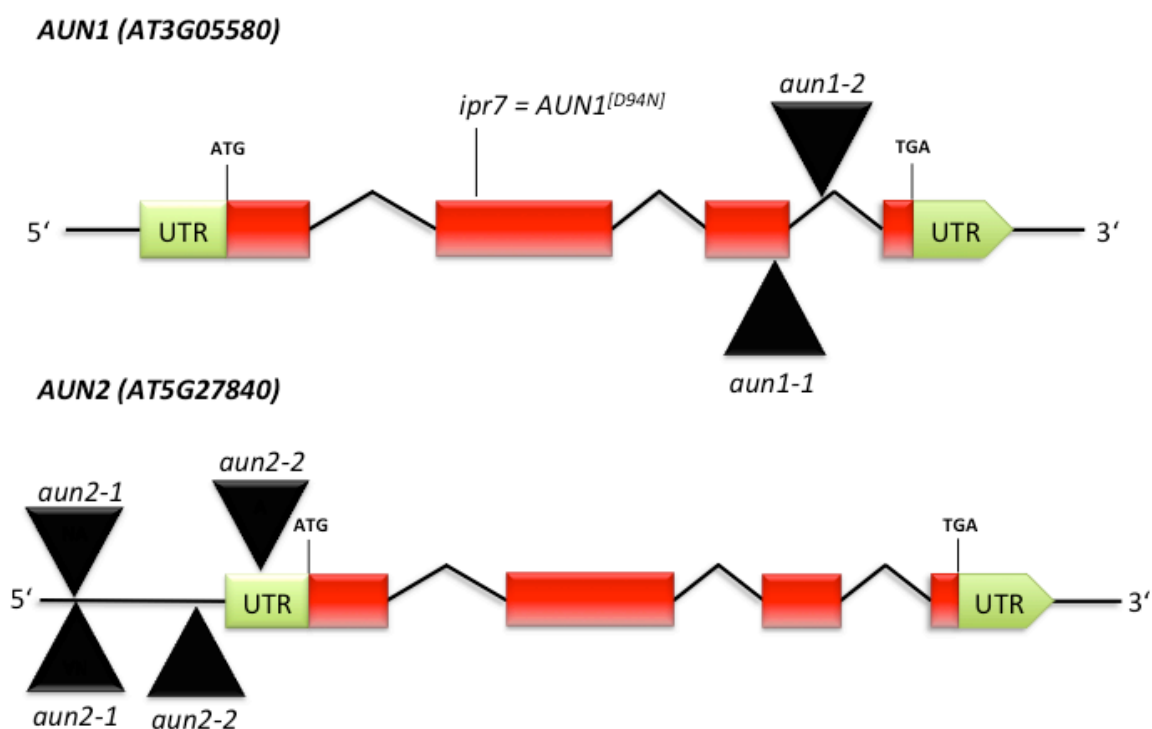
Fig. 31 Representation of the *AT3G05580* and the *AT5G27840* locus with introns, exons, and positions of the mutant alleles. Black triangles represent t-DNA insertions.
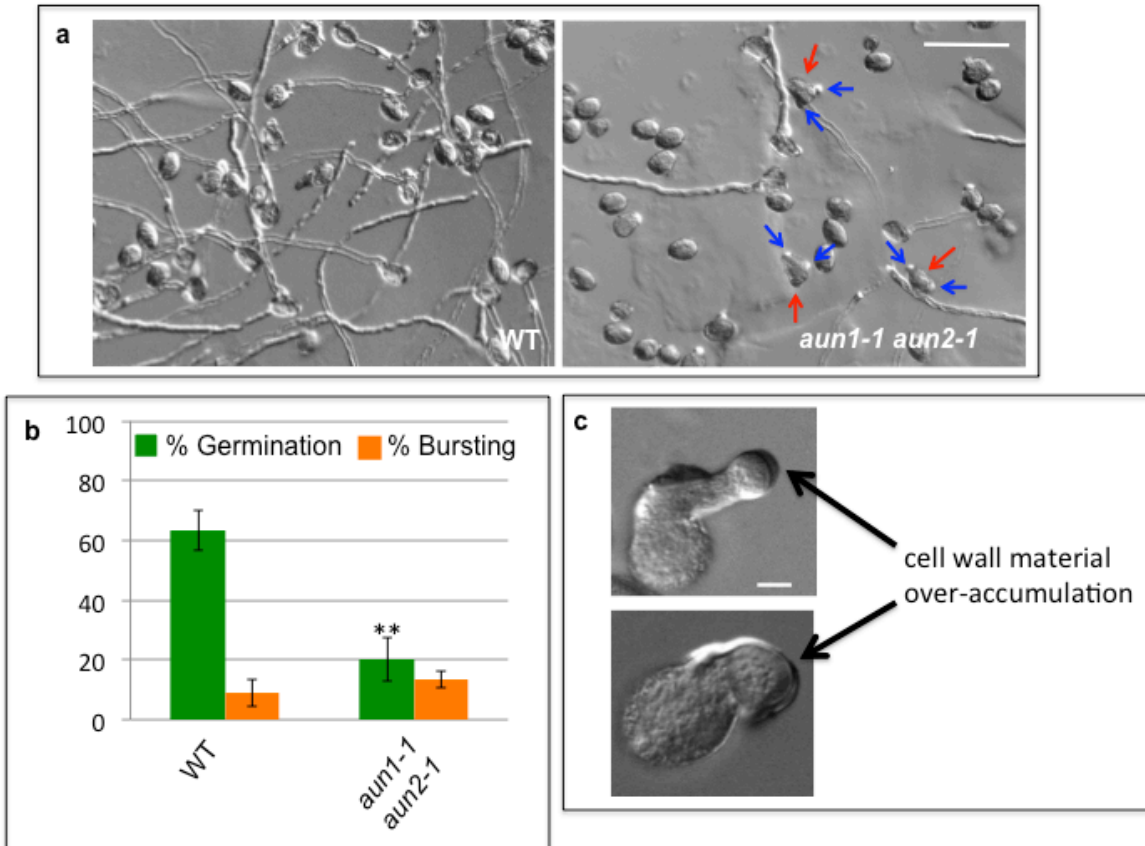
Fig. 32 *aun1-1 aun2-1* mutants are impaired in pollen germination. **a:** Representative images of WT and *aun1-1 aun2-1* pollen germination assays. Red arrows indicate pollen grains initiating PT outgrowth through 2 colpi, blue arrows indicate the colpi. Scale bar: 80μm. **b:** Germination and bursting rates of WT and *aun1-1 aun2-1* pollen. Data originates from three independent pollen germination assays. Black asterisks denote significant differences in the germination rate compared to WT plants (*P=0.003*, Student's *t* test). **c:** Pollen grain/tube with CW material over-accumulations. Scale bar: 5μm.

Interestingly, the *aun1-1 aun2-1* seed set is WT-like as well. However, when I conducted three independent pollen germination assays on WT and *aun1-1 aun2-1* pollen, I observed a striking difference (Fig. 32a and 32b). While on average 63.4% of WT pollen germinated and 8.9% of them burst, *aun1-1 aun2-1* pollen showed a drastic reduction of germination to 20.1% with an elevated bursting rate of 13.5%. Also, under closer examination, I frequently observed pollen grains unsuccessfully trying to initiate PT outgrowth through two or more colpi. Also, some pollen grains either only formed little bulges instead of PTs or PTs with wide tips from CW over-accumulation (Fig. 32c). This is reminiscent of the ANX1/2 over-expressor phenotype. Thus, it seems that in the absence of both AUN1 and AUN2, the CWI maintenance machinery is over-activated. This results in CW material over-accumulations that trigger such a strong inhibition of PT growth that the pollen grains are unable to properly germinate. The higher bursting rate in *aun1-1 aun2-1* pollen likely originates from a sampling artifact. When imaging a pollen germination assay, the zones with the best pollen germination are commonly chosen. However, these are also the zones with the most pollen bursting. In mutants with low pollen germination, the bursting rate consequently seems higher than it truly is.
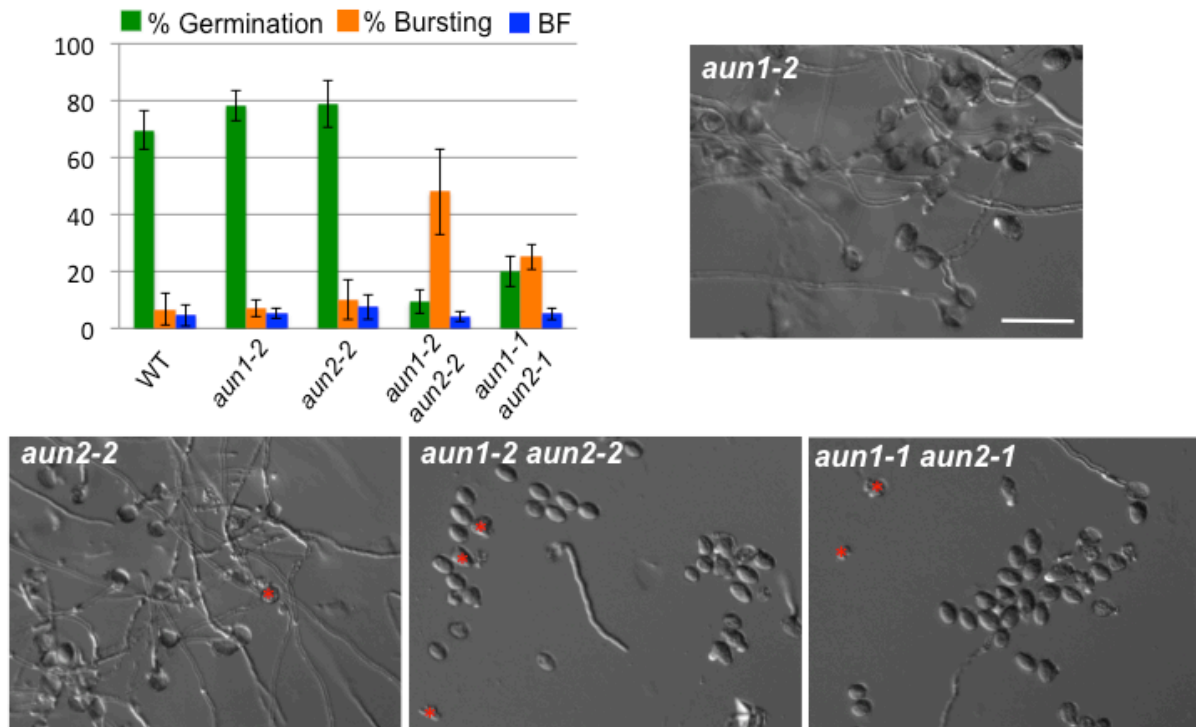
Fig. 33 *aun1-2* and *aun2-2* single mutants behave WT-like. Pollen germination assay of WT, *aun1-2, aun2-2, aun1-2 aun2-2* and *aun1-1 aun2-1* with germination and bursting rates as well as bursting fraction (BF). Representative images of *aun1-2, aun2-2, aun1-2 aun2-2* and *aun1-1 aun2-1* pollen germination assays. Red asterisks indicate burst pollen grains. Scale bar: 80μm.

We wanted to confirm this in a second independent allele and thus ordered the t-DNA insertion lines *aun1-2* (*GABI_600E08*) and *aun2-2* (*SALK_125184*) (Fig. 31). We crossed them and screened for an *aun2-1 aun2-2* double mutant in the T2 generation. We then conducted pollen germination assays on WT, *aun1-2, aun2-2, aun1-2 aun2-2* and *aun1-1 aun2-1* (Fig. 33). We found that WT, *aun1-2* and *aun2-2* had comparable germination rates of 69.4%, 77.9% and 78.6%, respectively, with bursting rates of 6.7%, 6.9% and 10.1%. In contrast, *aun1-2 aun2-2* pollen had a germination rate even lower than *aun1-1 aun2-1* (9.4% compared to 19.9%). The bursting rate of *aun1-2 aun2-2* was high with 47.8% compared to an already elevated 25.2% in *aun1-1 aun2-1*. These results show that the *aun1-2* and *aun2-2* single mutants have a WT-like phenotype, while the *aun1-2 aun2-2* mutant has severe pollen germination issues similar to the *aun1-1 aun2-1* mutant. Strikingly, we again obtain elevated bursting rates for the *aun1 aun2* double mutants with low pollen germination rates.

Thus, I had to find a way to distinguish between true and false elevated bursting rates. In contrast to the bursting rate that is defined as $100\% \times \frac{number\ of\ burst\ pollen\ grains}{number\ of\ germinated\ pollen\ grains}$, I decided to determine the bursting fraction (BF in the figures), defined as $100\% \times \frac{number\ of\ burst\ pollen\ grains}{total\ number\ of\ pollen\ grains}$. When doing so, the bursting fractions of *aun1-2 aun2-2* and *aun1-1 aun2-1* account to 4.3% and 5.1%, respectively, which is statistically not different to in WT (4.6%), *aun1-2* (5.5%) and *aun2-2* (7.6%) mutants.

In summary, we could show that *aun1* and *aun2* single mutants have a WT-like phenotype and that *aun1 aun2* double mutants have a low pollen germination phenotype with only seemingly elevated pollen bursting. Also, the bursting fraction is a means to distinguish between true pollen bursting and sampling artifacts. Furthermore, these results show that solely focusing on germination and bursting rates in pollen germination assays might be insufficient to accurately determine pollen bursting in lines with low pollen germination.
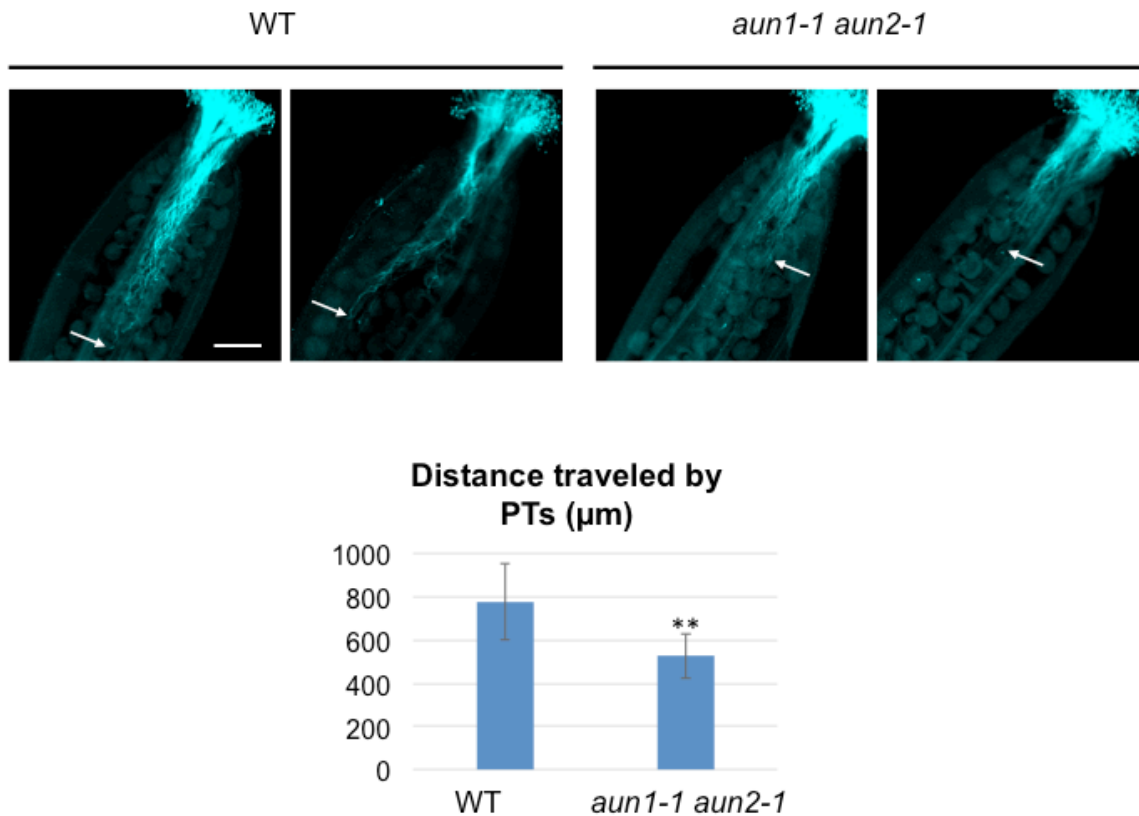
| | WT | aun1-1 aun2-1 |

Fig. 34 *aun1-1 aun2-1* pollen germination is impaired *in vivo* as well. Emasculated WT pistils manually pollinated by either WT or *aun1-1 aun2-1* pollen. Aniline blue staining 4 hours after pollination, n>19. White arrows indicate the PT traveling the fastest. Asterisks denote a significant difference in PT length (*P<0.0001*, unpaired Student's *t* test). Scale bar: 200µm.

Since the *aun1-1 aun2-1* seed set was WT-like, we decided on another way to check *aun1-1 aun2-1* PT growth behavior *in vivo*. Generally, as the transmitting tract is nutrient-rich and provides optimal conditions for PT growth, PTs tend to grow better *in vivo* than *in vitro*. We pollinated emasculated WT pistils with either WT or *aun1-1 aun2-1* pollen. After 4 and 16 hours, respectively, the pistils were harvested, fixed and subsequently stained with aniline blue according to Boisson-Dernier et al. (2015). The pistils were then imaged and the PT length was measured in FIJI. Interestingly, a clear delay in *aun1-1 aun2-1* PT growth could be observed after 4 hours after pollination (Fig. 34). While WT PTs traveled on average 777.4µm during this time, *aun1-1 aun2-1* PTs only traveled 525.1µm. However, after 16 hours, WT and *aun1-1 aun2-1* PT length was comparable to each other, which points towards an initial pollen germination/PT growth inhibition in *aun1-1 aun2-1* plants that is compensated over time. This might be the reason for the WT-like seed set of *aun1-1 aun2-1* plants.

3.2.3.2 The pollen tube growth inhibition is an exclusively male defect

To evaluate the impact of this pollen germination problem on fertilization, we next checked how the *aun1-1 aun2-1* mutation is transmitted to the next generation. Therefore, we crossed *aun1-1/AUN1 aun2-1/aun2-1* mutant with WT and genotyped the F1 generation for *aun1-1* presence to obtain the *aun1-1 aun2-1* transmission efficiency. Normally, half of the progeny carries the desired allele and thus, the transmission efficiency will be 100%. If the transmission efficiency of *aun1-1 aun2-1* would be close to 0%, as in *mri-1*, the effect of the observed pollen germination problem would be huge, if it is around 50%, the *in vitro* germination might artificially enhance the phenotype.

To test this, I had two different experimental setups: In the first one, I used *aun1-1/AUN1 aun2-1/aun2-1* as pollen donor for WT pistils, in the second one, I used WT pollen on *aun1-1/AUN1* pistils. When *aun1-1/AUN1* pollen was used, the *aun1-1 aun2-1* transmission efficiency was decreased to 50% (32 *aun1-1/AUN1* and 64 *AUN1/AUN1* out of 96 F1 plants genotyped). When WT was selected as pollen donor, the transmission efficiency was close to normal with 78% (39 *aun1-1/AUN1* and 50 *AUN1/AUN1* plants out of 89 F1 plants genotyped). Consequently, only if *aun1-1/AUN1* is used as male, the *aun1-1 aun2-1* transmission efficiency is noticeably decreased. Thus, the *aun1-1 aun2-1* PT growth phenotype is due to an exclusively male defect. Also, the *aun1-1 aun2-1* transmission efficiency of 50% on the pollen side suggests that the drastically lowered pollen germination in pollen germination assays might be artificially enhanced by the *in vitro* cultivation.
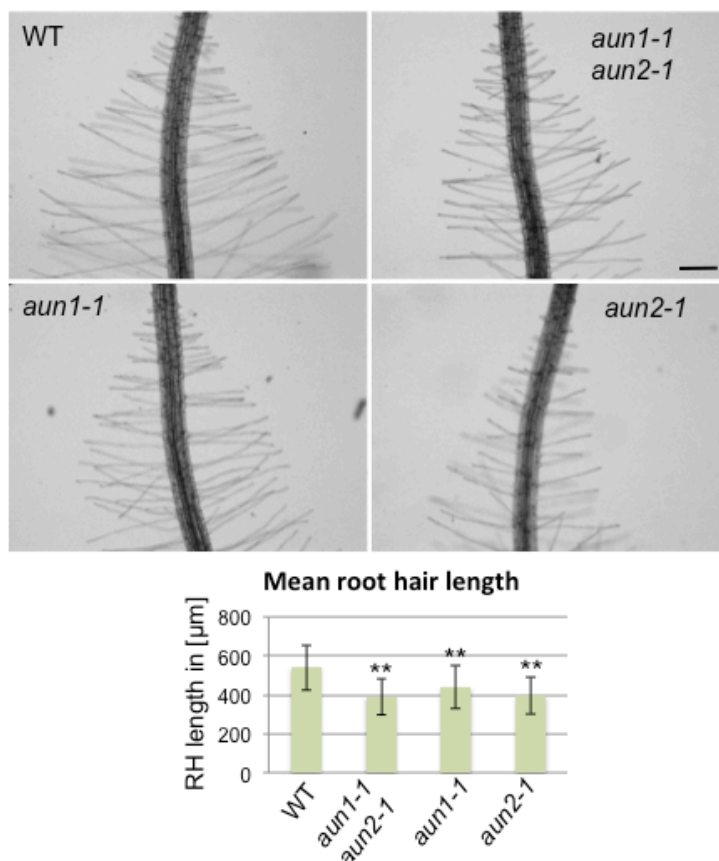
Fig. 35 Disruption of *AUN1* and/or *AUN2* triggers RH growth impairment. RH length measurements of WT (n= 153 from 14 individuals), *aun1-1* (n=181 from 16 individuals), *aun2-1* (n=161 from 18 individuals) and *aun1-1 aun2-1* (n=109 from 17 individuals) roots. Asterisks denote significant differences from WT *(P<0.0001*, unpaired Student's *t* test). Scale bar: 200μm.

3.2.3.3 *AUN1/2* disruption triggers root hair growth inhibition

After observing the growth inhibitory effect of *AUN1/2* loss on PTs, I wanted to check if this applies for RH growth as well. Thus, I conducted RH assays and measured the RH length of *aun1-1, aun2-1* and *aun1-1 aun2-1* plants compared to WT (Fig. 35). While WT plants exhibit average RH lengths of 541.3μm, the *aun1-1 aun2-1* double mutant has shorter RHs of average 391.9μm. Interestingly, unlike in PTs, the *aun1-1* and *aun2-1* single mutants depict the same short RH phenotype with 440.8μm and 394.1μm average RH length, respectively. This indicates that AUN1/2 have a function in CWI maintenance in both PTs and RHs. Also, while in PT growth knock-out of either *AUN1* or *AUN2* does not trigger a

phenotypic reaction, in RHs, disruption of one of the two genes is enough to obtain a growth inhibitory effect. This might point towards tissue-specific regulation of the two genes.

While these are very good indications that AUN1/2 are negative regulators of tip-growth, we wanted to test the hypothesis with another experiment.

3.2.3.4 Over-expression of *AUN1* and *AUN1[D94N]* leads to opposite phenotypes in pollen

If ANX1/2 truly negatively regulate AUN1/2 that inhibit the CWI maintenance machinery and if *AUN1[D94N]* indeed is a dominant negative form of AUN1, over-expression of *AUN1* and *AUN1[D94N]* should trigger opposite pollen phenotypes (Fig. 36). In our scenario, if there is an excess of AUN1, ANX1/2 would not be able to inhibit all of the AUN1 proteins. Thus, AUN1 would strongly inhibit the CWI maintenance machinery, which would result in pollen bursting. If *AUN1[D94N]* is expressed in addition to native *AUN1/2*, this would lead to a competition between the supposedly inactive form of AUN1, AUN1[D94N], and the native active AUN1/2. As we know that AUN1[D94N] is dominant over AUN1, the effect of this should be the same as if AUN1/2 are knocked out. AUN1/2 cannot inhibit the CWI maintenance machinery, which will consequently be over-activated. This would result in PT growth inhibition and possibly pollen germination problems.
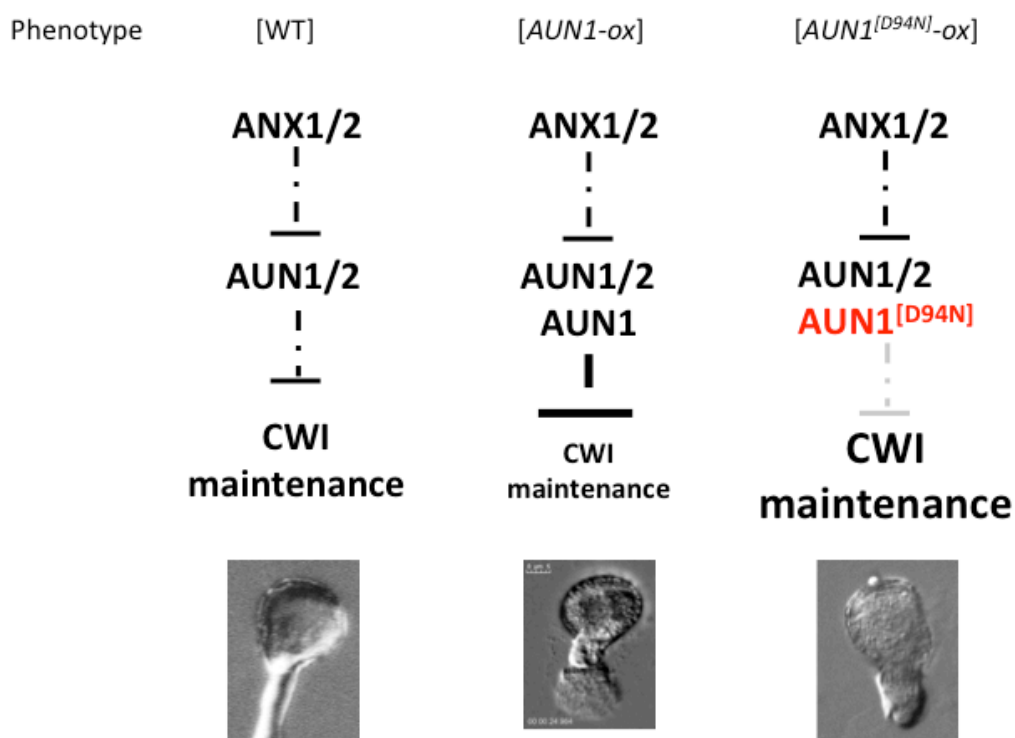
Fig. 36 Schematic representation of the expected over-expression phenotypes of *AUN1* and *AUN1[D94N]*.

To test this hypothesis, I transformed WT plants with both *p*LAT52:AUN1-YFP and *p*LAT52:AUN1[D94N]-YFP. I checked for expression of the constructs in the T1 generation by screening for fluorescence in pollen grains. In the T2 generation, I selected two independent lines homozygous for each of the respective constructs and subsequently investigated PT growth behavior *in vitro* in comparison to untransformed WT plants. Henceforth, the two WT lines homozygous for *AUN1-YFP* will be referred to as *AUN1-over-expressor 1 (AUN1-ox1)* and *AUN1-over-expressor 2 (AUN1-ox2)* whereas the two WT lines homozygous for

AUN1[D94N] will be called *AUN1[D94N]-over-expressor 1* and *2* (*AUN1[D94N]- ox1* and *AUN1[D94N]-ox2*).
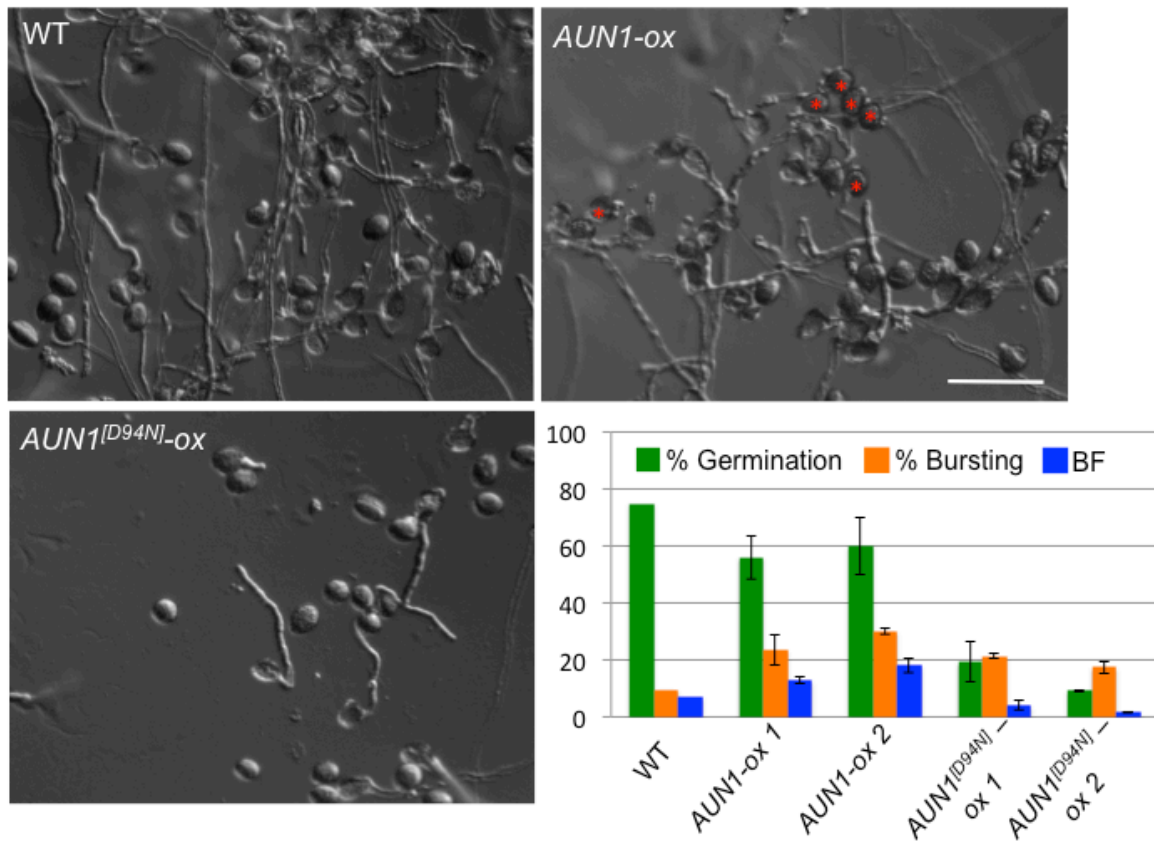
Fig. 37 Over-expression of *AUN1* and *AUN1[D94N]* triggers opposite phenotypes in pollen. Pollen germination assays of WT, *AUN1-ox1, AUN1-ox2, AUN1[D94N]-ox1* and *AUN1[D94N]-ox2* with germination and bursting rates as well as bursting fraction. Red asterisks indicate burst pollen grains. Scale bar: 80µm.

The seed set of all four over-expressor lines was WT-like. However, when I conducted pollen germination assays, I found substantial differences. Unfortunately, in three independent PG assays, I only was able to obtain one representative WT data set as these plants were treated with pesticides while the experiment was still ongoing. However, for the four over-expressor lines, I could get three independent data sets for each line as they were not treated. Interestingly, while WT pollen germinated at 75.0% and burst at 9.5%, *AUN1[D94N]-ox1* and *AUN1[D94N]- ox2* had significantly lower germination rates with 19.2% and 9.2%, respectively, and slightly elevated bursting rates of 21.3% and 17.4%, respectively (Fig. 37). *AUN1-ox1* pollen germinated at 56.0% and burst at 23.4%, while *AUN1-ox2* showed a germination rate of 60.1% and a bursting rate of 30.1%. Thus, while only the *AUN1[D94N]-ox* lines have a significantly lower germination rate than WT plants, it appears that all four over-expressor lines show elevated bursting rates. However, in case of the *AUN1[D94N]-ox* lines with low pollen germination rates, the higher bursting rate is likely a sampling artifact. To demonstrate this, we can determine the bursting fraction. In this case, WT pollen has an average bursting fraction of 7.14%, which is comparable to normal WT bursting fractions. *AUN1[D94N]-ox1* arrives at a mean bursting fraction of 4.1%, while *AUN1[D94N]-ox2* reaches 1.6%. In contrast, *AUN1-ox1* shows a bursting fraction of 12.9% and *AUN1-ox2* has a bursting fraction of 17.9%. This demonstrates that if the total number of counted pollen grains is concerned, the two *AUN1[D94N]-ox* lines have an average bursting fraction that is

comparable to, or possibly even lower than, the WT bursting fraction. However, when the two *AUN1-ox* lines are concerned, their average bursting fraction is higher than that of WT.

In summary, it appears that if *AUN1[D94N]* is expressed in a WT background, pollen germination is strongly inhibited. If *AUN1* is over-expressed in a WT background, a mild elevation of bursting pollen grains is observed while the pollen germination is not affected. The finding, that *AUN1* and *AUN1[D94N]* over-expression triggers opposite phenotypes in PT growth, supports our hypothesis that AUN1/2 indeed are negative regulators of CWI maintenance. Also, it demonstrates that AUN1[D94N] is a dominant negative form of AUN1.
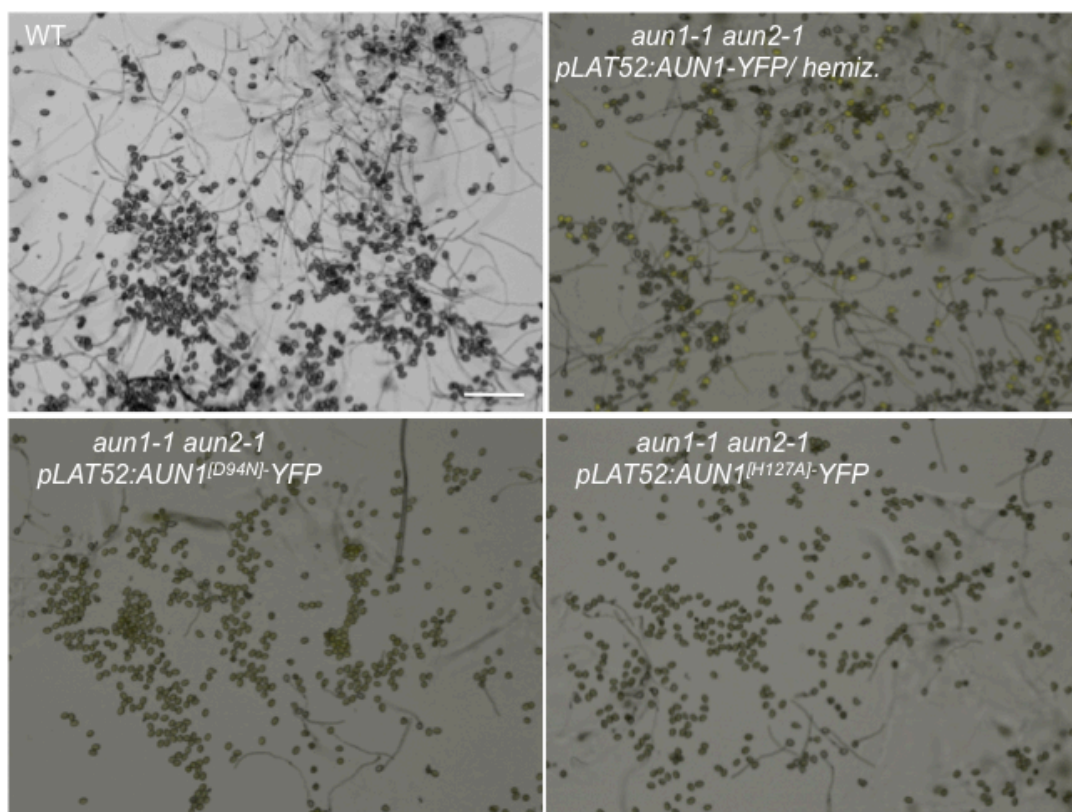
Fig. 38 *AUN1-YFP* complements the *aun1-1 aun2-1* low pollen germination phenotype. Representative images of WT, *aun1-1 aun2-1 AUN1-YFP (hemizygous), aun1-1 aun2-1 AUN1[D94N]-YFP* and *aun1-1 aun2-1 AUN1[H127A]-YFP.* Scale bar: 200µm.

3.2.3.5 *AUN1[D94N]* might be a constitutively inactive form of *AUN1*

The next question to be addressed is what makes AUN1[D94N] a negative form of AUN1. Until now, we hypothesize that AUN1[D94N] might have lost its catalytic activity and thus is constitutively inactive. To test this, I transformed *aun1-1 aun2-1* plants with *p*LAT52:AUN1-YFP, *p*LAT52:AUN1[D94N]-YFP and *p*LAT52:AUN1[H127A]-YFP, a phospho-dead version of AUN1. AUN1[H127A] should no longer have the phosphatase activity and thus be constitutively inactive (Boevink et al., 2016). The H127 is also located in the core catalytic conserved domain of *Arabidopsis* TOPPs (Fig. 26). I selected for construct expression in the T1 generation by screening for pollen grain fluorescence. In the T2 generation, two independent homozygous lines for AUN1[D94N]-YFP and AUN1[H127A]-YFP were selected, respectively, and two independent heterozygous lines for *AUN1-YFP*. In the T3 generation, I conducted pollen germination assays on one line for each construct and compared the lines to WT as positive control and *aun1-1 aun2-1* as negative control (Fig. 38 and 39). The aim of this experiment

was to see whether *AUN1-YFP*, *AUN1[D94N]-YFP* or *AUN1[H127A]-YFP* can complement the low pollen germination phenotype of *aun1-1 aun2-1* mutants and to obtain an idea where *AUN1* is localized in a subcellular context.
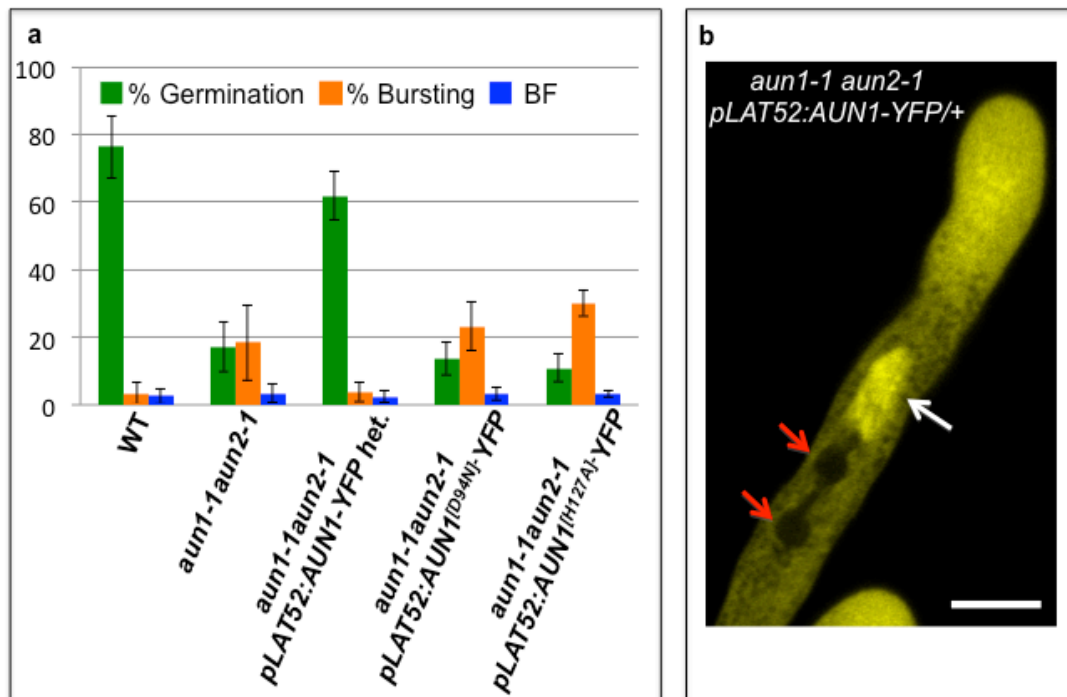
Fig. 39 *AUN1-YFP* complementation of *aun1-1 aun2-1* reveals AUN1 localization in the PT cytoplasm and vegetative nucleus. **a:** Germination and bursting rates as well as bursting fraction of WT, *aun1-1 aun2-1, aun1-1 aun2-1 AUN1-YFP (hemizygous), aun1-1 aun2-1 AUN1[D94N]-YFP* and *aun1-1 aun2-1 AUN1[H127A]-YFP*. **b:** Subcellular localization of *AUN1-YFP* in an *aun1-1 aun2-1* PT. Sperm cells are indicated by red arrows, vegetative nucleus is indicated by white arrow. Scale bar: 7µm.

In three independent pollen germination assays, WT pollen germinated on average at 76.4% with a bursting rate of 3.5% (Fig. 39a). *aun1-1 aun2-1* pollen had a low germination rate of 17.1% and a bursting rate of 18.4%. The *AUN1-YFP* hemizygous *aun1-1 aun2-1* line showed 61.8% germination and burst at 3.8%. The *aun1-1 aun2-1* line homozygous for *AUN1[D94N]-YFP* had a germination rate of 13.7% while the bursting rate accounted to 23.2%. The line homozygous for the *AUN1[H127A]-YFP* construct showed similar rates with 10.9% germination and 30.1% bursting.

The first conclusion we can draw from these results is that only the *AUN1-YFP* hemizygous line is capable of complementing the low pollen germination of *aun1-1 aun2-1*, restoring the germination rate to almost WT-like levels. The lines transformed with *AUN1[D94N]-YFP* and *AUN1[H127A]-YFP*, respectively, have a low germination rate similar to *aun1-1 aun2-1* pollen. Also, the bursting rate of *aun1-1 aun2-1* and the *AUN1[D94N]-YFP/AUN1[H127A]-YFP* transformed lines seems to be elevated. To test whether this is a sampling artifact, the bursting fraction can be determined. While the average bursting fraction of WT pollen is 2.6%, *aun1-1 aun2-1* reaches 3.3%. The hemizygous *AUN1-YFP* line has a bursting fraction of 2.3% and the two lines transformed with *AUN1[D94N]-YFP* and *AUN1[H127A]-YFP* depict bursting fractions of 3.3% and 3.2%, respectively (Fig. 39a). As all determined bursting fractions are comparable to WT, the elevated bursting rates of *aun1-1 aun2-1* and the *AUN1[D94N]-YFP/AUN1[H127A]-YFP* expressing lines indeed are sampling artifacts originating from the low germination rate.

The complementation assay also served as means to pinpoint the subcellular localization of AUN1. By live-imaging growing PTs hemizygous for the AUN1-YFP construct with confocal microscopy, we found that AUN1-YFP is present in both the PT cytoplasm and the

vegetative nucleus (Fig. 39b). This indicates that AUN1 could play a dual role in both the cytoplasm and the vegetative nucleus of the growing PT.

In summary, these results indicate that only native *AUN1* can complement the *aun1-1 aun2-1* mutant. As both the phospho-dead *AUN1[H127A]* and the dominant negative *AUN1[D94N]* versions fail to restore the low germination rate of *aun1-1 aun2-1* pollen, the phosphatase activity seems to be important for the function of *AUN1* in PT CWI maintenance. Furthermore, this supports the proposition that *AUN1[D94N]* identifies as a constitutive inactive form of AUN1. Also, these findings provide hints for a possible dual function of AUN1 in both the PT cytoplasm and the vegetative nucleus. However, the AUN1-YFP presence in the nucleus could also simply be an artifact. As AUN1 is a small protein of 36kDa and the YFP tag is also small, the fusion protein might just fit through the nuclear pores and enter the nucleus without having any function there. I will return to this topic in the discussion part of this thesis in more detail.
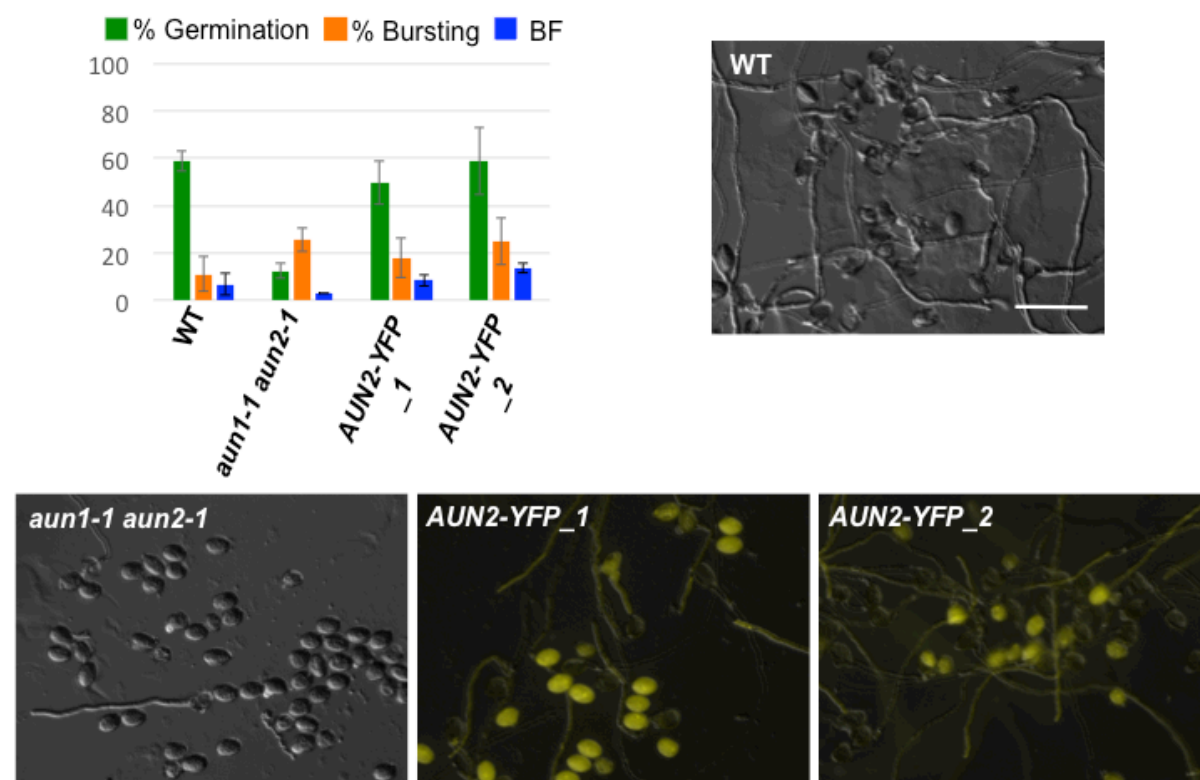
Fig. 40 *AUN2-YFP* complements the low pollen germination phenotype of *aun1-1 aun2-1.* Germination rates, bursting rates and bursting fractions of WT, *aun1-1 aun2-1* and two *aun1-1 aun2-1 AUN2-YFP* lines with representative pictures. Data originates from two independent pollen germination assays. Scale bar: 80µm.

3.2.3.6 *AUN2-YFP* is capable of complementing *aun1-1 aun2-1*

We also were interested whether *AUN2-YFP* is likewise able to complement the *aun1-1 aun2-1* low pollen germination phenotype. To address this, we cloned *AUN2* without stop codon into *p*LAT52:GW-YFP. We transformed *aun1-1 aun2-1* plants with this construct and screened for hemizygous transformants in the T1 generation by preselecting the seedlings on ½ MS plates with BASTA and subsequently monitoring fluorescence in pollen grains. We retrieved *aun1-1 aun2-1 AUN2-YFP* triple homozygous plants in the T2 generation and conducted pollen germination assays on two independent lines (referred to as *AUN2-YFP_1* and *AUN2-YFP_2* in the figure) compared to WT and untransformed *aun1-1 aun2-1* plants (Fig. 40). While WT had a germination rate of 58.8% and *aun1-1 aun2-1* pollen arrived at

12.5%, both *AUN2-YFP* expressing lines had germination rates close to WT with 49.8% and 58.5%, respectively. The bursting rates for WT and *aun1-1 aun2-1* accounted to 11.1% and 25.5%, respectively, while both *AUN2-YFP* expressing lines had bursting rates of 18.0% and 24.8%. To test, whether these high bursting rates originate from a sampling artifact in these pollen germination assays, we determined the bursting fraction. We found that the bursting fractions of the two *AUN2-YFP* lines were slightly elevated compared to the 6.7% in WT (8.6% and 13.9%, respectively) while *aun1-1 aun2-1* had a low bursting fraction of 3.1%. Furthermore, we could confirm that the *AUN2-YFP* localization is similar to the one of *AUN1-YFP* (Fig. 41). Thus, we can conclude that *AUN2-YFP* is also capable of complementing the *aun1-1 aun2-1* low pollen germination phenotype. The *AUN2-YFP* construct is clearly functional and similarly localized as *AUN1-YFP*. Also, the bursting fraction in the two *AUN2-YFP* expressing lines is slightly elevated compared to WT.
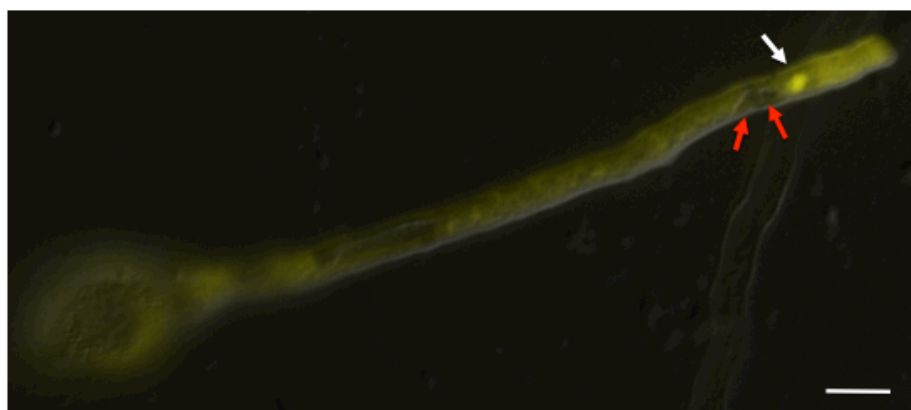
Fig. 41 Localization of *AUN2-YFP* in an *aun1-1 aun2-1* PT. Red arrows indicate the sperm cells, white arrow indicates the vegetative nucleus. Scale bar: 12µm.

3.2.4 AUN1 acts downstream of RALFL4/19 and RbohH/J in pollen tube growth

Next, we wanted to know where AUN1 is situated relative to the other members of the PT CWI pathway. From the suppressor screen and the ANX1/2-rescue assay, we already knew AUN1 was downstream of ANX1/2. To tackle this, we transformed *artificial microRNA line of rapid alkalinization factor-like 4/19 (amiRNA ralfl4/19), rbohH-3 rbohJ-3* and *mri-1/MRI* plants with *p*LAT52:AUN1-YFP and *p*LAT52:AUN1[D94N]-YFP.

RALFL4/19 are sister genes encoding putative ligands of ANX1/2 that are currently being investigated in the Grossniklaus lab and the Boisson-Dernier group. This is reminiscent of ANX1/2 homologue FER and its ligand RALF1 (Haruta et al., 2014). *RALFL4/19* are small, secreted RALF-like peptides. Downregulation of *RALFL4/19* by artificial microRNAs results in precocious pollen bursting and thus short siliques, just like in *anx1 anx2* and *rbohH rbohJ* mutants (Grossniklaus and Boisson-Dernier, unpublished).

All three lines exhibit a precocious pollen bursting phenotype but only *amiRNA ralfl4/19* and *rbohH-3 rbohJ-3* are male sterile. In contrast, *mri-1/MRI* plants exhibit an almost WT-like seed set. While *amiRNA ralfl4/19* and *rbohH-3 rbohJ-3* are homozygous lines, *mri-1/MRI* homozygous plants cannot be obtained.

The aim of this experiment was to investigate the seed set of homozygous transformed plants for each construct and subsequently conduct pollen germination assays, in order to see, if PT growth behavior of the male sterile plants is changed by transformation with any of the constructs.

3.2.4.1 AUN1 acts downstream of RALFL4/19

After transforming *amiRNA ralfl4/19* with *p*LAT52:AUN1-YFP and *p*LAT52:AUN1[D94N]-YFP, three independent lines with good fluorescence in pollen grains were selected in the T1 generation for each construct. In the T2 generation, the seed set of two or three homozygous plants per line was analysed (Fig. 42). As can be seen, *amiRNA ralfl4/19* siliques contain on average 7.8 seeds. In the 9 T2 lines homozygous for *AUN1[D94N]-YFP*, seed set values range between 21.1 and 36.2 seeds per silique. Thus, all of the investigated lines show a seed set rescue compared to untransformed *amiRNA ralfl4/19* plants. When it comes to the 8 *amiRNA ralfl4/19* plants homozygous for *AUN1-YFP*, the average seed set ranges between 4.6 and 13.9 seeds per silique, which is comparable to the seed set of *amiRNA ralfl4/19* plants. Consequently, *AUN1-YFP* transformation is not sufficient to increase the seed set of *amiRNA ralfl4/19* plants.
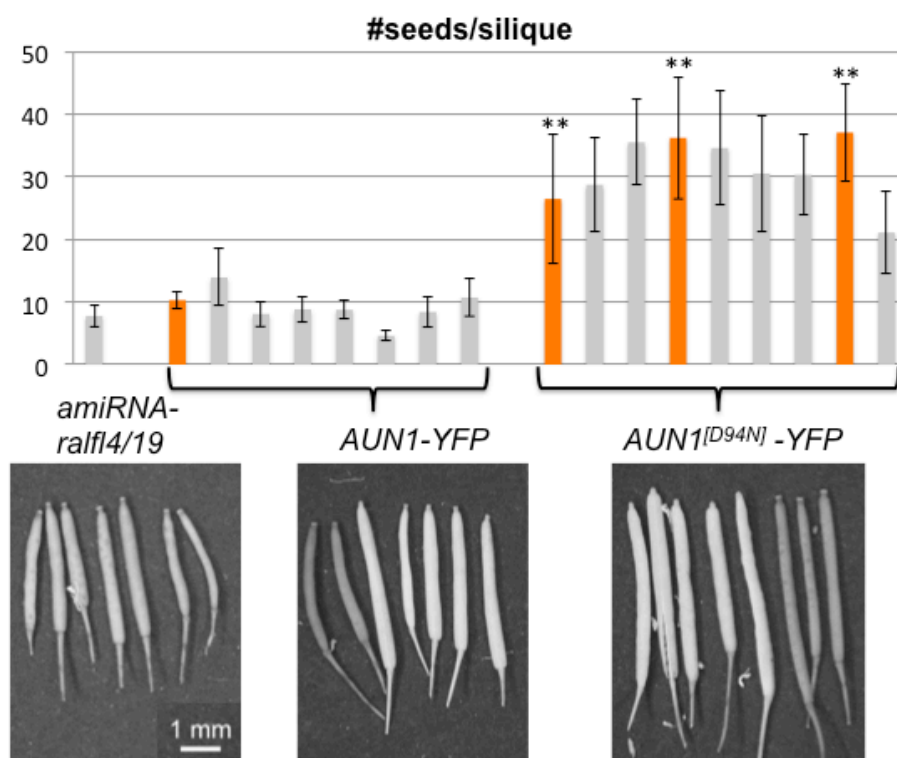
Fig. 42 *AUN1[D94N]-YFP* expression rescues the seed set of *amiRNA ralfl4/19* plants. Seed set analysis of *amiRNA ralfl4/19*, amiRNA ralfl4/19 *AUN1-YFP* and *amiRNA ralfl4/19 AUN1[D94N]-YFP* plants. All depicted data originates from 11-14 siliques. Orange color marks the lines selected for pollen germination assays. Asterisks denote significant differences in the seed set compared to *rbohH-3 rbohJ-3* plants (*P<0.001* for the three *AUN1[D94N]-YFP* lines, Student's *t* test).

If a seed set rescue can be observed after *amiRNA ralfl4/19* transformation with *AUN1[D94N]-YFP*, this could indicate that in these lines more seeds are formed, as more ovules are fertilized. Consequently, the precocious pollen bursting might be decreased. To test this, I took three representative *AUN1[D94N]-YFP* transformed lines and one representative *AUN1-YFP* transformed line to the T3 generation to assess the PT growth behavior *in vitro* compared to *amiRNA ralfl4/19* (Fig. 43)*. I conducted three independent rounds of pollen germination assays. Normally, *amiRNA ralfl4/19* pollen has a germination rate of 79.3% with a bursting rate of 47.7%. The three representative lines transformed with the *AUN1[D94N]-YFP* constructs have germination rates of 34.6%, 42.2% and 40.6%, respectively. Their bursting rates account to 26.6%, 29.6% and 31.9%, respectively. The one line expressing *AUN1-YFP*

shows a pollen germination rate of 69.1% and a bursting rate of 52.5%. These results demonstrate that the *AUN1-YFP* transformed line behaves *amiRNA ralfl4/19*-like *in vitro* as well. Thus, *AUN1-YFP* is definitely not capable of rescuing the *amiRNA ralfl4/19* pollen bursting phenotype. When the three *AUN1[D94N]-YFP* homozygous lines are concerned, both, the germination and the bursting rate, are decreased compared to *amiRNA ralfl4/19* pollen. This shows that AUN1[D94N] executes two tasks: it inhibits pollen germination and it prevents pollen bursting. A decreased bursting rate can either originate from an increased production of PTs or a decreased frequency of pollen bursting. If the bursting fraction is determined, we find that *amiRNA ralfl4/19* pollen and *AUN1-YFP* transformed pollen have comparable bursting fractions of 37.5% and 32.8%, respectively. In contrast, the three *AUN1[D94N]-YFP* transformed lines depict considerably decreased bursting fractions of 8.9%, 12.3% and 13.0%. Thus, the observed decrease in the bursting rate of pollen from the *AUN1[D94N]-YFP* lines originates from a lower number of pollen bursting events.
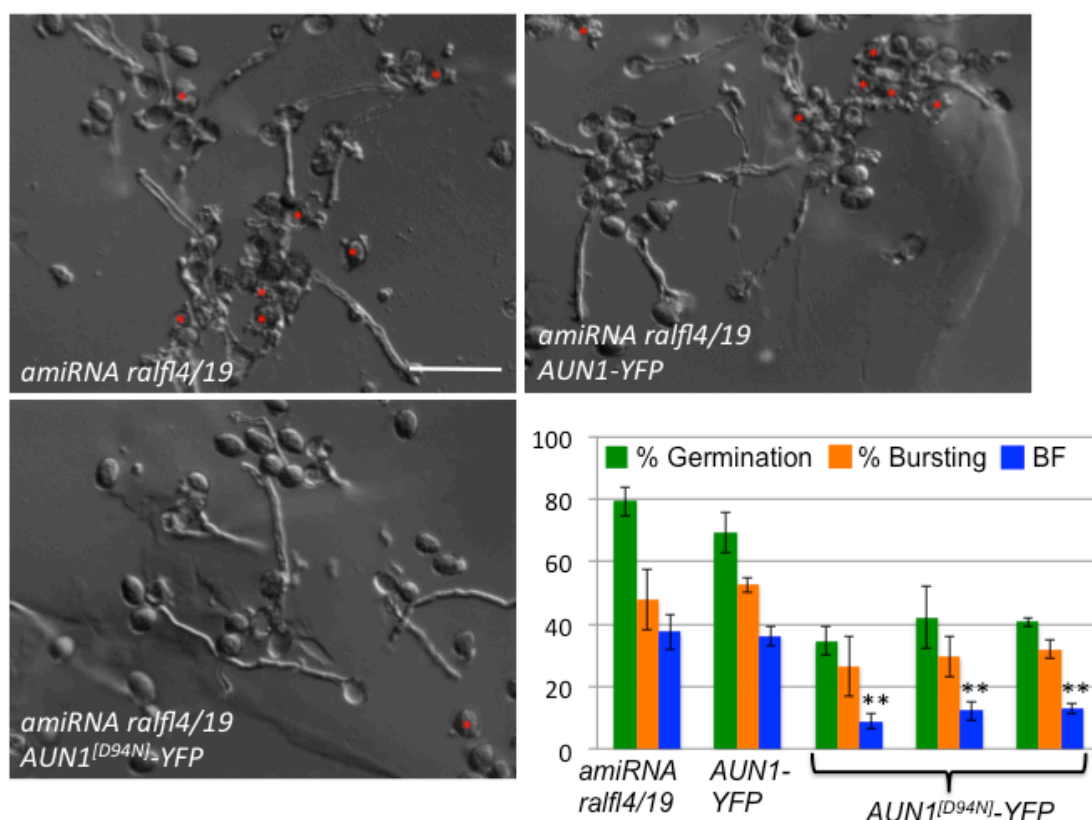
Fig. 43 *AUN1[D94N]-YFP* expression rescues the pollen bursting of *amiRNA ralfl4/19* plants. Representative images of *amiRNA ralfl4/19, amiRNA ralfl4/19 AUN1-YFP* and *amiRNA ralfl4/19 AUN1[D94N]-YFP* pollen germination assays. Red asterisks indicate burst pollen grains. Scale bar: 80µm. Germination rate, bursting rate and bursting fraction from three independent pollen germination assays. Black asterisks indicate significant differences in the bursting fraction compared to *amiRNA ralfl4/19* ($P<0.0024$ for all three *AUN1[D94N]-YFP* lines, Student's *t* test).

In summary, these results indicate that AUN1[D94N], but not AUN1, is capable of rescuing the pollen bursting phenotype of *amiRNA ralfl4/19 in vivo* and *in vitro,* possibly by reducing the frequency of pollen bursting events. Also, this confirms that AUN1 acts downstream of RALFL4/19, which makes sense in light of the fact that AUN1 acts downstream of ANX1/2 which likely interact with RALFL4/19 (Grossniklaus, pers. comm.).

3.2.4.2 AUN1 acts downstream of RbohH/J

Following the transformation of *rbohH-3 rbohJ-3* plants with *p*LAT52:AUN1-YFP and *p*LAT52:AUN1[D94N]-YFP, a screen for fluorescence in pollen grains was performed in the T1 generation. For the AUN1[D94N]-YFP construct, three lines were selected, for AUN1-YFP, one line was selected. In the T2 generation, a seed set analysis was conducted for two-three plants per line that were homozygous for the respective construct. The seed set was compared to untransformed *rbohH-3 rbohJ-3* plants. The number of siliques analysed was 9-13 per plant.

rbohH-3 rbohJ-3 plants exhibit an average of 6.3 seeds per silique (Fig. 44). In the eight homozygous lines for *AUN1[D94N]-YFP*, the seed set values ranged between 22.8 and 41.8 seeds/silique. The three lines homozygous for *AUN1-YFP* had seed set numbers between 11.5 and 16.8 seeds/silique. Thus, all of the *AUN1[D94N]-YFP* transformed *rbohH-3 rbohJ-3* plants show a strong increase in seed set and, surprisingly, the *AUN1-YFP* expressing lines show a slight seed set rescue as well. Thus, *in vivo,* both constructs appear to be able to rescue *rbohH-3 rbohJ-3* sterility. I picked three representative lines for *AUN1[D94N]-YFP* and one line for *AUN1-YFP* to conduct pollen germination assays in the T3 generation with *rbohH-3 rbohJ-3* as pollen bursting control.
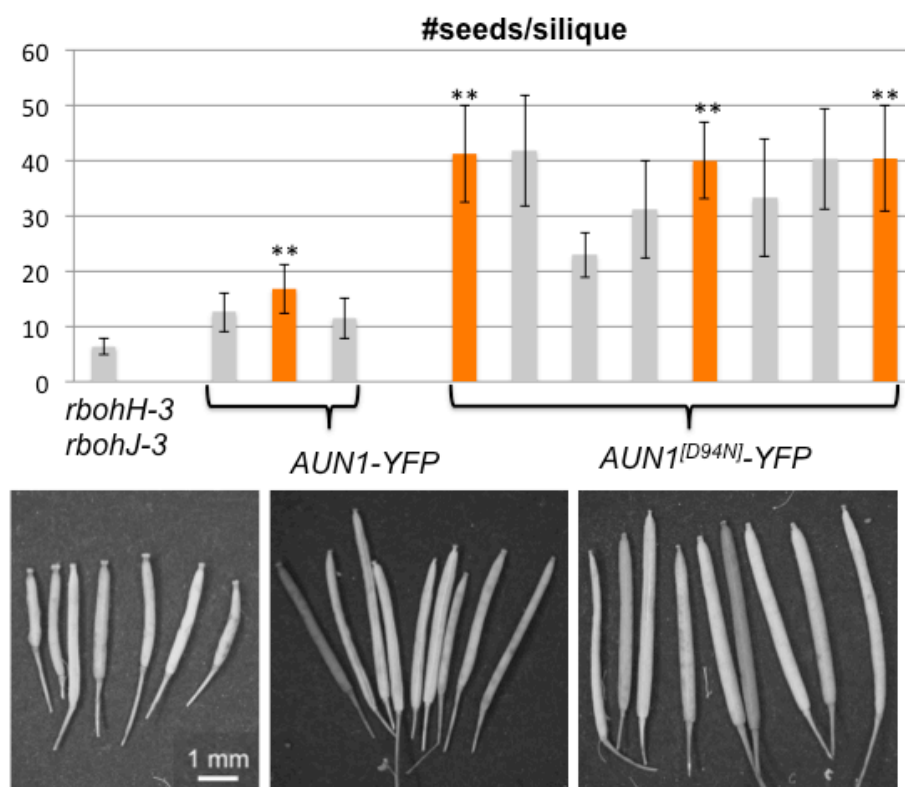
Fig. 44 *AUN1[D94N]-YFP* and *AUN1-YFP* expression rescues the seed set of *rbohH-3 rbohJ-3* plants. Seed set analysis of untransformed *rbohH-3 rbohJ-3, rbohH-3 rbohJ-3 AUN1-YFP* and *rbohH-3 rbohJ-3 AUN1[D94N]-YFP* plants. The lines chosen for pollen germination assays are marked in orange. Asterisks denote significant differences in the seed set compared to *rbohH-3 rbohJ-3* plants ($P<0.001$ for the three *AUN1[D94N]-YFP* lines and the *AUN1-YFP* line, Student's *t* test).

In three independent pollen germination assays, *rbohH-3 rbohJ-3* pollen germinated at 81.5% and burst at 84.1% (Fig. 45). The three *AUN1[D94N]-YFP* expressing lines showed low germination rates of 46.2%, 26.7% and 46.4%, respectively, with bursting rates of 78.7%, 81.4% and 76.1%. The *AUN1-YFP* line depicted a pollen germination rate of 65.7% with a

bursting rate of 78.8%. The most striking discovery in this result is that it appears that none of the constructs appears to be able to reduce pollen bursting even though all lines depicted a seed set rescue. The only parameter that changes is the germination rate. While the three *AUN1[D94N]-YFP* exhibit a strongly reduced pollen germination rate, *AUN1-YFP* appears to be slightly impaired in pollen germination. For *AUN1[D94N],* this PT growth inhibitory effect is familiar from when we expressed the construct in WT or *amiRNA ralfl4/19* background. However, why AUN1 shows a slight reduction of germination as well is unclear. As the *AUN1[D94N]* transformed lines exhibit such a low germination rate, I determined the bursting fraction to rule out that the bursting rate is artificially elevated by a sampling artifact. *rbohH-3 rbohJ-3* pollen exhibits a bursting fraction of 68.5%. The three *AUN1[D94N]* expressing lines have bursting fraction values of 36.4%, 21.6% and 35.7%, respectively. The *AUN1-YFP* line has a bursting fraction of 51.7%. Thus, if we consider the total number of pollen grains, the pollen bursting fraction - and thus the pollen bursting frequency - is significantly reduced in all four lines compared to *rbohH-3 rbohJ-3*. Consequently, the elevated amount of non-germinating pollen grains in these lines might originate from pollen grains that would have burst under normal *rbohH-3 rbohJ-3* conditions. This means that AUN1 and AUN1[D94N] in fact do influence the *rbohH-3 rbohJ-3* pollen bursting but in a very subtle way that brings the pollen germination assay to the limits of its sensitivity. In the discussion part of the thesis, I will review possible interpretations of this result in detail.
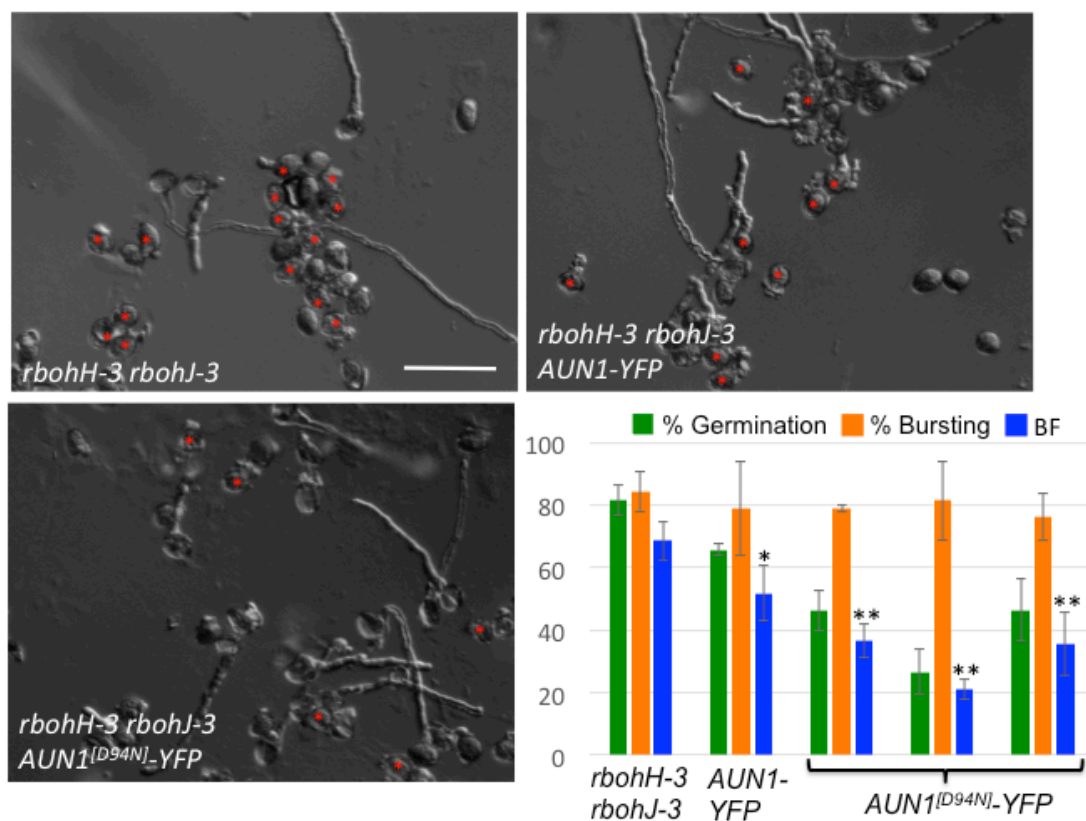
Fig. 45 *AUN1[D94N]-YFP* and *AUN1-YFP* expression rescues the pollen bursting of *rbohH-3 rbohJ-3* plants. Representative images of pollen germination assays of untransformed *rbohH-3 rbohJ-3* and selected *rbohH-3 rbohJ-3 AUN1-YFP* as well as *rbohH-3 rbohJ-3 AUN1[D94N]-YFP* lines. Red asterisks indicate burst pollen grains. Black asterisks denote significant differences in the bursting fraction compared to *rbohH-3 rbohJ-3* plants ($P<0.0082$ for the three *AUN1[D94N]-YFP* lines, $P=0.043$ for the *AUN1-YFP* line, Student's *t* test). Scale bar: 80μm.

To summarize, it appears that both *AUN1* and *AUN1[D94N]* are capable of rescuing the sterility of *rbohH-3 rbohJ-3* to various extents *in vivo*. However, *in vitro* pollen germination

experiments could not demonstrate a reduction in pollen bursting rate for any of the two constructs. If the entire pool of counted pollen grains is considered, the pollen bursting fraction is significantly reduced in all three $AUN1^{[D94N]}$-YFP expressing lines and a bit weaker also in the $AUN1$-YFP expressing line. Thus, we can conclude that $AUN1^{[D94N]}$ and $AUN1$ can rescue the male sterility of rbohH-3 rbohJ-3 and that AUN1 acts downstream of RbohH/J.

3.2.4.3 AUN1 does not act downstream of MRI

As previously reported, homozygous mri-1 plants cannot be found. Thus, we transformed mri-1/MRI plants with pLAT52:AUN1-YFP and pLAT52:AUN1$^{[D94N]}$-YFP to screen for homozygous mri-1 plants in the T2 generation. This would indicate that the respective construct is capable of rescuing the mri-1 male sterility phenotype and that AUN1 acts downstream of MRI. In the T1 generation, I selected two lines with good fluorescence in pollen for $AUN1$-YFP and four lines for $AUN1^{[D94N]}$-YFP. In the T2-generation, I screened for homozygous $AUN1$-YFP / $AUN1^{[D94N]}$-YFP mri-1/MRI plants. Subsequently, in the T3 generation, I chose one homozygous $AUN1$-YFP / $AUN1^{[D94N]}$-YFP plant per line, respectively, and genotyped 24 plants of each of the two $AUN1$-YFP and the four $AUN1^{[D94N]}$-YFP expressing lines in search for mri-1 homozygous plants. However, I could not retrieve a single mri-1 homozygous plant out of 48 genotyped $AUN1$-YFP and 96 $AUN1^{[D94N]}$-YFP expressing plants. This is striking, compared to how we obtained 29 mri-1/mri-1 plants in the T2 generation when we introduced MRI-YFP in mri-1/MRI plants (Boisson-Dernier et al., 2015). Thus, AUN1 does not seem to act downstream of MRI, as in this case homozygous mri-1 plants should have been found.

These results indicate that AUN1 can be positioned in the PT CWI pathway downstream of RALFL4/19, ANX1/2 and RbohH/J and upstream - or at the same level in a parallel pathway - of MRI (Fig. 46).
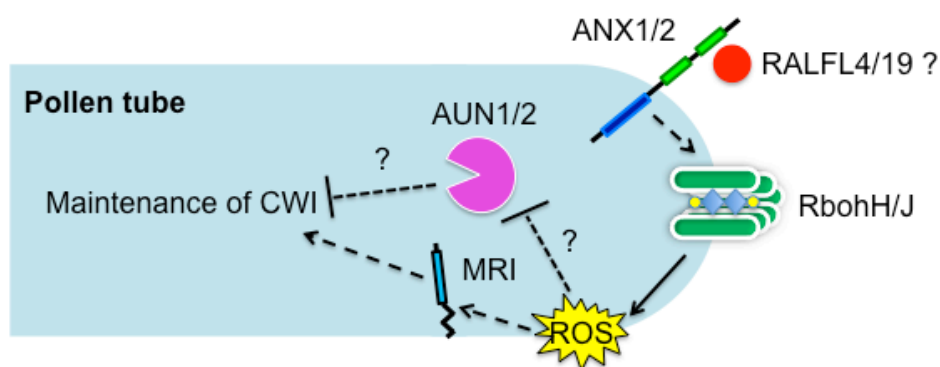
Fig. 46 Schematic representation of AUN1/2 in the PT CWI pathway.

3.2.5 Summary

In summary, we could show that AUN1/2 are negative regulators of the CWI pathway in PTs and possibly in RHs as well. Disruption of AUN1/2 has growth inhibitory effects on both PTs and RHs. AUN1/2 are Ser/Thr-protein phosphatases that localize to the cytoplasm and the vegetative nucleus of growing PTs. AUN1 acts downstream of ANX1/2 and RbohH/J. Also, AUN1$^{[D94N]}$ is a dominant inactive variant of AUN1 that is capable of rescuing amiRNA

ralfl4/19, anx1 anx2 and *rbohH-3 rbohJ-3* pollen bursting. *AUN1*$^{[D94N]}$ expression in WT background has a strong growth inhibitory effect on pollen and a weaker inhibitory effect on RH growth.

4. DISCUSSION

The aim of this work was the elucidation of novel components in the PT CWI pathway. PTs require a close coordination between internal growth machineries and CWI maintenance in order to sustain stable growth. If this coordination is disturbed, cessation of growth or precocious bursting of the PT can be the consequences. The discovery of the importance of *Cr*RLK1Ls ANX1/2 in PT growth laid the foundation for this PhD thesis. ANX1/2 are localized at the PT plasma membrane and preferentially at the tip-region. *anx1 anx2* double mutant pollen were found unable to form a PT *in vitro,* due to precocious pollen bursting (Boisson-Dernier et al., 2009; Miyazaki et al., 2009). In contrast, *ANX1/2* over-expressor pollen was found to form short PTs with wide tips from pectinuous CW-material over-accumulations. In addition, invaginations of the plasma membrane frequently accompanied this phenotype (Boisson-Dernier et al., 2013).

With the finding, that NADPH-oxidases RbohH/J act downstream of ANX1/2 in PT growth, the first downstream constituents were described (Boisson-Dernier et al., 2013). Not only was the presence of RbohH/J important for observing the ANX1/2 over-expressor phenotype, but the two partially redundant Rbohs were found to be vital for producing ROS at the PT tip and for the maintenance of a stable tip-focussed Ca^{2+} gradient during PT growth. In *rbohH rbohJ* double mutants, Ca^{2+} and ROS homeostasis is perturbed, leading to oscillatory growth behavior and precocious bursting in these PTs (Boisson-Dernier et al., 2013; Lassig et al., 2014).

To discover novel signaling constituents in the ANX1/2-dependent CWI pathway, we treated *anx1 anx2* mutant seeds with EMS and screened for a rescue of the *anx1 anx2* male sterility in the M1 generation. By this means, we were able to identify 32 suppressor mutants, the *ipr*s. Two of these were investigated in detail in this PhD thesis, namely *ipr7 (AUN1^[D94N])* and *ipr19 (MRI^[R240C]).* The *ipr19* mutation targets a gene encoding a RLCK-VIII member, MRI, and appears to render the kinase more efficient in activating the downstream CWI maintenance machinery. In contrast, the *ipr7* mutation is situated in a gene encoding a TOPP family member, AUN1, with a close homologue, AUN2. AUN1 and AUN2 show partial functional redundancy in PT growth. The D94N substitution apparently renders the phosphatase non-functional and constitutively inhibits its downstream signaling cascade.

4.1 The role of MRI and AUN1/2 in pollen tube growth

With MRI and AUN1/2, we have discovered three novel regulators of the ANX1/2-dependent CWI pathway in PTs. MRI is a positive regulator of PT growth while AUN1/2 act as negative regulators. All three genes act downstream of RbohH/J. However, whether AUN1/2 act in a parallel pathway or upstream of MRI remains to be elucidated. We crossed *aun1-1 aun2-1* plants with *mri-1/MRI* plants and were able to retrieve 2 *aun1-1 aun2-1 mri-1/MRI* plants in the T2 generation by genotyping (out of 11 plants total). Pollen germination assays on these plants might provide hints on whether AUN1/2 are upstream of MRI or in a parallel pathway (Fig. 47). If MRI were upstream of AUN1/2, which is to be excluded from our previous experiments, we would expect very low pollen germination, just as with *aun1 aun2* pollen. If AUN1/2 were upstream of MRI, *aun1-1 aun2-1 mri-1/MRI* pollen would burst like *mri-1/MRI* pollen. In the case that MRI and AUN1/2 were in parallel pathways, the outcome cannot be predicted so clearly. We either could envision the occurrence of pollen bursting together with low pollen germination or even normal growth, as the contradicting phenotypes could cancel each other out. However, this hypothesis remains to be tested.
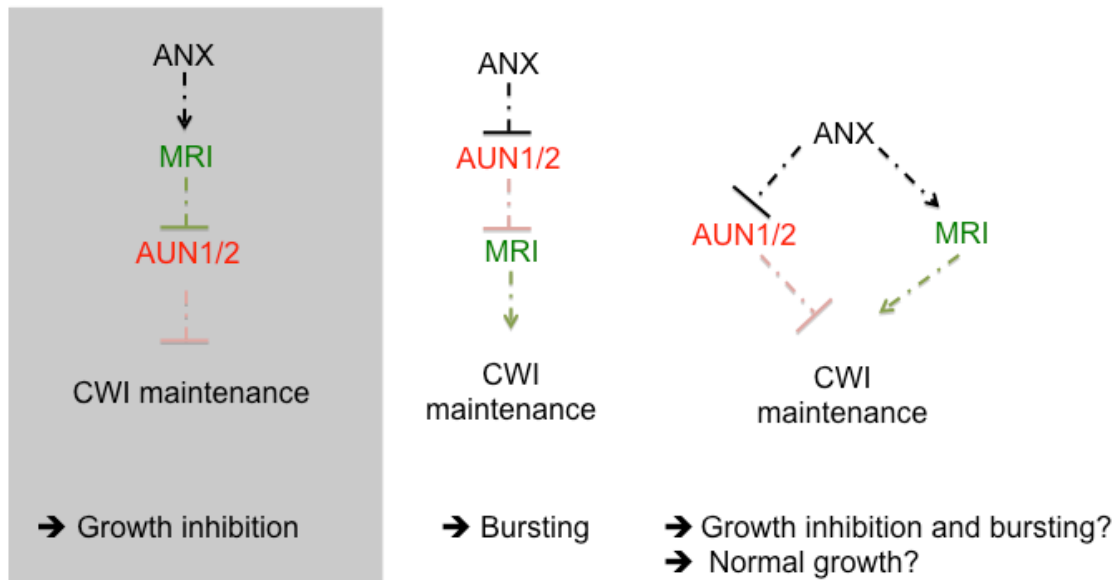
Fig. 47 Putative scenarios for MRI and AUN1/2 with predicted outcomes of the triple *aun1-1 aun2-1 mri-1/MRI* mutant indicated below. Grey color indicates least expected scenario.

4.1.1 The hypermorphic MRI[R240C] allele

MRI is essential for PT growth, since we discovered that *mri* knock-out pollen bursts just as *anx1 anx2* or *rbohH rbohJ* pollen. Transformation with the hypermorphic *MRI[R240C]* allele is able to efficiently rescue pollen bursting in *anx1 anx2* and *rbohH rbohJ* mutant background. Also, WT plants transformed with *MRI[R240C]* show a strong reduction in pollen germination. This indicates that MRI[R240C] is more efficient than native MRI in activating the CWI pathway, possibly due to constitutive over-activation of the downstream pathway triggered by the R240C amino acid substitution. This over-activation could have several reasons. First, the kinase activity of MRI itself might be enhanced (Boisson-Dernier et al., 2015). Also, MRI[R240C] might be more resistant to degradation or inactivation than native MRI. Additionally, MRI[R240C] could be more efficient in interacting with up-/ or downstream interaction partners.

To test whether the kinase activity is enhanced in MRI[R240C], a kinase assay with MRI and MRI[R240C] could be initiated. This could elucidate whether MRI and its mutant form R240C have functional kinase activity in the first place and whether the kinase activity is required for MRI function during PT growth. Also, if MRI has functional kinase activity, this would demonstrate whether there are differences in the activity of MRI and MRI[R240C].

Another arising question is why the R240 substitution renders MRI more active. The R240 is part of the conserved STR motif in RLCK-VIII proteins. MRI is a member of the RLCK-VIII family of RLKs, just like tomato Pti1. Pti1 is phosphorylated by kinase Pto at Threonin 233 (Sessa et al., 2000). In contrast, in *Arabidopsis,* kinase OXI1 phosphorylates Pti1-2 at T238 (Anthony et al., 2006). In MRI, this T corresponds to T239, next to R240 in the conserved STR motif. It is thus likely that the R240C substitution either facilitates phosphorylation at T239 or mimics a phosphorylated T239.

Recently, Aurélien Boisson-Dernier tackled these questions (Boisson-Dernier, unpublished). He generated several MRI variants by site-directed mutagenesis. First, he substituted the K100 with either N or E, generating MRI[K100N] and MRI[K100E]. The invariant K is a conserved residue in protein kinases that is critical for orienting ATP for catalysis (Roskoski, 2012). Thus, replacing the K100 with other amino acids should generate kinase-dead versions of

MRI (Hanks et al., 1988). This would help to elucidate whether the kinase activity of MRI is required for its function in tip-growth. Boisson-Dernier also generated MRI[T239A] and MRI[T239E], substituting the T239, to test whether phosphorylation at this residue is essential for MRI functionality. Lastly, he obtained MRI[R240M], MRI[R240A] and MRI[R240S] to test whether the loss of the R residue or the introduction of the C renders MRI[R240C] over-active.

First, he introduced all of these *MRI* variants into *p*MRI:GW-YFP and transformed *mri-1/MRI* plants with them. In the T2 generation, he screened for the occurrence of *mri-1* homozygous lines by genotyping, which would indicate that the respective construct is functional and complements *mri-1*. Indeed, he obtained *mri-1* homozygous plants in all transformed lines, even in MRI[K100N]- and MRI[K100E]- transformed progeny. This indicates that all constructs are functional, that the kinase activity of MRI is not required for its function in tip-growth and that there is no requirement of phosphorylation at the T239.

Next, he wanted to test whether MRI[R240C] really is an over-active form of MRI. From the previous experiments, we knew that MRI[R240C] expression in *rbohH-3 rbohJ-3* plants rescues the *rbohH rbohJ* male sterility. To test whether any of the other *MRI[R240x]* variants can rescue *rbohH rbohJ* male sterility, Boisson-Dernier transformed *rbohH rbohJ* mutants with the *MRI* variants (Boisson-Dernier, unpublished). He discovered that all R240 variants were able to trigger the production of elongated siliques with higher seed set than *rbohH rbohJ* untransformed plants. Thus, all R240 variants of MRI are over-active, as is MRI[R240C]. This demonstrates that the loss of the R rather than the introduction of the C renders MRI[R240C] over-active. The mechanism for this auto-inhibition by R remains unknown to date.

4.1.2 Putative targets of MRI

Another intriguing question in this context is what kind of targets MRI could have. In the Boisson-Dernier group, it could be demonstrated that *mri-2* PTs depict similar irregular growth rates and Ca^{2+}-gradient instabilities as *rbohH rbohJ* PTs (Westermann and Boisson-Dernier, unpublished). This was investigated by means of combining the expression of the genetically encoded Ca^{2+} sensor YellowCameleon3.6 with confocal laser-scanning microscopy, as described in Franck et al. (2017). This indicates that MRI might be acting upstream of and possibly interacting with Ca^{2+}-channels that maintain and finetune the Ca^{2+}-gradient vital for tip-growing cells. Interestingly, Ogasawara et al. (2008) demonstrated that RbohD, a homologue of RbohH/J, is synergistically activated by phosphorylation and Ca^{2+}. Thus, it might also be possible that MRI interacts with the pollen-expressed RbohH/J.

4.1.3 The low pollen germination of *aun1 aun2* requires a novel pollen bursting quantification method

In contrast to *MRI*, *AUN1/2* are essential for pollen germination, since *aun1 aun2* pollen display very low germination rates. At the same time, *aun1 aun2* pollen exhibits seemingly higher bursting rates. This however is a sampling artifact originating from the selection of imaging zones in a pollen germination assay. During the latter, we consistantly choose the zones with the highest germination rates that include both PTs and burst pollen grains. However, with mutants that struggle to produce PTs, the imaged zones thus consist of mostly burst pollen grains, which artificially boost the bursting rate. To eliminate this artifact, I have found a different way to interpret the data, which is by determining the bursting fraction. The bursting fraction takes the total number of pollen grains into account instead of only the germinated ones. Therefore, we can compare whether the amount of burst pollen grains relative to all observed pollen grains changes in between lines. For mutants with low pollen

germination phenotypes, this can be a more accurate approach to quantify changes in pollen bursting.

4.1.4 The bursting fraction appropriately reflects pollen bursting differences in lines with low germination

The high bursting fraction of *amiRNA ralfl4/19* and *rbohH-3 rbohJ-3* plants can be decreased by transformation with the amorphic allele *AUN1[D94N]*. In *amiRNA ralfl 4/19* background, the bursting rate is already visibly decreased in *AUN1[D94N]* transformed lines and the rescue effect is merely emphasized when determining the bursting fractions. In *rbohH-3 rbohJ-3* background however, the bursting rates of untransformed and *AUN1/AUN1[D94N]* transformed lines are similar. This is striking, since in the seed set analysis, we previously had discovered that both *AUN1* and *AUN1[D94N]* were able to rescue the seed set of *rbohH rbohJ* plants to various extents. This means that with our traditional counting method of the bursting rate, the pollen germination assay is at the limits of its sensitivity. However, when the bursting fraction is determined, we observed a significant decrease in pollen bursting of the *AUN1/ AUN1[D94N]* transformed lines, reflecting what we observed during the seed set analysis. Thus, the bursting fraction more accurately represents pollen bursting in lines with low pollen germination.

4.1.5 AUN1[D94N] might be a constitutively inactive form of AUN1

When we transformed WT plants with *AUN1* and *AUN1[D94N]*, respectively, we observed opposite phenotypes in pollen. While *AUN1* transformed WT pollen moderately burst, *AUN1[D94N]* transformed pollen had strongly decreased pollen germination rates. This is in concordance with the low germination rates in *AUN1[D94N]* transformed *amiRNA ralfl4/19* and *rbohH-3 rbohJ-3* plants. This indicates, that AUN1[D94N] might be a constitutively inactive, dominant form of AUN1. It might no longer possess its phosphatase activity, as we found that *AUN1[D94N]* cannot complement the *aun1 aun2* low pollen germination phenotype just as the phospho-dead *AUN1[H127A]*. To test whether this is true, we are currently trying to establish a protein phosphatase assay with AUN1, AUN1[D94N] and AUN1[H127A]. I cloned the three coding sequences into expression vectors with an N-terminal GST and a C-terminal His-Tag. The constructs are then transformed in *E. coli BL21 RIL* cells and protein expression is induced via IPTG. Subsequently, the proteins are isolated and purified in a pull-down assay. The two tags make the fusion protein suitable for two distinct pull-down methods, in case one method does not work. Thereafter, the protein phosphatase assay with a suitable substrate and a control phosphatase would reveal, whether native AUN1 possesses phosphatase activity and whether AUN1[D94N] and AUN1[H127A] indeed lack phosphatase activity.

It would also be interesting to test, whether *anx1 anx2* and *rbohH rbohJ* pollen bursting phenotypes can be rescued by transformation with AUN1[H127A]-YFP. This would be an indication, that any mutation in the core catalytic domain of AUN1 that renders the phosphatase inactive also constitutively inhibits the downstream pathway. Additionally, WT plants could be transformed with AUN1[H127A]-YFP to see if this triggers a similar decrease in pollen germination as transformation with AUN1[D94N]-YFP.

4.1.6 AUN1 might play a dual role in both the vegetative nucleus and the pollen tube cytoplasm

When we complemented the *aun1 aun2* low pollen germination phenotype with AUN1-YFP and AUN2-YFP, we also discovered that AUN1/2 are localized in the PT cytoplasm and vegetative nucleus. While this localization pattern could be an artifact, originating from AUN1/2 being small proteins and thus able to enter the nucleus via nuclear pores without executing a function, there are indications that indicate otherwise. It is known for other members of the *Arabidopsis* TOPP family that they are negative regulators in their respective pathways and that they can be localized in different areas within the cell. *TOPP4* is known to be a negative regulator involved in processes like gibberellic acid-mediated growth, where it controls the degradation of nuclear localized DELLA proteins (Qin et al., 2014), pavement cell morphogenesis, where it mediates PIN1 dephosphorylation at the plasma membrane (Guo et al., 2015), and phytochrome-dependent light responses, where it regulates PIF5 stability in the nucleus (Yue et al., 2016). It is found in the cytoplasm, vegetative nucleus and at the plasma membrane. Another family member, *TOPP1,* negatively regulates abscisic acid signaling (Hou et al., 2016) and has been reported to localize to both cytoplasm and nucleus. Thus, the AUN1/2 localization in the PT suits prior observations in other TOPP family members. However, to date we have not identified possible downstream targets of AUN1/2. Thus, it remains to be elucidated whether AUN1/2 primary function is in the nucleus or in the cytoplasm.

To date, proteins interacting with TOPP family members are still largely unknown. The TOPP family is related to PP1, a eukaryotic Ser/Thr phosphatase mediating various cellular processes in animals like cell cycle progression, transcription, protein synthesis, carbohydrate metabolism, muscle contraction and neuronal signaling (Bollen, 2001; Cohen, 2002; Ceulemans and Bollen, 2004; Takemiya et al., 2009). It consists of a catalytic subunit (PP1c) and diverse distinct regulatory subunits that determine specificity of the catalytic activity, specificity of the substrate and subcellular localization. The PP1c itself is highly conserved throughout eukaryots and it has 9 *Arabidopsis* isoforms, comprised in the TOPP family, three isoforms in humans, four in *Vicia faba* and five in *Oryza sativa* (Kaul et al., 2000; Kerk et al, 2002; Matsumoto et al., 2005; Takemiya et al., 2006).

Takemiya et al. (2009) identified inhibitor-3 (Inh3) in both *Vicia faba* and *Arabidopsis* as regulatory subunit of plant PP1. They found that Inh3 interacts with all 9 TOPPs *in vitro* and with TOPP4 *in vivo* and that Inh3 localizes to the cytoplasm and nucleus, in concordance with previously described TOPP4 and AUN1/2 localizations. Inh3 inhibits the PP1c catalytic activities. Takemiya et al. propose that *At*Inh3 either targets PP1cs to the nucleus or stabilizes them by forming complexes that aggregate in the nucleus. Interestingly, they also discovered reduced fertility in *At*Inh3-RNA interference lines. They report that all 3 lines exhibit shorter siliques. It would be interesting to test if the reduced fertility of these lines originates from precocious pollen bursting. The reasoning behind is that AUN1/2 and Inh-3 could maybe also interact in PTs. According to the *Arabidopsis* eFP Browser, Inh-3 shows strongest expression in mature pollen. Moreover, Inh-3 was shown to inhibit PP1c catalytic activity. Thus, reduced levels of Inh-3 could result in higher AUN1/2 phosphatase activity. This could be mimicked by over-expression of AUN1, as higher AUN1 levels would lead to a similar effect as normal levels of over-active AUN1. We previously demonstrated that in WT background, transformation with *AUN1-YFP* leads to moderate pollen bursting. Thus, it is not unlikely that the reduced fertility in these RNAi lines partially originates from precocious pollen bursting, which could be tested by requesting the *At*Inh3-RNAi lines and performing pollen germination assays on them.

Another possible downstream constituent of AUN1/2 is the GTPase ROP1. This hypothesis is based on an interesting finding of ROP1 homologue ROP2 regulating cytoskeleton reorganization during pavement cell lobe formation and outgrowth. The cortical F-actins, promote pavement cell lobe formation and outgrowth while the cortical MTs are arranged transversely at the neck regions and restrict cell expansion in pavement cells (Fu et al., 2005). ROP2 has two functions in pavement cell lobes: it activates RIC4, which promotes diffuse cortical F-actin assembly, and it represses RIC1 that promotes MT assembly. This reminds of the previously described contradictory functions of ROP1, which activates RIC4 promoting F-actin assembly and also activates RIC3 promoting F-actin disassembly (Gu et al., 2005). Guo et al. (2005) discovered that TOPP4 positively regulates ROP2. Consequently, in *topp4-1* mutants, the cytoskeleton of pavement cells was disorganized and the pavement cells exhibited less lobes compared to WT plants. Thus, it is possible that in PTs, AUN1/2 also regulate cytoskeleton reorganization via ROP1. The *aun1 aun2* low pollen germination rate could originate from slower cytoskeleton reorganization, as ROP1 would no longer be activated by AUN1/2 and thus would not activate RIC3 and RIC4. However, this hypothesis remains to be tested e.g. by visualizing the cytosekeleton with a cytoskeleton marker in *aun1 aun2* PTs.

Additionally, there are two other candidates we could envision as AUN1 targets. For example, proton pump AHA2 in RHs and/or a pollen homologue AHA8 would be possible. This hypothesis is based on the observation that fungal *Fusarium oxysporum* –RALF (F-RALF) mimics RALF1 during infection and invasion (Masachis et al., 2016). F-RALF supposedly binds to FER, which in response might phosphorylate AHA2. The phosphorylation renders AHA2 less active and subsequently, the extracellular pH increases. This alkalinization is sensed by the fungal kinase FMK1 that is phosphorylated and subsequently increases the infection potential. Furthermore, it is known that RALF1 triggers alkalinization of the extracellular matrix in roots that correlates with stall of growth (Haruta et al., 2014). The alkalinization renders the CW less extensible. In growing PTs, the tip-focused Ca^{2+}-gradient, ROS levels and the pH must be tightly regulated, as previously discussed. Till date, the involvement of a proton pump in the PT CWI pathway was not demonstrated. Also, if the activity of AHA2 is regulated by its phosphorylation status, a phosphatase to remove the activity inhibiting phosphorylation should be involved in AHA regulation as well. We have already cloned AHA8 and AHA2 in order to find out whether AUN1/2 regulate AHA activity.

AUN1/2 could also be involved in the regulation of previously identified members of the PT CWI pathway like RbohH/J. Ogasawara et al. (2008) previously demonstrated that a RbohH/J homologue, RbohD, is synergistically activated by Ca^{2+} and phosphorylation. It is possible that AUN1/2 regulate the activity of RbohH/J in a negative feedback loop. To test if any of the ANX1/2 PT CWI pathway members interact with each other, we are currently initiating BIFC tests for all PT CWI members and AHA8.

4.2 The role of MRI and AUN1/2 in root hair growth

As demonstrated, PT growth shares many features with RH growth. We were able to show that MRI has a function in both, the ANX1/2-dependent CWI pathway in PTs as well as in the FER-dependent pathway in RHs. This was a novelty, as in these largely uncharacterized CWI pathways till then no gene was discovered that is shared amongst them. We demonstrated that *fer* RH bursting is rescued in seedlings transformed with the hypermorphic *MRI*[R240C] allele. Also, *mri* RHs were found to burst just like *fer* RHs. In the original *ipr19* mutant, we observed a strong growth inhibition of RHs. In contrast to *mri* RHs, the *ipr19* RHs were intact but had a bulge-like appearance with pectinuous CW material over-accumulations at the tip, reminding of *ANX1/2* over-expressing PTs.

Interestingly, the original *ipr7* mutant showed RH growth inhibition as well, although milder than the original *ipr19* mutant. However, this fits the observation that compared to *ipr19, ipr7* is a weak suppressor mutant. We also discovered that disruption of *AUN1/2* triggers a similar RH growth impairment. Interestingly though, compared to *AUN1/2* disruption in PTs, knocking out *AUN1* or *AUN2* is already sufficient to replicate the *aun1 aun2* phenotype. Thus, *AUN1/2* might be regulated tissue specifically. It will be interesting to see whether AUN1/2 act in the FER-dependent CWI pathway and if so, if they are at the same position relative to the ANX1/2- dependent PT CWI pathway. To test this, we have transformed *fer-4* and *mri-2* mutants with *p*FER:AUN1[D94N]-GFP and *p*FER:AUN1-GFP as a control and will soon start selecting for transformants in the T1 generation. If the constructs are functional, we would expect AUN1[D94N]-GFP but not AUN1-GFP to rescue *fer* RH bursting and, if the PT CWI pathway is in concordance with the RH CWI pathway, that none of the constructs complements the *mri-2* RH bursting as MRI seemingly is not acting upstream of AUN1/2.

4.3 A novel role for ANX1/2 in immunity

A recent study revealed a novel role of ANX1/2, aside from CWI maintenance. ANX1/2 were found to be involved in plant immunity, where they negatively regulate both PAMP-triggered immunity (PTI) and effector-triggered immunity (ETI) (Mang et al., accepted). *anx1 anx2, anx1* and *anx2* plants exhibit enhanced resistance to the pathogen *Pseudomonas syringae pv. tomato* and they initiate stronger defense responses in reaction to *flg22* treatment than WT plants. Thus, ROS production and MAPK activation is enhanced in these mutants. These phenotypes were originally discovered in the *aggie101* mutant that harbors a C-to-T conversion at 1073 bp from the start codon, which triggers an A-to-V substitution at the 358th residue of the ANX1 protein. This A358V mutation is located in the second malectin-like domain of ANX1. Furthermore, ANX1 was found to associate with *flg22* receptor FLS2 and the kinases BAK1 and BIK1. However, in response to *flg22* treatment, ANX1 preferentially associates with BAK1 and thereby attenuates the FLS2/BAK1 ligand-induced complex formation. This weakens PTI responses. In ETI, ANX1 was found to destabilize nucleotide-binding domain leucine-rich repeat protein RPS2, which acts as a guard for RIN4. If RIN4, the guardee, is degraded by effector AvrRpt2, RPS2 initiates cell-death and defense responses. However, if ANX1 destabilizes RPS2, these defense responses are attenuated.

We were able to contribute to these intriguing findings by showing that the function of ANX1/2 in immunity appears to be separated from ANX1/2 function in CWI maintenance. While the *ANX1[A358V]* mutation enhances PTI responses, we discovered that PT growth is not affected in the *anx1 [A358V] anx2-2* mutant compared to the *anx1-2 anx2-2* mutant (Mang et al., accepted). This argues for a differential regulation of ANX1/2 in CWI maintenance and immunity, possibly by binding of different ligands.

4.4 The different roles of FER in plant life

This new role of ANX1/2 is very exciting, since recently multiple related roles are being discovered for other *Cr*RLK1L members as well. For example, FER, the closest homologue of ANX1/2, is involved in a plethora of different processes in the plant, involving plant fertilization, CWI maintenance in tip-growing cells and immunity. As previously described, FER is a positive regulator in RH CWI maintenance. Duan et al. (2010) first showed that *fer* RHs burst precociously. Also, Foreman et al. (2003) identified RbohC that supposedly acts downstream of FER in RH growth as positive signaling constituent, similar to RbohH/J in PT growth. We discovered that MRI is a novel positive downstream constituent of the FER-

dependent CWI pathway and it will be interesting to see, if, with AUN1/2, we can describe the first negative signaling constituents in this pathway.

In fertilization, FER/SIRENE (SRN) was found to be required for mediating PT recognition and rupture (Huck et al., 2003; Rotman et al., 2003; Escobar-Restrepo et al., 2007). In WT plants, during PT reception, the PT enters one of the two synergid cells, the receptive synergid. Signaling between the male and female gametophyte subsequently mediates PT rupture and release of the sperm cells. In *fer/srn* ovules, the PT is not properly recognized by the female gametophyte and consequently, the PT continues growing after entering the synergid cell without releasing the sperm cells. This phenomenon is called PT overgrowth. Recent publications have demonstrated that FER orchestrates the male-female dialogue during PT reception via ROS and Ca^{2+} signaling (Duan et al., 2014; Ngo et al., 2014), which is of importance for PT/RH growth and immunity as well.

In immunity, FER was proposed to have a pathosystem-specific role. It acts as a negative regulator during plant defense against several fungal pathogens (Kessler et a., 2010; Masachis et al., 2016) but similarly acts as a scaffold enhancing ligand-induced FLS2/BAK1 complex formation in response to *flg22* treatment, thereby boosting immunity (Stegmann et al., 2017). This appears to be in contrast to the described negative role of ANX1/2 in immunity (Mang et al., accepted). It will be interesting to see whether ANX1/2 and FER compete for association with the FLS2/BAK1 complex, and if the balance of FER and ANX1 is under control of different RALF peptides.

4.5 RALF peptides, ligands for FER and ANX1/2?

Interestingly, while for ANX1/2 no ligand has been described until now, FER has been shown to bind to RALF peptides (Haruta et al., 2014; Stegmann et al., 2017). RALF1 binds FER during cell elongation and prompts rapid alkalinization of the extracellular matrix, causing growth stall. This was demonstrated for root and hypocotyl growth. It was proposed that RALF1 regulates this rapid alkalinization via FER-dependent phosphorylation of the proton pump AHA2. The phosphorylation would render the proton pump less active and thus diminish the number of protons secreted to the extracellular matrix. As a result, the extracellular pH would increase and the CW would be less extensible, causing growth stall.

Stegmann et al. (2017) recently demonstrated that RALF23 is capable of binding the FER ectodomain as well. In immunity, RALF23, possibly by binding to FER, attenuates FLS2/BAK1 and EFR/BAK1 ligand-induced complex formation in response to *flg22* and *elf18* treatment, respectively.

Recent advances argue for a role of RALFL4/19 in PT CWI maintenance (Grossniklaus, pers. comm.). *amiRNA ralfl4/19* pollen show a similar bursting phenotype as *anx1 anx2* or *rbohH rbohJ* pollen. Also, we could demonstrate that the pollen bursting phenotype of *amiRNA ralfl4/19* can be rescued by transformation with AUN1[D94N]-YFP, which is another indication that RALFL4/19 act in the ANX1/2-dependent PT CWI pathway.

There are about 37 RALFs in *Arabidopsis* (Campbell and Turner, 2017). It will be interesting to see whether RALF peptides can also bind other *Cr*RLK1Ls like THE1 and if they can differentially regulate their functions. Also, future research in the field could bring novel insights, which other common signaling modules play a role within *Cr*RLK1L signaling in general and FER and ANX1/2 signaling pathways in particular.

4.6 Outlook

In summary, the results of this PhD project can help to better understand CWI maintenance mechanisms in tip-growing plant cells as RHs and PTs. The knowledge obtained from these kinds of "basic research" studies in *Arabidopsis* might be relevant for agronomy in the future. As more and more *Cr*RLK1L homologues are being identified in species like maize, rice, common bean, Chinese pear or cotton (reviewed in Franck et al., submitted), some of the knowledge obtained in *Arabidopsis* might be transferable to these and other crucial nutritional plants. Generally, the transfer of knowledge about CW signaling obtained in scientific models to field crops would be valuable for many human activities such as human and animal nutrition, pharmacology, textile, wood and biofuel production.

Also, more *Cr*RLK1L studies in non-seed plants could provide a more detailed evolutionary perspective on the topic and could help understanding evolutionary conserved signaling mechanisms.

5. REFERENCES

Anthony, R. G., Khan, S., Costa, J., Pais, M. S. and Bögre, L. (2006). The Arabidopsis protein kinase PTI1-2 is activated by convergent phosphatidic acid and oxidative stress signaling pathways downstream of PDK1 and OXI1. *Journal of Biological Chemistry*, *281*(49): 37536-37546.

Baroux, C., Spillane, C. and Grossniklaus, U. (2002). Evolutionary origins of the endosperm in flowering plants. *Genome Biology*, *3*(9): reviews1026-1.

Barnett, D. W., Garrison, E. K., Quinlan, A. R., Strömberg, M. P. and Marth, G. T. (2011). BamTools: a C++ API and toolkit for analyzing and managing BAM files. *Bioinformatics*, *27*(12): 1691-1692.

Becker, J. D., Takeda, S., Borges, F., Dolan, L. and Feijó, J. A. (2014). Transcriptional profiling of Arabidopsis root hairs and pollen defines an apical cell growth signature. *BMC plant biology*, *14*(1): 197.

Bergonci, T., Ribeiro, B., Ceciliato, P. H., Guerrero-Abad, J. C., Silva-Filho, M. C. and Moura, D. S. (2014). *Arabidopsis thaliana* RALF1 opposes brassinosteroid effects on root cell elongation and lateral root formation. *Journal of experimental botany*, *65*(8): 2219-2230.

Berken, A., Thomas, C. and Wittinghofer, A. (2005). A new family of RhoGEFs activates the Rop molecular switch in plants. *Nature*, *436*(7054): 1176.

Boavida, L. C. and McCormick, S. (2007). TECHNICAL ADVANCE: Temperature as a determinant factor for increased and reproducible in vitro pollen germination in Arabidopsis thaliana. *The Plant Journal*, *52*(3): 570-582.

Boevink, P. C., Wang, X., McLellan, H., He, Q., Naqvi, S., Armstrong, M. R., ... , and Birch, P. R. (2016). A Phytophthora infestans RXLR effector targets plant PP1c isoforms that promote late blight disease. *Nature communications*, *7*.

Boisson-Dernier, A., Roy, S., Kritsas, K., Grobei, M. A., Jaciubek, M., Schroeder, J. I. and Grossniklaus, U. (2009). Disruption of the pollen-expressed *FERONIA* homologs *ANXUR1* and *ANXUR2* triggers pollen tube discharge. *Development (Cambridge, England)*, *136*(19): 3279–3288.

Boisson-Dernier, A., Lituiev, D.S., Nestorova, A., Franck, C.M., Thirugnanarajah, S. and Grossniklaus, U. (2013). ANXUR Receptor-Like Kinases Coordinate CWI with Growth at the Pollen Tube Tip Via NADPH Oxidases. *PLOS Biology,* 11(11): e1001719.

Boisson-Dernier, A., Franck, C.M., Lituiev, D.S. and Grossniklaus, U. (2015). Receptor-like cytoplasmic kinase MARIS functions downstream of *Cr*RLK1L-dependent signaling during tip growth. *Proceedings of the National Academy of Sciences of the United States of America*, *112*(39): 12211–12216.

Bosch, M. and Hepler, P. K. (2005). Pectin Methylesterases and Pectin Dynamics in Pollen Tubes. *The Plant Cell*, *17*(12): 3219–3226.

Bibikova, T. N., Zhigilei, A. and Gilroy, S. (1997). Root hair growth in Arabidopsis thaliana is directed by calcium and an endogenous polarity. *Planta*, *203*(4): 495-505.

Bibikova, T. N., Jacob, T., Dahse, I. and Gilroy, S. (1998). Localized changes in apoplastic and cytoplasmic pH are associated with root hair development in Arabidopsis thaliana. *Development*, *125*(15): 2925-2934.

Bleckmann, A., Alter, S. and Dresselhaus, T. (2014). The beginning of a seed: regulatory mechanisms of double fertilization. *Frontiers in plant science*, *5*.

Bollen, M. (2001). Combinatorial control of protein phosphatase-1. *Trends in biochemical sciences*, *26*(7): 426-431.

Cai, G. and Cresti, M. (2008). Organelle motility in the pollen tube: a tale of 20 years. *Journal of experimental botany*, *60*(2): 495-508.

Campbell, L. and Turner, S. R. (2017). A Comprehensive Analysis of RALF Proteins in Green Plants Suggests There Are Two Distinct Functional Groups. *Frontiers in plant science*, *8*.

Cárdenas, L., Lovy-Wheeler, A., Kunkel, J. G. and Hepler, P. K. (2008). Pollen Tube Growth Oscillations and Intracellular Calcium Levels Are Reversibly Modulated by Actin Polymerization. *Plant Physiology*, *146*(4): 1611–1621.

Ceulemans, H. U. G. O. and Bollen, M. (2004). Functional diversity of protein phosphatase-1, a cellular economizer and reset button. *Physiological reviews*, *84*(1): 1-39.

Chebli, Y., Kaneda, M., Zerzour, R. and Geitmann, A. (2012). The cell wall of the Arabidopsis pollen tube-spatial distribution, recycling, and network formation of polysaccharides. *Plant Physiology,* 160(4): 1940-55.

Chebli, Y., Kroeger, J. and Geitmann, A (2013). Transport Logistics in Pollen Tubes*, Molecular Plant,* 6(4): 1037-1052.

Cheung, A. (1996). Pollen—pistil interactions during pollen-tube growth. *Trends in Plant Science,* 1(2): 45-51.

Cheung, A. Y., Niroomand, S., Zou, Y. and Wu, H. M. (2010). A transmembrane formin nucleates subapical actin assembly and controls tip-focused growth in pollen tubes. *Proceedings of the National Academy of Sciences*, *107*(37): 16390-16395.

Clough, S. J. and Bent, A. F. (1998). Floral dip: a simplified method for *Agrobacterium*-mediated transformation of *Arabidopsis thaliana*. *The Plant Journal*, 16: 735–743.

Cohen, P. T. (2002). Protein phosphatase 1–targeted in many directions. *Journal of cell science*, *115*(2): 241-256.

Cosgrove, D. (2005). Growth of the plant cell wall*. Nature Reviews Molecular Cell Biology.* 6: 850-861.

Deslauriers, S. D. and Larsen, P. B. (2010). FERONIA is a key modulator of brassinosteroid and ethylene responsiveness in Arabidopsis hypocotyls. *Molecular Plant*, *3*(3): 626-640.

do Canto, A. M., Ceciliato, P. H., Ribeiro, B., Morea, F. A. O., Garcia, A. A. F., Silva-Filho, M. C. and Moura, D. S. (2014). Biological activity of nine recombinant *At*RALF peptides: implications for their perception and function in Arabidopsis. *Plant Physiology and Biochemistry*, *75*: 45-54.

Du, C., Li, X., Chen, J., Chen, W., Li, B., Li, C., ... , and Liu, X. (2016). Receptor kinase complex transmits RALF peptide signal to inhibit root growth in Arabidopsis. *Proceedings of the National Academy of Sciences*, *113*(51): E8326-E8334.

Duan, Q., Kita, D., Li, C., Cheung, A. Y. and Wu, H. M. (2010). FERONIA receptor-like kinase regulates RHO GTPase signaling of root hair development. *Proceedings of the National Academy of Sciences*, *107*(41): 17821-17826.

Duan, Q., Kita, D., Johnson, E. A., Aggarwal, M., Gates, L., Wu, H. M. and Cheung, A. Y. (2014). Reactive oxygen species mediate pollen tube rupture to release sperm for fertilization in Arabidopsis. *Nature Communications*, *5*: 3129.

Dresselhaus, T. and Franklin-Tong, N. (2013). Male–female crosstalk during pollen germination, tube growth and guidance, and double fertilization. *Molecular Plant*, *6*(4): 1018-1036.

Dresselhaus, T., Sprunck, S. and Wessel, G. M. (2016). Fertilization mechanisms in flowering plants. *Current Biology*, *26*(3): R125-R139.

Duan, Q., Kita, D., Li, C., Cheung, A. Y., and Wu, H. M. (2010). FERONIA receptor-like kinase regulates RHO GTPase signaling of root hair development. *Proceedings of the National Academy of Sciences*, *107*(41): 17821-17826.

Escobar-Restrepo, J. M., Huck, N., Kessler, S., Gagliardini, V., Gheyselinck, J., Yang, W. C. and Grossniklaus, U. (2007). The FERONIA receptor-like kinase mediates male-female interactions during pollen tube reception. *Science*, *317*(5838): 656-660.

Felle, H. H. and Hepler, P. K. (1997). The cytosolic Ca2+ concentration gradient of Sinapis alba root hairs as revealed by Ca2+-selective microelectrode tests and fura-dextran ratio imaging. *Plant Physiology*, *114*(1): 39-45.

Foreman, J., Demidchik, V., Bothwell, J. H., Mylona, P., …, and Dolan, L. (2003). Reactive oxygen species produced by NADPH oxidase regulate plant cell growth. *Nature*, *422*(6930): 442.

Franck, C. M., Westermann, J. and Boisson-Dernier, A. (2017). Imaging Ca2+ Dynamics in Wild-Type and NADPH Oxidase-Deficient Mutant Pollen Tubes with Yellow Cameleon and Confocal Laser Scanning Microscopy. *In Plant Germline Development (pp. 103-116). Humana Press, New York, NY.*

Franck, C.M., Westermann, J. and Boisson-Dernier, A. Plant Malectin-like Receptor kinases: from CWI to immunity and beyond. *Annual Reviews of Plant Biology.* (submitted)

Free, S. J. (2013). Fungal cell wall organization and biosynthesis. *Adv Genet*, *81*: 33-82.

Fry, S.C. (1998). Oxidative scission of plant cell wall polysaccharides by ascorbate-induced hydroxyl radicals. *Biochemical Journal*, 332: 507–515.

Fu, Y., Wu, G. and Yang, Z. (2001). Rop GTPase–dependent dynamics of tip-localized F-actin controls tip growth in pollen tubes. *The Journal of cell biology*, *152*(5): 1019-1032.

Fu, Y., Gu, Y., Zheng, Z., Wasteneys, G., and Yang, Z. (2005). Arabidopsis interdigitating cell growth requires two antagonistic pathways with opposing action on cell morphogenesis. *Cell*, *120*(5): 687-700.

Fuchs, U., Manns, I. and Steinberg, G. (2005). Microtubules are dispensable for the initial pathogenic development but required for long-distance hyphal growth in the corn smut fungus Ustilago maydis. *Molecular biology of the cell*, *16*(6): 2746-2758.

Garrison, E. and Marth, G. (2012). Haplotype-based variant detection from short-read sequencing. *arXiv preprint arXiv:1207.3907*.

Grierson, C., Nielsen, E., Ketelaarc, T. and Schiefelbein, J. (2014). Root hairs. *The Arabidopsis Book*, *12*: e0172.
Guan, Y., Guo, J., Li, H. and Yang, Z. (2013). Signaling in Pollen Tube Growth: Crosstalk, Feedback, and Missing Links. *Molecular Plant*, *6*(4): 1053–1064.

Gu, Y., Fu, Y., Dowd, P., Li, S., Vernoud, V., Gilroy, S. and Yang, Z. (2005). A Rho family GTPase controls actin dynamics and tip growth via two counteracting downstream pathways in pollen tubes. *J Cell Biol*, *169*(1): 127-138.

Guo, H., Li, L., Ye, H., Yu, X., Algreen, A. and Yin, Y. (2009). Three related receptor-like kinases are required for optimal cell elongation in Arabidopsis thaliana. *Proceedings of the National Academy of Sciences*, *106*(18): 7648-7653.

Guo, X., Qin, Q., Yan, J., Niu, Y., Huang, B., Guan, L., …, and Hou, S. (2015). TOPP4 Regulates Pavement Cell Interdigitation by Modulating PIN1 Polarity and Trafficking in Arabidopsis. *Plant Physiology*, pp-114.

Hamann, T. (2014). The plant CWI maintenance mechanism—concepts for organization and mode of action. *Plant and Cell Physiology*, *56*(2): 215-223.

Hanks, S. K., Quinn, A. M. and Hunter, T. (1988). The Protein Kinase Family: Conserved Features and Deduced Phylogeny. *Science*, *241*: 42-52.

Haruta, M., Sabat, G., Stecker, K., Minkoff, B. B., and Sussman, M. R. (2014). A peptide hormone and its receptor protein kinase regulate plant cell expansion. *Science*, *343*(6169): 408-411.

Hématy, K., Sado, P. E., Van Tuinen, A., Rochange, S., Desnos, T., Balzergue, S., ... , and Höfte, H. (2007). A receptor-like kinase mediates the response of Arabidopsis cells to the inhibition of cellulose synthesis. *Current Biology*, *17*(11): 922-931.

Herrmann, A. and Felle, H. H. (1995). Tip growth in root hair cells of Sinapis alba L.: significance of internal and external Ca2+ and pH. *New Phytologist*, *129*(3): 523-533.

Honys, D. and Twell, D. (2004). Transcriptome analysis of haploid male gametophyte development in Arabidopsis. *Genome biology*, *5*(11): R85.

Hou, Y. J., Zhu, Y., Wang, P., Zhao, Y., Xie, S., Batelli, G., …, and Lei, M. (2016). Type one protein phosphatase 1 and its regulatory protein inhibitor 2 negatively regulate ABA signaling. *PLoS genetics*, *12*(3): e1005835.

Hruz, T., Laule, O., Szabo, G., Wessendorp, F., Bleuler, S., Oertle, L., ... , and Zimmermann, P. (2008). Genevestigator v3: a reference expression database for the meta-analysis of transcriptomes. *Advances in bioinformatics*, *2008*.

Huck, N., Moore, J. M., Federer, M. and Grossniklaus, U. (2003). The Arabidopsis mutant feronia disrupts the female gametophytic control of pollen tube reception. *Development*, *130*(10), 2149-2159.

Iwano, M., Entani, T., Shiba, H., Kakita, M., Nagai, T., Mizuno, H., …, and Takayama, S. (2009). Fine-Tuning of the Cytoplasmic Ca2+ Concentration Is Essential for Pollen Tube Growth. *Plant Physiology*, 150(3): 1322–1334.

Jakoby, M. J., Falkenhan, D., Mader, M. T., Brininstool, G., Wischnitzki, E., Platz, N., ... , and Schnittger, A. (2008). Transcriptional profiling of mature Arabidopsis trichomes reveals that NOECK encodes the MIXTA-like transcriptional regulator MYB106. *Plant Physiology*, *148*(3): 1583-1602.

Jones, L., Milne, J. L., Ashford, D. and McQueen-Mason, S. J. (2003). Cell wall arabinan is essential for guard cell function. *Proceedings of the National Academy of Sciences*, *100*(20): 11783-11788.

Johnson, M.A. and Preuss, D. (2002). Plotting a Course: Multiple Signals Guide Pollen Tubes to Their Targets, *Developmental Cell*, 2(3): 273-281.

Johnson, M. and Lord, E. (2006). Extracellular Guidance Cues and Intracellular Signaling Pathways that Direct Pollen Tube Growth, in: Malhó, R. (Ed.), The Pollen Tube, Plant Cell Monographs. *Springer Berlin Heidelberg*, 3: 223–242.

Jurczak, M. J., Zapater, J. L., Greenberg, C. C., & Brady, M. J. (2010). Generation of a Dominant-Negative Glycogen Targeting Subunit for Protein Phosphatase-1. *Obesity, 18*(10), 1881-1887.

Katzen, F. (2007). Gateway® recombinational cloning: a biological operating system. *Expert opinion on drug discovery*, *2*(4): 571-589.

Kaul, S., Koo, H. L., Jenkins, J., Rizzo, M., Rooney, T., Tallon, L. J., ... , and Town, C. D. (2000). Analysis of the genome sequence of the flowering plant Arabidopsis thaliana. *nature*, *408*(6814): 796-815.

Kavi Kishor, P. B., Hima Kumari, P., Sunita, M. S. L. and Sreenivasulu, N. (2015). Role of proline in cell wall synthesis and plant development and its implications in plant ontogeny. *Frontiers in Plant Science*, 6: 544.

Keinath, N. F., Kierszniowska, S., Lorek, J., Bourdais, G., Kessler, S. A., Shimosato-Asano, H., ... , and Panstruga, R. (2010). PAMP (pathogen-associated molecular pattern)-induced changes in plasma membrane compartmentalization reveal novel components of plant immunity. *Journal of Biological Chemistry*, *285*(50): 39140-39149.

Kerk, D., Bulgrien, J., Smith, D. W., Barsam, B., Veretnik, S., and Gribskov, M. (2002). The complement of protein phosphatase catalytic subunits encoded in the genome of Arabidopsis. *Plant physiology*, *129*(2): 908-925.

Kessler, S. A., Shimosato-Asano, H., Keinath, N. F., Wuest, S. E., Ingram, G., Panstruga, R. and Grossniklaus, U. (2010). Conserved molecular components for pollen tube reception and fungal invasion. *Science*, *330*(6006): 968-971.

Kessler, S. A., Lindner, H., Jones, D. S. and Grossniklaus, U. (2014). Functional analysis of related *Cr*RLK1L receptor-like kinases in pollen tube reception. *EMBO reports*, e201438801.

Ketelaar, T., De Ruijter, N. C. and Emons, A. M. C. (2003). Unstable F-actin specifies the area and microtubule direction of cell expansion in Arabidopsis root hairs. *The Plant Cell*, *15*(1): 285-292.

Kohorn, B. D. and Kohorn, S. L. (2012). The cell wall-associated kinases, WAKs, as pectin receptors. *Frontiers in Plant Science*, 3: 88.

Krebs, M., Held, K., Binder, A., Hashimoto, K., Den Herder, G., Parniske, M., …, and Schumacher, K. (2012). FRET-based genetically encoded sensors allow high-resolution live cell imaging of Ca^{2+} dynamics. *The Plant Journal*, *69*(1): 181-192.

Lassig, R., Gutermuth, T., Bey, T. D., Konrad, K. R. and Romeis, T. (2014). Pollen tube NAD(P)H oxidases act as a speed control to dampen growth rate oscillations during polarized cell growth. *The Plant Journal*, 78: 94–106.

Lehti-Shiu, M.D., Zou, C., Hanada, K., Shiu, S.-H. (2009). Evolutionary History and Stress Regulation of Plant Receptor-Like Kinase/Pelle Genes. *Plant Physiology,* 150(1):12-26.

Leshem, Y., Johnson, C. and Sundaresan, V. (2013). Pollen tube entry into the synergid cell of Arabidopsis is observed at a site distinct from the filiform apparatus. *Plant reproduction*, *26*(2): 93-99.

Levin, D. E. (2005). CWI signaling in Saccharomyces cerevisiae. *Microbiology and molecular biology reviews*, *69*(2): 262-291.

Levin, D. E. (2011). Regulation of cell wall biogenesis in Saccharomyces cerevisiae: the CWI signaling pathway. *Genetics*, *189*(4): 1145-1175.

Li, H., Handsaker, B., Wysoker, A., Fennell, T., Ruan, J., Homer, N., ... , and Durbin, R. (2009). The sequence alignment/map format and SAMtools. *Bioinformatics*, *25*(16): 2078-2079.

Lin, D., Lopez-Sanchez, P. and Gidley, M. J. (2015). Binding of arabinan or galactan during cellulose synthesis is extensive and reversible. *Carbohydrate polymers*, *126*: 108-121.

Lindner, H., Müller, L.M., Boisson-Dernier, A. and Grossniklaus, U. (2012). *Cr*RLK1L receptor-like kinases: Not just another brick in the wall. *Current Opinion in Plant Biology*,15(6): 659-69.

Lindner, H., Raissig, M. T., Sailer, C., Shimosato-Asano, H., Bruggmann, R. and Grossniklaus, U. (2012). SNP-Ratio Mapping (SRM): identifying lethal alleles and mutations in complex genetic backgrounds by next-generation sequencing. *Genetics*, *191*(4): 1381-1386.

Liszkay, A., van der Zalm, E. and Schopfer, P. (2004). Production of reactive oxygen intermediates O_2^- , H_2O_2, and OH by maize roots and their role in wall loosening and elongation growth. *Plant Physiology*, 136: 3114–3123.

Loraine, A. E., McCormick, S., Estrada, A., Patel, K. and Qin, P. (2013). RNA-seq of Arabidopsis pollen uncovers novel transcription and alternative splicing. *Plant physiology*, *162*(2): 1092-1109.

Mang, H., Feng, B., Hu, Z., Boisson-Dernier, A., Franck, C.M., Meng, X., Xu, G., Wang, T., Shan, L. and He, P. Differential regulation of two-tiered plant immunity and sexual reproduction by ANXUR receptor-kinases. *The Plant Cell.* (accepted)

Márton, M. L., Cordts, S., Broadhvest, J. and Dresselhaus, T. (2005). Micropylar pollen tube guidance by egg apparatus 1 of maize. *Science*, *307*(5709): 573-576.

Márton, M. L., Fastner, A., Uebler, S. and Dresselhaus, T. (2012). Overcoming hybridization barriers by the secretion of the maize pollen tube attractant ZmEA1 from Arabidopsis ovules. *Current Biology*, *22*(13): 1194-1198.

Masachis, S., Segorbe, D., Turrà, D., Leon-Ruiz, M., Fürst, U., El Ghalid, M., ... , and Di Pietro, A. (2016). A fungal pathogen secretes plant alkalinizing peptides to increase infection. *Nature microbiology*, *1*: 16043.

Mashigo, M., Combrinck, S., Regnier, T., Du Plooy, W., Augustyn, W. and Mokgalaka, N. (2015). Chemical variations, trichome structure and antifungal activities of essential oils of *Helichrysum splendidum* from South Africa. *South African Journal of Botany,* 96: 78-84.

Matsumoto, T., Wu, J. Z., Kanamori, H., Katayose, Y., Fujisawa, M., Namiki, N., ... , and Sakata, K. (2005). The map-based sequence of the rice genome. *Nature*, *436*(7052), 793-800.

Michard, E., Filipa, A. and Feijó, J.A. (2009). The role of ion fluxes in polarized cell growth and morphogenesis: the pollen tube as an experimental paradigm. *The International Journal of Developmental Biology*, 53: 1609 - 1622.

Miyazaki, S., Murata, T., Sakurai-Ozato, N., Kubo, M., Demura, T., Fukuda, H. and Hasebe, M. (2009). ANXUR1 and 2, Sister Genes to FERONIA/SIRENE, Are Male Factors for Coordinated Fertilization.*Current Biology*, 19(15): 1327-1331.

Mollet, J.-C., Leroux, C., Dardelle, F. and Lehner, A. (2013). Cell Wall Composition, Biosynthesis and Remodeling during Pollen Tube Growth. *Plants*, *2*(1): 107–147.

Monshausen, G. B., Bibikova, T. N., Messerli, M. A., Shi, C. and Gilroy, S. (2007). Oscillations in extracellular pH and reactive oxygen species modulate tip growth of Arabidopsis root hairs. *Proceedings of the National Academy of Sciences, 104*(52): 20996-21001.

Mouriño-Pérez, R. R., Roberson, R. W. and Bartnicki-García, S. (2006). Microtubule dynamics and organization during hyphal growth and branching in Neurospora crassa. *Fungal Genetics and Biology, 43*(6), 389-400.

Müller, K., Linkies, A., Vreeburg, R.A., Fry, S.C., Krieger-Liszkay, A. and Leubner-Metzger, G. (2009). *In vivo* cell wall loosening by hydroxyl radicals during cress seed germination and elongation growth. *Plant Physiology*, 150: 1855–1865.

Ngo, Q. A., Vogler, H., Lituiev, D. S., Nestorova, A. and Grossniklaus, U. (2014). A calcium dialog mediated by the FERONIA signal transduction pathway controls plant sperm delivery. *Developmental Cell, 29*(4): 491-500.

Nibau, C., Wu, H. M. and Cheung, A. Y. (2006). RAC/ROP GTPases: 'hubs' for signal integration and diversification in plants. *Trends in plant science, 11*(6): 309-315.
Nibau, C. and Cheung, A. (2011). New insights into the functional roles of CrRLKs in the control of plant cell growth and development. *Plant signaling & behavior, 6*(5): 655-659.

Ogasawara, Y., Kaya, H., Hiraoka, G., Yumoto, F., Kimura, S., Kadota, Y., …, and Nara, M. (2008). Synergistic activation of the Arabidopsis NADPH oxidase AtRbohD by Ca^{2+} and phosphorylation. *Journal of Biological Chemistry, 283*(14): 8885-8892.

Okuda, S., Tsutsui, H., Shiina, K., Sprunck, S., Takeuchi, H., Yui, R., ... , and Kawano, N. (2009). Defensin-like polypeptide LUREs are pollen tube attractants secreted from synergid cells. *Nature, 458*(7236): 357-361.

Parton, R. M., Fischer, S., Malhó, R., Papasouliotis, O., Jelitto, T. C., Leonard, T. and Read, N. D. (1997). Pronounced cytoplasmic pH gradients are not required for tip growth in plant and fungal cells. *Journal of Cell Science, 110*(10): 1187-1198.

Potocký, M., Jones, M. A., Bezvoda, R., Smirnoff, N. and Žárský, V. (2007). Reactive oxygen species produced by NADPH oxidase are involved in pollen tube growth. *New Phytologist*, 174: 742–751.

Preuss, D., Rhee, S. Y. and Davis, R. W. (1994). Tetrad analysis possible in Arabidopsis with mutation of the QUARTET (QRT) genes. *Science-AAAS-Weekly Paper Edition-including Guide to Scientific Information, 264*(5164): 1458-1459.

Qin, Q., Wang, W., Guo, X., Yue, J., Huang, Y., Xu, X., …, and Hou, S. (2014). Arabidopsis DELLA protein degradation is controlled by a type-one protein phosphatase, TOPP4. *PLoS genetics, 10*(7): e1004464.

Raudaskoski, M., Mao, W. Z. and Yli-Mattila, T. A. P. A. N. I. (1994). Microtubule cytoskeleton in hyphal growth. Response to nocodazole in a sensitive and a tolerant strain of the homobasidiomycete Schizophyllum commune. *European journal of cell biology, 64*(1): 131-141.

Rayle, L. and Cleland, R. (1970). Enhancement of Wall Loosening and Elongation by Acid Solutions. *Plant Physiology*, 46 (2): 250-253.

Ridley, B. L., O'Neill, M. A. and Mohnen, D. (2001). Pectins: structure, biosynthesis, and oligogalacturonide-related signaling. *Phytochemistry, 57*(6): 929-967.

Ringli, C. (2010). Monitoring the Outside: Cell Wall-Sensing Mechanisms. *Plant Physiology, 153*(4): 1445–1452.

Roskoski, R. (2012). MEK1/2 dual-specificity protein kinases: structure and regulation. *Biochemical and biophysical research communications*, *417*(1): 5-10.

Rotman, N., Rozier, F., Boavida, L., Dumas, C., Berger, F., and Faure, J. E. (2003). Female control of male gamete delivery during fertilization in Arabidopsis thaliana. *Current Biology*, *13*(5): 432-436.

Schallus, T., Jaeckh, C., Fehér, K., Palma, A.S., Liu, Y.,..., and Muhle-Goll, C. (2008). Malectin: A Novel Carbohydrate-binding Protein of the Endoplasmic Reticulum and a Candidate Player in the Early Steps of Protein N-Glycosylation. *Molecular Biology of the Cell,* 19(8): 3404–14.

Schindelin, J., Arganda-Carreras, I., Frise, E., Kaynig, V., Longair, M., Pietzsch, T., ... , and Tinevez, J. Y. (2012). Fiji: an open-source platform for biological-image analysis. *Nature methods*, *9*(7): 676-682.

Schindelin, J., Rueden, C. T., Hiner, M. C. and Eliceiri, K. W. (2015). The ImageJ ecosystem: An open platform for biomedical image analysis. *Molecular reproduction and development*, *82*(7-8): 518-529.

Schiøtt, M., Romanowsky, S. M., Bækgaard, L., Jakobsen, M. K., Palmgren, M. G. and Harper, J. F. (2004). A plant plasma membrane Ca2+ pump is required for normal pollen tube growth and fertilization. *Proceedings of the National Academy of Sciences of the United States of America*, *101*(25): 9502-9507.

Schulze-Muth, P., Irmler, S., Schröder, G. and Schröder, J. (1996). Novel Type of Receptor-like Protein Kinase from a Higher Plant (Catharanthus roseus): cDNA, gene, intramolecular autophosphorylation, and identification of a threonine important for auto- and substrate phosphorylation. *Journal of Biological Chemistry,* 271(43): 26684–89.

Sedlazeck, F. J., Rescheneder, P. and Von Haeseler, A. (2013). NextGenMap: fast and accurate read mapping in highly polymorphic genomes. *Bioinformatics*, *29*(21): 2790-2791.

Sessa, G., D'Ascenzo, M. and Martin, G. B. (2000). The major site of the Pti1 kinase phosphorylated by the Pto kinase is located in the activation domain and is required for Pto–Pti1 physical interaction. *The FEBS Journal*, *267*(1): 171-178.

Simpson, M., Plant Systematics (2006). *Academic Press*,1: 399 et sqq.

Singh, P. and Zimmerli, L. (2013). Lectin receptor kinases in plant innate immunity. *Frontiers in Plant Science*, 4: 124.

Staiger, C. J., Yuan, M., Valenta, R., Shaw, P. J., Warn, R. M. and Lloyd, C. W. (1994). Microinjected profilin affects cytoplasmic streaming in plant cells by rapidly depolymerizing actin microfilaments. *Current biology*, *4*(3): 215-219.

Stegmann, M., Monaghan, J., Smakowska-Luzan, E., Rovenich, H., Lehner, A., Holton, N., ... , and Zipfel, C. (2017). The receptor kinase FER is a RALF-regulated scaffold controlling plant immune signaling. *Science*, *355*(6322): 287-289.

Steinhorst, L. and Kudla, J. (2013). Calcium - a central regulator of pollen germination and tube growth. *Biochimica et Biophysica Acta - Molecular Cell Research*,1833(7): 1573-1581.

Takemiya, A., Kinoshita, T., Asanuma, M. and Shimazaki, K. I. (2006). Protein phosphatase 1 positively regulates stomatal opening in response to blue light in Vicia faba. *Proceedings of the National Academy of Sciences*, *103*(36): 13549-13554.

Takemiya, A., Ariyoshi, C. and Shimazaki, K. I. (2009). Identification and functional characterization of inhibitor-3, a regulatory subunit of protein phosphatase 1 in plants. *Plant physiology*, *150*(1): 144-156.

Takeuchi, H. and Higashiyama, T. (2012). A species-specific cluster of defensin-like genes encodes diffusible pollen tube attractants in Arabidopsis. *PLoS Biology*, *10*(12): e1001449.

Torres, M. A., Onouchi, H., Hamada, S., Machida, C., Hammond-Kosack, K. E. and Jones, J. D. (1998). Six Arabidopsis thaliana homologues of the human respiratory burst oxidase (gp91phox). *The Plant Journal*, *14*(3): 365-370.

Twell, D., Wing, R., Yamaguchi, J. and McCormick, S. (1989). Isolation and expression of an anther-specific gene from tomato. *Molecular and general genetics Mgg*, *217*(2): 240-245.

van der Geer, P., Hunter, T. and Lindberg, R.A. (1994). Receptor protein-tyrosine kinases and their signal transduction pathways. *Annual Reviews of Cell Biology,* 10: 251–33.

Vincken, J. P., Schols, H. A., Oomen, R. J., McCann, M. C., Ulvskov, P., Voragen, A. G. and Visser, R. G. (2003). If homogalacturonan were a side chain of rhamnogalacturonan I. Implications for cell wall architecture. *Plant physiology*, *132*(4): 1781-1789.

Wagner, G. J. (1991). Secreting Glandular Trichomes: More than Just Hairs. *Plant Physiology*, *96*(3): 675–679.

Willats, W. G., McCartney, L., Mackie, W. and Knox, J. P. (2001). Pectin: cell biology and prospects for functional analysis. In *Plant Cell Walls* (pp. 9-27). Springer Netherlands.

Wu, G., Gu, Y., Li, S., and Yang, Z. (2001). A genome-wide analysis of Arabidopsis Rop-interactive CRIB motif–containing proteins that act as Rop GTPase targets. *The Plant Cell*, *13*(12): 2841-2856.

Wymer, C. L., Bibikova, T. N. and Gilroy, S. (1997). Cytoplasmic free calcium distributions during the development of root hairs of Arabidopsis thaliana. *The Plant Journal*, *12*(2): 427-439.

Ye, J., Zheng, Y., Yan, A., Chen, N., Wang, Z., Huang, S. and Yang, Z. (2009). Arabidopsis formin3 directs the formation of actin cables and polarized growth in pollen tubes. *The Plant Cell*, *21*(12): 3868-3884.

Yuan, F., Leng, B. and Wang, B. (2016). Progress in Studying Salt Secretion from the Salt Glands in Recretohalophytes: How Do Plants Secrete Salt? *Frontiers in Plant Science*, 7: 977.

Yue, J., Qin, Q., Meng, S., Jing, H., Gou, X., Li, J. and Hou, S. (2016). TOPP4 Regulates the Stability of PHYTOCHROME INTERACTING FACTOR5 during Photomorphogenesis in Arabidopsis. *Plant physiology*, *170*(3): 1381-1397.

Ich versichere, dass ich die von mir vorgelegte Dissertation selbständig angefertigt, die benutzten Quellen und Hilfsmittel vollständig angegeben und die Stellen der Arbeit − einschließlich Tabellen, Karten und Abbildungen −, die anderen Werken im Wortlaut oder dem Sinn nach entnommen sind, in jedem Einzelfall als Entlehnung kenntlich gemacht habe; dass diese Dissertation noch keiner anderen Fakultät oder Universität zur Prüfung vorgelegen hat; dass sie − abgesehen von unten angegebenen Teilpublikationen − noch nicht veröffentlicht worden ist, sowie, dass ich eine solche Veröffentlichung vor Abschluss des Promotionsverfahrens nicht vornehmen werde. Die Bestimmungen der Promotionsordnung sind mir bekannt. Die von mir vorgelegte Dissertation ist von Dr. Aurélien Boisson-Dernier betreut worden.

Lebenslauf

Persönliche Daten

Name: Franck
Vorname: Christina Maria
Geburtsdatum: 17. August 1991
Geburtsort: Moosburg a.d. Isar
Staatsangehörigkeit: Deutschland
E-mail: c.franck@uni-koeln.de

Ausbildung

Studienverlauf

Ab März 2015   Promotionsstudium am Botanischen Institut der Universität zu Köln, betreut von Dr. Aurélien Boisson-Dernier

August 2013 – Januar 2015   Master of Science (Molecular Cell Biology) in der Arbeitsgruppe von Prof. Dr. Ueli Grossniklaus am Institut für Botanik und Mikrobiologie der Universität Zürich (Schweiz), betreut von Dr. Hannes Vogler

Thema der Masterarbeit: „Assessing the role of NADPH oxidases RbohH and RbohJ in pollen tube growth with Cellular Force Microscopy. "

Abschlussnote 5,5 (entspricht 1,5 in Deutschland)

September 2010 – Juni 2013 Bachelor of Science (Biology) an der Universität Zürich (Schweiz)

Abschlussnote 5,1 (entspricht 1,9 in Deutschland)

Schulbildung

Bis Juli 2010   Allgemeine Hochschulreife

Gymnasiale Oberstufe am Maristenkolleg Mindelheim (Deutschland)

Abschlussnote 1,5